

การเพิ่มประสิทธิภาพของระบบเซลล์เชื้อเพลิงชนิดออกไซด์ชนิดแข็งป้อนด้วยมีเทน



นายสุภวัฒน์ วิวรรณภัทรกิจ

สถาบันวิทยบริการ

วิทยานิพนธ์นี้เป็นส่วนหนึ่งของการศึกษาตามหลักสูตรปริญญาวิศวกรรมศาสตรบัณฑิต

สาขาวิชาวิศวกรรมเคมี ภาควิชาวิศวกรรมเคมี

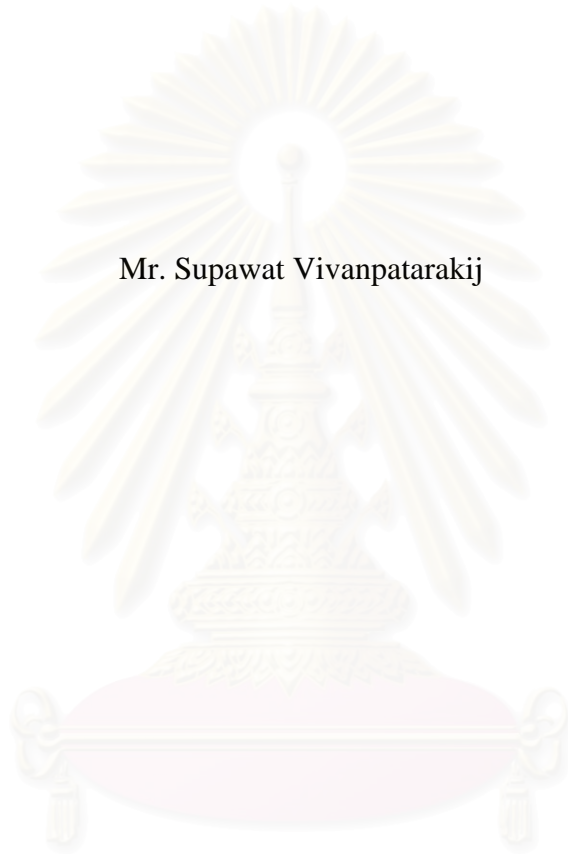
คณะวิศวกรรมศาสตร์ จุฬาลงกรณ์มหาวิทยาลัย

ปีการศึกษา 2550

ลิขสิทธิ์ของจุฬาลงกรณ์มหาวิทยาลัย

PERFORMANCE IMPROVEMENT OF
SOLID OXIDE FUEL CELL SYSTEM FED BY METHANE

Mr. Supawat Vivanpatarakij



A Dissertation Submitted in Partial Fulfillment of the Requirements
for the Degree of Doctor of Engineering Program in Chemical Engineering

Department of Chemical Engineering

Faculty of Engineering


Chulalongkorn University

Academic Year 2007

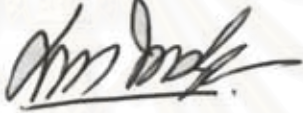
Copyright of Chulalongkorn University

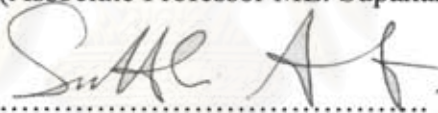
Thesis Title PERFORMANCE IMPROVEMENT OF SOLID OXIDE
FUEL CELL SYSTEM FED BY METHANE
By Mister Supawat Vivanpatarakij
Field of Study Chemical Engineering
Thesis Advisor Associate Professor Suttichai Assabumrungrat, Ph.D.

Accepted by the Faculty of Engineering, Chulalongkorn University in Partial
Fulfillment of the Requirements for the Doctoral Degree



..... Dean of the Faculty of Engineering
(Associate Professor Boonsom Lerdkhironwong, Dr. Ing.)


THESIS COMMITTEE


..... Chairman
(Associate Professor ML. Supakanok Thongyai, Ph.D.)


..... Thesis Advisor
(Associate Professor Suttichai Assabumrungrat, Ph.D.)


..... External Member
(Assistant Professor Navadol Laosiripojana, Ph.D.)


..... Member
(Assistant Professor Amornchai Arpornwichanop, D.Eng.)


..... Member
(Akawat Sirisuk, Ph.D.)

ศุภวัฒน์ วิวรรักษ์ภทกิจ : การเพิ่มประสิทธิภาพของระบบเซลล์เชื้อเพลิงชนิดออกไซด์ชนิดแข็งป้อนด้วยมีเทน (PERFORMANCE IMPROVEMENT OF SOLID OXIDE FUEL CELL SYSTEM FED BY METHANE) อ. ที่ปรึกษา: รศ. ดร. ศุทธิชัย อุตตะปารุ่งรัตน์, 104 หน้า.

งานวิจัยนี้ศึกษาการเพิ่มสมรรถนะของระบบเซลล์เชื้อเพลิงชนิดออกไซด์ชนิดแข็งที่ป้อนด้วยมีเทน โดยแนวทางการพัฒนาระบบนี้สามารถแบ่งออกได้เป็น 3 หัวข้อหลัก ดังนี้ 1) การดำเนินงานเซลล์เชื้อเพลิงภายใต้ความดันสัทธิที่ไม่คงที่ (SOFC-NUP) 2) การใช้เครื่องปฏิกรณ์แบบเชื้อเพลิงผ่านชนิดพลาสมาเพื่อดำเนินงานร่วมกับเซลล์เชื้อเพลิงชนิดออกไซด์ชนิดแข็ง (SOFC-MR) 3) การเพิ่มหน่วยกำจัดคาร์บอนไดออกไซด์ที่ดำเนินงานร่วมกับเซลล์เชื้อเพลิงชนิดออกไซด์ชนิดแข็ง (SOFC-CaO) ผลการศึกษาพบว่าสำหรับการดำเนินงานแบบความดันสัทธิที่ไม่คงที่นั้น กรณีที่ทำการแบ่งเซลล์เชื้อเพลิงเป็น 2 ส่วนที่ดำเนินงานที่ความดันสัทธิไม่เท่ากัน จะได้ค่าความหนาแน่นพลังงานที่เพิ่มขึ้นสูงสุดถึง 9.2% เมื่อใช้ค่าสัดส่วนการแบ่งเซลล์ (split ratio) ที่เหมาะสมคือ ชั้นที่หนึ่งเท่ากับ 0.55 และชั้นที่สองเท่ากับ 0.45 นอกจากนี้ยังพบว่า การเพิ่มจำนวนการแบ่งช่วงของการดำเนินงานแบบความดันสัทธิไม่เท่ากันของเซลล์เชื้อเพลิงจะสามารถเพิ่มสมรรถนะของเซลล์เชื้อเพลิงชนิดออกไซด์ชนิดแข็งได้ แต่เมื่อเพิ่มมากกว่า 3 ช่วงนั้น จะเพิ่มสมรรถนะเพียงเล็กน้อยเท่านั้น สำหรับกรณีที่ใช้เครื่องปฏิกรณ์แบบเชื้อเพลิงผ่านร่วมกับเซลล์เชื้อเพลิงชนิดออกไซด์ชนิดแข็ง (MR-SOFC) ได้ศึกษาวิธีการดำเนินงานของเครื่องปฏิกรณ์แบบเชื้อเพลิงผ่าน 3 รูปแบบ คือ 1) กรณีใช้ความดันสูงเพียงอย่างเดียว (MR-HPC) 2) กรณีใช้ความดันสูญญากาศเพียงอย่างเดียว (MR-V) และ 3) กรณีใช้ความดันสูงควบคู่กับความดันสูญญากาศ (MR-HPC-V) การศึกษาพบว่าความหนาแน่นพลังงานไฟฟ้าจะขึ้นอยู่กับปริมาณของไฮโดรเจนที่สามารถแยกออกมาได้ กล่าวคือ ค่าความหนาแน่นพลังงานไฟฟ้าจะมีค่าสูงขึ้นเมื่อสามารถแยกไฮโดรเจนออกได้มากขึ้น ซึ่งเมื่อเปรียบเทียบกับในเชิงเศรษฐศาสตร์พบว่าระบบเซลล์เชื้อเพลิงร่วมกับเครื่องปฏิกรณ์แบบเชื้อเพลิงจะเหมาะสมกว่าระบบดั้งเดิมเมื่อดำเนินงานที่ค่าประสิทธิภาพทางไฟฟ้าสูง นอกจากนี้ยังพบว่า การใช้กรณีที่ใช้ทั้งความดันสูงควบคู่กับความดันสูญญากาศเป็นวิธีที่เหมาะสมที่สุดในการดำเนินงาน ในส่วนของการศึกษาการเพิ่มหน่วยกำจัดคาร์บอนไดออกไซด์ ที่ทำงานร่วมกับเซลล์เชื้อเพลิงชนิดออกไซด์ชนิดแข็ง ได้พิจารณาแบบที่ติดตั้งหน่วยกำจัดคาร์บอนไดออกไซด์ที่ตำแหน่งต่างๆ ของระบบ คือ 1) ติดตั้งก่อนเข้าเซลล์เชื้อเพลิง 2) ติดตั้งหลังเข้าเซลล์เชื้อเพลิง และ 3) ติดตั้งหลังหน่วยเผา (after burner) พบว่าการติดตั้งก่อนเข้าเซลล์เชื้อเพลิงจะสามารถช่วยเพิ่มสมรรถนะของเซลล์เชื้อเพลิงได้เนื่องจากความเข้มข้นของไฮโดรเจนที่สูงขึ้นในสายป้อนเข้าเซลล์เชื้อเพลิง อย่างไรก็ตาม การติดตั้งที่ตำแหน่งนี้สามารถดำเนินงานได้เมื่อคาร์บอนไดออกไซด์ที่ต้องการแยกนั้นน้อยกว่า 40% จากการศึกษาทางด้านเศรษฐศาสตร์ที่ระดับความต้องการในการแยกคาร์บอนไดออกไซด์ต่างๆ พบว่า ที่การดำเนินงานโดย ที่สัดส่วนการใช้เชื้อเพลิงสูง จะสามารถลดค่าใช้จ่ายได้ และการติดตั้งหน่วยกำจัดคาร์บอนไดออกไซด์ก่อนเข้าเซลล์เชื้อเพลิงชนิดออกไซด์ชนิดแข็งจะคุ้มค่าที่สุด แต่เมื่อต้องการลดปริมาณคาร์บอนไดออกไซด์มากกว่า 40% นั้น ระบบที่มีความเหมาะสมที่สุดคือระบบที่ติดตั้งหลังเข้าเซลล์เชื้อเพลิง

ภาควิชา..... วิศวกรรมเคมี.....

สาขาวิชา..... วิศวกรรมเคมี.....

ปีการศึกษา..... 2550.....

ลายมือชื่อนิสิต..... ศุภวัฒน์ วิวรรักษ์ภทกิจ.....

ลายมือชื่ออาจารย์ที่ปรึกษา.....

4771833921: MAJOR CHEMICAL ENGINEERING

KEYWORDS : SOLID OXIDE FUEL CELL (SOFC)/ NON-UNIFORM POTENTIAL OPERATION (NUP)/ Pd-MEMBRANE REACTOR (Pd-MR)/ CaO-CO₂ ACCEPTOR

SUPAWAT VIVANPATARAKIJ : PERFORMANCE IMPROVEMENT OF SOLID OXIDE FUEL CELL SYSTEM FED BY METHANE. THESIS ADVISOR: ASSOCIATE PROFESSOR SUTTICHA ASSABUMRUNGRAT, Ph.D., 104 pp.

The research focuses on the improvement of methane-fuelled solid oxide fuel cell system. Three improvements of the system were considered: 1) Operating under a non-uniform potential operation (SOFC-NUP), 2) Implementing a membrane reactor to the SOFC system (SOFC-MR) and 3) Integrating a CaO-CO₂ acceptor with the SOFC system (SOFC-CaO). For SOFC-NUP, the optimum split ratios of $S_{p,1} = 0.55$ and $S_{p,2} = 0.45$ was found to improve power density as high as 9.2%. In addition, the increase in the number of separated section (n) of the cell could increase the achieved maximum power density but less pronounced after $n > 3$. For SOFC-MR, an SOFC system integrated with a palladium membrane reactor operating at different modes; i.e., high pressure compressor (MR-HPC), vacuum pump (MR-V) and combined high pressure compressor and vacuum pump (MR-HPC-V) was considered. The power density of the SOFC was improved, depending on the increasing hydrogen recovery (ξ). At high electrical efficiency, the SOFC-MR system became more attractive than the conventional system. It was found that the MR-HPC-V was the best operation mode among MR-SOFC systems. For the CaO-CO₂ acceptor SOFC systems, the CO₂ capture efficiency (E_c) depends on fresh feed CaO (F_0), recycled CaO (F_R) and amount of CO₂ fed through. The CaO-CO₂ SOFC systems (i.e. CaO-After-Burner, CaO-After-SOFC and CaO-Before-SOFC) were compared with the conventional SOFC. Only CaO-Before-SOFC can improve SOFC performance which depends on both CO₂ capture efficiency (E_c) and fuel utilization (U_f). The CaO-SOFC system can operate at lower cost than the conventional SOFC. The total added cost/reduced CO₂ (\$/mol⁻¹) are in the sequence of the CaO-After-Burner > CaO-After-SOFC > CaO-Before-SOFC. Unfortunately, CaO-Before-SOFC can not reduce CO₂ more than 40%. When the CO₂ reduction was required more than 40%, the CaO-After-SOFC was a suitable choice for the SOFC-CaO system.

Department Chemical Engineering....
 Field of Study .Chemical Engineering...
 Academic year2007.....

Student's signature*Supawat Vivonpatarakij*.....
 Advisor's signature*Suttichai Assabumrungrat*.....

ACKNOWLEDGEMENTS

The author would like to express his highest gratitude to Associate Professor Suttichai Assabumrungrat, advisor, many good advices throughout this research study. In addition, the authors wish to thank Associate Professor ML. Supakanok Thongyai, as the chairman, Assistant Professor Navadol Laosiripojana, Dr. Akawat Sirisuk and Dr. Amornchai Arpornwichanop as the members of the thesis committee.

Many thanks for the financial supports from The Thailand Research Fund (TRF) throughout the doctoral course.

Most of all, the author would like to express his highest gratitude to his parents, sister and brother. Their unyielding support and generous love not only made this work possible but worth while doing the first place.

Finally, grateful thanks to members in Center of Excellence on Catalysis and Catalytic Reaction Engineering, Department of Chemical Engineering, Chulalongkorn University who have assisted him over the years of his study.

สถาบันวิทยบริการ
จุฬาลงกรณ์มหาวิทยาลัย

CONTENTS

	page
ABSTRACT (IN THAI).....	iv
ABSTRACT (IN ENGLISH).....	v
ACKNOWLEDGEMENTS.....	vi
CONTENTS.....	vii
LIST OF TABLES.....	x
LIST OF FIGURES.....	xi
NOMENCLATURE.....	xiv
CHAPTERS	
I INTRODUCTION.....	1
II THEORY.....	5
2.1 Methane Steam Reforming.....	5
2.2 Fuel Cell Description.....	5
2.1.1 Basic Principle.....	5
2.1.2 Type of Fuel Cell.....	6
2.1.2.1 Alkaline Fuel Cell (AFC).....	6
2.1.2.2 Proton Exchange Membrane Fuel Cell (PEMFC).....	7
2.1.2.3 Phosphoric Acid Fuel Cell (PAFC).....	7
2.1.2.4 Molten Carbonate Fuel Cell (MCFC)....	7
2.1.2.5 Solid Oxide Fuel Cell (SOFC).....	8
2.3 Solid Oxide Fuel Cell (SOFC).....	10
2.4 Fuel Cell Performance.....	11
2.4.1 Ohmic Overpotential (η_{Ohm}).....	12
2.4.2 Activation Overpotential (η_{Act}).....	12
2.4.3 Concentration Overpotential (η_{Conc}).....	12
2.5 Palladium Membrane.....	13
2.5.1 Mechanism of Hydrogen Permeation Through Palladium Membrane.....	13
2.6 CaO-CO ₂ Acceptors.....	15

	page
CHAPTERS	
III LITERATURE REVIEWS.....	17
3.1 Methane steam reforming.....	17
3.2 Solid Oxide Fuel Cell (SOFC).....	19
3.3 Non-Uniform Potential Operation (NUP).....	21
3.4 Pd Membrane.....	22
3.5 CaO-CO ₂ Acceptor.....	24
IV MODELING.....	26
4.1 Calculation of the Converted Mole of Methane Steam Reforming.....	26
4.1.1 Thermodynamic Equilibrium Method.....	26
4.1.2 Kinetic Model.....	28
4.2 Calculation of the SOFC Performance.....	29
4.2.1 Electromotive Force (E_0).....	30
4.2.2 Overpotentials.....	30
4.2.3 SOFC Performances.....	33
4.3 Pd Membrane Reactor.....	34
4.4 CaO-CO ₂ Acceptor.....	35
4.5 Economic Analysis.....	38
4.6 Simulation of SOFC System by Using <i>MATLAB</i> TM	38
V IMPROVEMENT OF SOLID OXIDE FUEL CELL PERFORMANCE BY USING NON- UNIFORMPOTENTIAL OPERATION.....	43
5.1 Results and Discussion.....	43
5.2 Conclusions.....	50
VI PERFORMANCE IMPROVEMENT OF SOLID OXIDE FUEL CELL SYSTEM USING PALLADIUM MEMBRANE REACTOR WITH DIFFERENT OPERATION MODES.....	51
6.1 Results and Discussion.....	51
6.2 Conclusions.....	62

	page
CHAPTERS	
VII SOLID OXIDE FUEL CELL	63
SYSTEMS INCORPORATED WITH SEQUENTIAL CaO- CO ₂ CAPTURE.....	
7.1 Results and Discussion.....	63
7.2 Conclusions.....	79
VIII CONCLUSION AND RECOMMENDATION.....	80
8.1 Conclusion of Improvement of Solid Oxide Fuel Cell Performance by Using Non-Uniform Potential Operation.....	80
8.2 Conclusion of Performance Improvement of Solid Oxide Fuel Cell System Using Palladium Membrane Reactor with Different Operation Modes.....	80
8.3 Conclusion of Solid Oxide Fuel Cell Systems Incorporated with Sequential CaO-CO ₂ Capture.....	81
8.4 Recommendation and future work.....	81
REFERENCES.....	86
APPENDICES.....	93
Appendix A. THERMODYNAMIC DATA OF SELECTED COMPONENT.....	94
Appendix B. DETERMINING GIBBS ENERGY.....	95
B.1 Determining Gibbs Energy (<i>G</i>).....	95
B.2. Determining the Equilibrium Constant (<i>K</i>).....	95
Appendix C. NEWTON'S METHOD.....	97
Appendix D. POWER CALCULATION OF COMPRESSOR BY USING <i>Aspen Plus</i> TM SIMULATOR.....	99
Appendix E. LIST OF PUBLICATIONS.....	102
VITA.....	104

LIST OF TABLES

	page
Table 2.1 The description of fuel cell types.....	10
Table 2.2 Regressed parameter for the diffusion of hydrogen through Pd membrane.....	15
Table 4.1 Kinetic parameters for methane steam reforming (Xu and Froment, 1989).....	28
Table 4.2 Resistivity and thickness of cell component.....	31
Table 4.3 Summary of activation polarization parameters (Hernandez-Pacheco et al., 2004).....	32
Table 5.1 Comparison of power density between SOFCs with different number of section and section splits.....	48
Table 6.1 Economic analysis of the SOFC systems with different operation modes.....	60
Table 7.1 Standard condition.....	69
Table 7.2 Economic analysis of CaO-SOFC system and conventional SOFC system (At $U_f=80\%$).....	72
Table 7.3 Economic analysis of CaO-SOFC system and conventional SOFC system (At $U_f=90\%$).....	73
Table A.1 Heat capacities of selected component (C_p)	94
Table A.2 Heat of formation (H_f), and entropy (S^0) of selected component.....	94

LIST OF FIGURES

	page
Fig. 2.1 Diagram of basic-fuel cell.....	6
Fig. 2.2 Schemes of all fuel cell types: a.) Alkaline Fuel Cell (AFC), b.) Proton Exchange Membrane (PEM), c.) Phosphoric Acid Fuel Cell (PAFC), d.) Molten Carbonate Fuel Cell (MCFC), e.) Solid Oxide Fuel Cell (SOFC).....	9
Fig. 2.3 Mechanism of hydrogen diffusion in palladium membrane.....	14
Fig. 4.1 Schematic diagram of a CaO-CO ₂ acceptor system.....	36
Fig. 4.2 Flowchart of non-uniform potential operation of solid oxide fuel cell.....	40
Fig. 4.3 Flowchart of SOFC incorporated with Pd-membrane reactor.....	41
Fig. 4.4 Flowchart of SOFC incorporated with CaO-CO ₂ acceptor.....	42
Fig. 5.1 Schematic diagram of SOFC-NUP.....	44
Fig. 5.2 Performance characteristic curves of typical SOFC-UP (H ₂ O/CH ₄ ratio = 2.2 and $T_{SOFC} = 1173$ K).....	45
Fig. 5.3 Relationship between power density and electrical efficiency of SOFC-UP and SOFC-NUP ($U_f = 80\%$ and $T = 1173$ K; for SOFC-NUP: $n = 2$, $S_{p,1} = 0.5$).....	46
Fig. 5.4 Effect of operating voltages on performance of SOFC-NUP ($n = 2$, $U_f = 80\%$, $T = 1173$ K, $S_{p,1} = 0.5$ and $S_{p,2} = 0.5$).....	47
Fig. 5.5 Effect of section split on power density improvement of SOFC- NUP ($n = 2$, $U_f = 80\%$ and $T = 1173$ K).....	48
Fig. 5.6 Effect of number of stage on power density improvement of SOFC-NUP ($U_f = 80\%$, $T = 1173$ K and $S_{p,k} = 1/n$).....	50
Fig. 6.1 Schematic diagrams of SOFC systems with different operation modes: (a) conventional reformer, (b) MR-HPC, (c) MR-V, (d) MR-HPC-V.	53
Fig. 6.2 Validation of the reformer model with experimental results from the literature (Pfafferodt <i>et al.</i> , 2005) ($P = 1$ atm and H ₂ O:CH ₄ = 3).....	54
Fig. 6.3 Validation of SOFC model with results from the literature (Hernandez-Pacheco <i>et al.</i> , 2005) (Pure H ₂ feed and $U_f = 80\%$)..	54

	page
Fig. 6.4 Improvement of SOFC performance by using Pd membrane reactor ($U_f=80\%$ and $T_{SOFC} = 1073$ K).....	55
Fig. 6.5 Effect of reaction pressure on required Pd membrane area and compressor power ($T = 773$ K, $P_R = 1$ atm and $H_2O:CH_4 = 3$)...	56
Fig. 6.6 Effect of permeation pressure on required Pd membrane area and vacuum pump power ($T_{SOFC} = 773$ K, $P_P = 1$ atm and $H_2O:CH_4 = 3$).....	57
Fig. 6.7 Effect of reaction and permeation pressure on required Pd membrane area and power consumption ($\xi = 90\%$, $T_{SOFC} = 773$ K and $H_2O:CH_4 = 3$).....	58
Fig. 6.8 Economic analysis of different SOFC systems: (a) $\eta = 40.7\%$, (b) $\eta = 45.3\%$ and (c) $\eta = 47.7\%$ ($U_f = 80\%$ and $T = 1073$ K)...	62
Fig. 7.1 Elements composition of conventional SOFC system (at $U_f = 90\%$, $T_{ref}=973$ K and $T_{SOFC}=1073$ K).....	64
Fig. 7.2 a.) Conventional SOFC system, b.) CaO-Before-SOFC, c.) CaO-After-SOFC and d.) CaO-After- burner.....	65
Fig. 7.3 Effect of CaO fresh feed (F_0) and CaO recycle (F_R) on CO_2 capture efficiency (E_c) a.) CaO-Before-SOFC, b.) CaO-After-SOFC and c.) CaO-After-Burner. (At $T_{ref} = 973$ K).....	67
Fig. 7.4 Effect of reformer temperature on produced CO_2 and effect of CO_2 capture efficiency (E_c) on partial pressure of H_2	68
Fig. 7.5 Comparison SOFC performance of CaO-SOFC system with conventional SOFC system at varies CO_2 capture efficiency (E_c) and fuel utilization (U_f) (At $T_{ref} = 973$ K, $T_{SOFC} = 1073$ K).....	70
Fig. 7.6 Performance improvement of CaO-SOFC system (At $V=0.56$ V, $T_{ref} = 973$ K, $T_{SOFC} = 1073$ K).....	71
Fig. 7.7 Minimum total CaO (F_0+F_R) a.)CaO-Before-SOFC, b.) CaO-After-SOFC and c.) CaO-After-Burner.....	75
Fig. 7.8 The required SOFC area a). $U_f = 80\%$ and b). $U_f = 90\%$, (At $T_{SOFC} = 1073$ K, CO_2 capture = 0.424 mol s^{-1}).....	76

	page
Fig. 7.9 The CO ₂ reduction of CaO-SOFC system (CaO-accepter Before-SOFC, After SOFC and After-burnner) from conventional SOFC system (At $T_{ref}= 973$ K, $T_{SOFC}= 1073$ K)...	77
Fig. 7.10 Economics analysis of CaO-After-SOFC and CaO-After-Burner at higher percentage of reduced CO ₂ (75%).....	78
Fig. 8.1 a).non-uniform potential operation of SOFC (NUP-SOFC), b).implementing a membrane reactor to the SOFC system (MR-SOFC) and c).integrating a CaO-CO ₂ acceptor with the SOFC system (CaO-SOFC).....	83
Fig. 8.2 Scheme of the non-uniform potential operation of SOFC (NUP-SOFC) operates with membrane reactor to the SOFC system (MR-SOFC).....	83
Fig. 8.3 Scheme of the non-uniform potential operation of SOFC (NUP-SOFC) operates with a CaO-CO ₂ acceptor with the SOFC system (CaO-SOFC).....	83
Fig. 8.4 a.) SOFC system incorporated with silica membrane reactor, b.) SOFC system incorporated with silica membrane.....	85
Fig. D.1 Schematic diagram of compressor.....	99
Fig. D.2 Inputting parameter at <i>Steam 1(Material)</i>	100
Fig. D.3 Setting compressor parameter at Block B1 (Compr).....	100
Fig. D.4 Calculation results.....	101

NOMEMCLATURE

a_j	Constant in Eq. 4.34	($\Omega \text{ m}$)
A_j	Kinetic parameters in Eq. 4.18	(-)
A_{Pd}	Pd membrane area	(m^2)
A_{SOFC}	SOFC area	(m^2)
b	Constant in Eq. 4.51	(-)
b_j	Constant in Eq. 4.34	(K)
B_j	Kinetic parameters in Eq. 4.19	(-)
d_p	Partial diameter	(m)
E	Open circuit voltage (OCV)	(V)
E_0	Reversible potential	(V)
	Activation energy for diffusion through	
E_D	membrane	(kJ mol^{-1})
$E_{A,pol}$	Activation polarization energy in Eq. 4.35-4.36	(kJ mol^{-1})
f	Constant in Eq. 4.51	(-)
f_g	Gas friction factor	(-)
f_s	Solid friction factor -	(-)
F	Faraday constant (96485.34)	(C mol^{-1})
F_0	Fresh CaO	(mol s^{-1})
F_{CO_2}	Molar flow rate of CO_2	(mol s^{-1})
F_R	Recycle CaO	(mol s^{-1})
	Enthalpy of formation of kinetic parameters in	
H_i	Eq. 9.	(kJ.mol^{-1})
HP	Parameter in Eq. 4.63	(HP)
i_0	Exchange current density	(A m^{-2})
k_i	Adsorption parameters	(-)
K_i	Equilibrium constant	(-)
LHV	Lower heating value of methane feed	(W)
m	Constant polarization parameters in Eq. 4.35-4.36	(-)
n	Number of separated section	(-)
n_e	Electron transfer	(-)

N_{H_2}	Hydrogen flux	(mol s ⁻¹ m ⁻²)
p_i	Partial pressure	(atm)
P	Power density	(W cm ⁻²)
P_{com}, P_{vac}	Power requirement of compressor, vacuum pump	(kW)
Q_0	Pre-exponential constant for membrane permeability (4.40x10 ⁻⁷)	(mol m ⁻¹ s ⁻¹ Pa ^{-0.5})
Q_{MR}	Heat of membrane reactor	(kW)
Q_R	Heat of reformer	(kW)
r	Activation polarization parameters in Eq. (xx-xx)	(A m ⁻²)
r_{ext}	External radius tube reactor	(m)
r_i	Rate of reaction	(-)
r_{int}	Internal radius tube reactor	(m)
R	Universal gas constant (8.31447x10 ⁻³)	(kJ mol ⁻¹ K ⁻¹)
$S_{p,i}$	Section split	(-)
T_j	Absolute temperature	(K)
u_f	Fluid velocity	(m s ⁻¹)
u_p	Partial velocity	(m s ⁻¹)
U_f	Fuel utilization	(%)
v	Gas velocity	(m s ⁻¹)
v_t	Gas terminal velocity	(m s ⁻¹)
V	Operating voltage	(V)
W_{elec}	Electrical work	(W)
\bar{x}_c	Carbonation conversion	(%)
x_i	Converted moles associated to the reactions (Eq. 4.1-4.2)	(mol)
X	Parameter in Eq. 4.64	(lbs.H ₂ /h/suction Torr)
y_i^I	Mole fraction of component i in bulk phase	(-)
z_{Pd}	Length of Pd membrane reactor	(m)

Greeks letters

η	Electrical efficiency	(%)
η_i	Overpotential	($\Omega \text{ m}^2$)
ε_{elec}	Electrical efficiency	(%)
ε	Bed void	(-)
δ	Thickness	(m)
ρ	Density	(kg m^{-3})
ρ_i	Specific ohmic resistance	($\Omega \text{ m}$)
φ	Potential	(V)
ξ	Hydrogen recovery	(%)

Subscripts

<i>A</i>	Anode
<i>Act</i>	Activation
<i>C</i>	Cathode
<i>Conc</i>	Concentration
<i>k</i>	Section number
<i>Ohm</i>	Ohmic
<i>Ref</i>	Reformer
<i>SOFC</i>	Solid oxide fuel cell

สถาบันวิทยบริการ
จุฬาลงกรณ์มหาวิทยาลัย

CHAPTER I

INTRODUCTION

Fuel cells are electrochemical devices, which directly convert chemical energy to electrical energy. Solid oxide fuel cell (SOFC), one of the most promising fuel cell nowadays, can use various types of fuel such as hydrogen (H_2), methane (CH_4), methanol (CH_3OH) and ethanol (C_2H_5OH) due to its high temperature operation. The fuel can be internally reformed to hydrogen within an SOFC stack (Achenbach, 1994; Aguiar *et al.*, 2002; Yamada *et al.*, 2002). Among various fuels, methane is a favorable fuel choice because it is a major component of natural gas. In order to convert methane to hydrogen, a number of reactions; i.e. steam reforming, dry reforming, partial oxidation and auto-thermal reforming have been proposed. However, the steam reforming is the most popular, because it can produce higher amount of hydrogen and excess heat co-generated with the electrochemical reaction can be utilized for the endothermic steam reforming reaction, resulting in an increase of overall efficiency.

Many researches on fuel cell technology have been carried out in various approaches with a main goal to improve performance of fuel cells and their systems. Numerous researchers have focused on development of cell components with superior characteristics (Yoon *et al.*, 2004; Kim *et al.*, 2005; and Simner *et al.*, 2003). Although most current SOFC technology is based on the use of oxygen ion-conducting materials as an electrolyte, it was theoretically demonstrated that using a proton-conducting electrolyte could offer higher SOFC performance compared to the conventional oxygen ion-conducting electrolyte (Assabumrungrat *et al.*, 2005). Several gas turbine cycles such as steam injected gas turbine cycle, gas turbine/steam turbine combined cycle, and humid air turbine cycle have been integrated with SOFC to further utilize waste heat from the SOFC system (Kuchonthara *et al.*, 2003). An operation with re-circulating anodic off-gas was proposed for a polymer electrolyte membrane fuel cell (PEMFC) system equipped with a fuel processor. Under this operation, a significant efficiency increase for the fuel processor and the gross efficiency of the combined system of 30% were reported (Heinzel *et al.*, 2005). The

performance improvement of PEMFC from the increased operating pressure was investigated taking into account the power loss due to air compression at various operating current densities (Kazim, 2005).

In this study, we have attempted to improve the SOFC performance by using various strategies; i.e., a non-uniform potential operation, replacing a conventional reformer with a palladium membrane reactor for increasing hydrogen concentration in the feed and integration of SOFC with a CO₂ acceptor for reducing CO₂ emission. In most fuel cell operation, the cell is operated in a uniform potential condition. It was demonstrated that multistage operation of proton exchange membrane fuel cell (PEMFC) can improve power density by 6.5% compared with conventional operation (Sen *et al.*, 2005). The concept was also applied to molten carbonate fuel cell (MCFC). Au *et al.* (2003) reported that the two stages operation with two directions of feed on MCFC can increase efficiency by 0.3-0.6%. It is still interesting to apply this non-uniform potential operation concept to SOFC. A suitable operating condition should be carefully selected to achieve a superior obtained performances.

Regarding the concept of performance improvement by increasing hydrogen concentration in a feed, it is known that the hydrogen concentration influences the electromotive force of the cell and, consequently, the performance characteristic curves. The use of additional units to increase hydrogen concentration can increase the SOFC performance. The palladium membrane reactor has been effectively applied to many hydrogen-producing reactions (Kikuchi *et al.*, 2000). By selective removal of hydrogen from the reaction zone, the reaction can proceed at higher extent and pure hydrogen can be obtained. It was previously demonstrated that although the use of palladium membrane reactor in the SOFC system could improve the cell performance, the conventional operation of the palladium membrane using a high pressure compressor required high energy consumption for operating the compressor, and, hence, made the overall system economical (Paper 8). In this study, we will focus on the uses of a palladium membrane reactor with different operation modes (i.e., high pressure compressor (MR-HPC), vacuum pump (MR-V) and combined high pressure compressor and vacuum pump (MR-HPC-V)), aiming to find a suitable operation mode which makes the overall system more economical.

Nowadays, the global warming is big ours problem. Carbon dioxide is major cause of this trouble. So, the technology selection should be low or zero CO₂ emission. A solid oxide fuel cell (SOFC) is a promising electrical power generator compared to conventional systems as it offers a wide range of applications, low emissions and high system efficiency. Although, SOFC can use hydrogen for produce electrical energy, zero CO₂ emission. In general, hydro-carbon compounds were supplied for SOFC, such as methane, methanol and ethanol etc. Methane is a promising fuel as it is a rich element in natural gas and the methane steam reforming technology is relatively well established. Therefore, it is the fuel of interest in this study. An alternative way to increase hydrogen partial pressure in the SOFC feed can be carried out by using a CO₂-acceptor unit containing CaO as an adsorbent. It was found that the added CaO in commercial methane steam reformer catalyst can produce hydrogen as pure as 95% in laboratory-scale experiment (Balasubramanian *et al.*, 1999). The CO₂-capture capacity of CaO-carbonation was reported to be larger than hydrotalcite-base sorbent (Ding and Alpay, 2000; Xiu *et al.*, 2002). However, when the CaO-carbonation becomes CaCO₃, the activity of CaO-carbonation is decreased. Some researchers have proposed methods to recycle CaO with integrated calcinations unit. Abanades (2002) showed that after 14 cycles of carbonation-calcination, the conversion of CaO-carbonation decreased to 20%. By integrating the CO₂-acceptor unit before the SOFC, the hydrogen partial pressure in the feed becomes higher, resulting in an improved cell performance. Apart from this benefit, the removed CO₂ offers a possibility for CO₂ sequestration following the environmental concern.

Objective

The main objective of this work is to investigate various alternatives for improving performance of SOFC system. The particular scope of work in this study can be summarized as follows:

1. Compare performances of SOFC fed by methane between the non-uniform cell potential operation and the conventional uniform potential operation.

2. Compare performances of SOFC fed by methane between conventional SOFC and SOFC integrated with a palladium membrane reactor.
3. Compare performances of SOFC fed by methane between conventional SOFC and SOFC system integrated with a CaO-CO₂ acceptor.



สถาบันวิทยบริการ
จุฬาลงกรณ์มหาวิทยาลัย

CHAPTER II

THEORY

2.1 Methane Steam Reforming

Methane steam reforming is a conventional method of hydrogen production. The major reactions taking place in the reactor are methane steam reforming (Eq. 2.1), water gas shift reaction (Eq. 2.2) and carbon dioxide methanation (Eq. 2.3).



In order to avoid carbon formation problem, the feed containing a H₂O:CH₄ molar ratio of 2.5 (or high) is usually employed [Renner *et al.*, 1985].

2.2 Fuel Cell Description

2.2.1 Basic Principle

Fuel cells are electrochemical devices that convert the chemical energy of a reaction directly into electrical energy. The basic physical structure or building block of a fuel cell consists of an electrolyte layer in contact with a porous anode and cathode on either side. Fuel cells and batteries are similar in that both of them can convert the chemical reactance with chemical reaction into electricity, but the batteries, being used up, must be recharged. Fuel cells can be operated as long as with feed continues fuel and oxidant. Fuel cells are based on the simple combustion (Eq. 2.4).



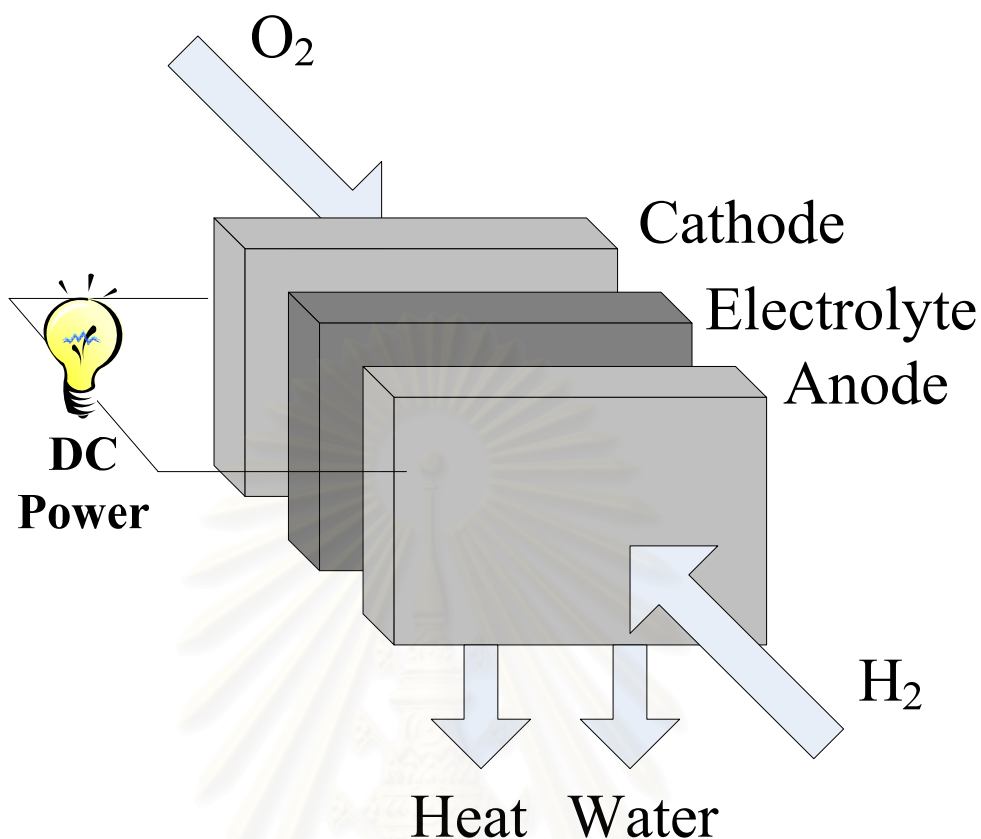


Fig. 2.1 Diagram of basic-fuel cell.

2.1.2 Type of Fuel Cell

The fuel cells are composed of two electrodes (anode and cathode) and an electrolyte. They can be classified according to the types of electrolyte as follows. Figure 2.2 shows schematic diagrams of different fuel cell types.

2.1.2.1 Alkaline Fuel Cell (AFC)

A concentrated solution of potassium hydroxide (35-50%) is used as an electrolyte for AFC. The operating temperature is about 393 K. The fuel supply is limited to pure hydrogen (purity > 99.99 %), and air must be always purified before use because CO is a poison and carbon dioxide (CO_2) can react with hydroxyl ions (OH^-) to form carbonate ions (CO_3^{2-}), thus damaging the electrolyte. At the anode,

hydrogen is oxidized by hydroxyl ions (OH^-), generating water (H_2O) and releasing two electrons. The electrons flow through an external circuit and return to the cathode where hydroxyl ions (OH^-) are generated.

2.1.2.2 Proton Exchange Membrane Fuel Cell (PEMFC)

The electrolyte is an ion exchange polymer membrane and porous carbon electrodes containing a platinum catalyst. The electrolyte membrane must be saturated with water to conduct protons from the anode side to the cathode side. The electrolyte membrane must be saturated with water to conduct protons from the anode side to the cathode side; hence, corrosion troubles are minimal. The Pt catalyst is also highly sensitive to carbon monoxide (CO) poisoning, making it necessary to use an additional reactor to reduce CO in the fuel gas when hydrogen is derived from an alcohol or hydrocarbon fuel. Developers are currently exploring platinum/ruthenium (Pt/Ru) catalysts that are more resistive to CO.

2.1.2.3 Phosphoric Acid Fuel Cell (PAFC)

Phosphoric Acid Fuel Cell (PAFC) was the first commercial fuel cell. PAFC uses concentrated 100% phosphoric acid, H_3PO_4 , as its electrolyte. Anode and cathode are made of graphite with a platinum catalyst, and operating temperature is 423-493 K. PAFC is more tolerant to impurities in the fuel than PEM. The degree of tolerance is dependent on temperature; the CO tolerance increased which increasing temperature. The fuel has to be reformed external of the cell. PAFC is less powerful than other fuel cells, given the same weight and volume. As a result, these fuel cells are typically large and heavy, suitable for stationary.

2.1.2.4 Molten Carbonate Fuel Cell (MCFC)

Molten carbonate fuel cell (MCFC) has an electrolyte made of a molten carbonate salt. In MCFC, it is necessary to supply both oxygen and carbon dioxide to the cathode to produce carbonate ions (CO_3^{2-}) which are transported within the electrolyte. Unlike other fuel cells, MCFC does not require an external reformer to convert more energy-dense fuels to hydrogen. Due to the high temperatures at which

they operate, these fuels are converted to hydrogen within the fuel cell itself by a process called “internal reforming”. If natural gas is used, carbon dioxide is also produced but at the anode side. It can be separated from the anode exhaust and fed to the cathode. The anode is porous nickel while the cathode consists of nickel oxide (NiO) and lithium oxide (Li₂O) because they operate at high temperatures of 923 K or above, noble-metals are not used as catalysts.

2.1.2.5 Solid Oxide Fuel Cell (SOFC)

Solid oxide fuel cell is operated in the region of high temperature and usually uses Y₂O₃-stabilized ZrO₂ as an electrolyte. SOFC can be operated with an internal reformer within the fuel cell due to its high temperature operation (973-1273 K). Typically, Ni-ZrO₂ cerment and Sr-doped LaMnO₃ are used as the anode and cathode catalyst, respectively.



สถาบันวิทยบริการ
จุฬาลงกรณ์มหาวิทยาลัย

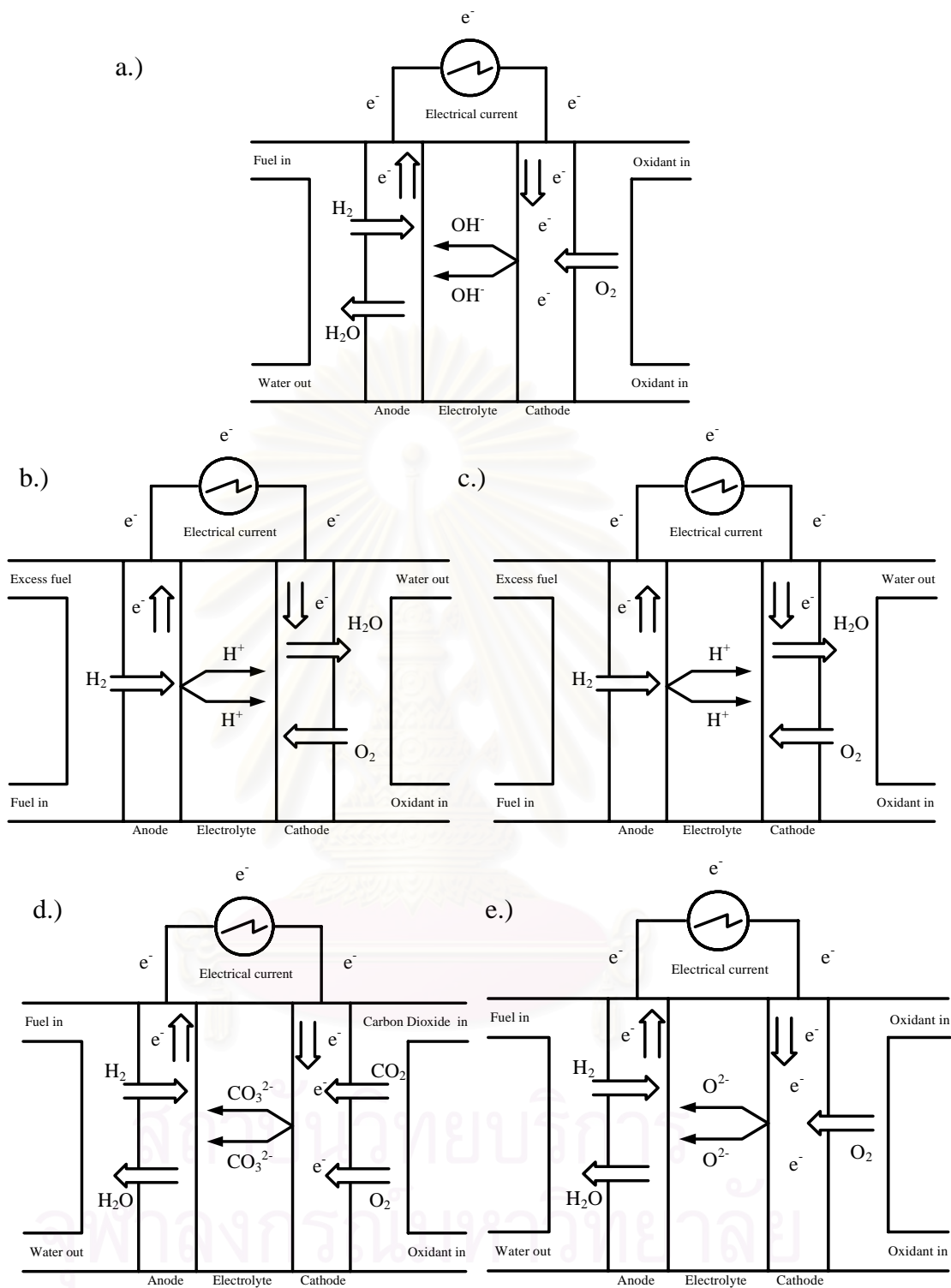


Fig. 2.2 Schemes of all fuel cell types: a.) Alkaline Fuel Cell (AFC), b.) Proton Exchange Membrane (PEM), c.) Phosphoric Acid Fuel Cell (PAFC), d.) Molten Carbonate Fuel Cell (MCFC), e.) Solid Oxide Fuel Cell (SOFC)

The description of fuel cell types are shown in Table 2.1 (Rayment *et al.*, 2003):

Table 2.1 The description of fuel cell types

	AFC	PAFC	MCFC	PEMFC	SOFC
Electrolyte	Mobilized or Immobilized Potassium Hydroxide	Immobilized Liquid Phosphoric Acid	Immobilized Liquid Molten Carbonate	Ion Exchange membrane	Ceramic
Operating Temperature	338-493 K	473 K	923 K	353 K	1073-1273 K
Catalyst	Pt	Pt	Ni	Pt	Perovskite
Fuels	H ₂	H ₂	CO, H ₂	H ₂	CO, H ₂ , CH ₄
Poisons	CO, CH ₄ , CO ₂ , H ₂ O, S*	CO, S*	S*	CO, S*	S*
Diluents	-	CO ₂ , H ₂ O, CH ₄	CO ₂ , H ₂ O	CO ₂ , H ₂ O, CH ₄	CO ₂ , H ₂ O

S* = Sulfur compound for example H₂S and COS

From different operating temperature and supplied electric power, the fuel cell applications are selected by type of fuel cell. The main of applications are as stationary electric power plants, as motive power for vehicles and as batteries for portable electric devices.

2.3 Solid Oxide Fuel Cell (SOFC)

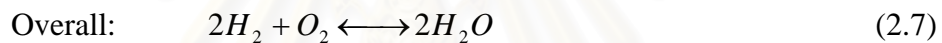
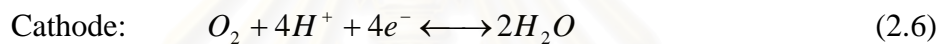
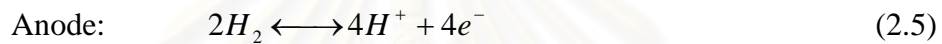
Solid oxide fuel cell is a high temperature fuel cell. It offers several advantages as summarized below.

- SOFC offers the highest electrical efficiency among various fuel cells.
- The solid electrolyte eliminates problems of electrolyte containment and migration and allows for design, that utilizes the electrolyte as part of the structural members of the cells.
- The operation of SOFC can use at high temperature, that allows for internal reforming of gases fuel within the cells, promotes rapid kinetics with non-precious materials and produces high quality heat for energy conversion or other uses.

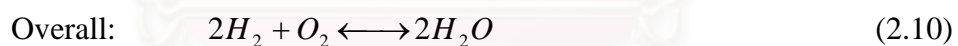
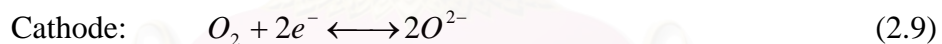
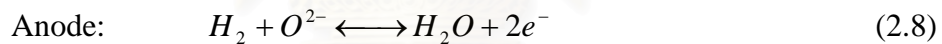
- The SOFC can appear in small-scale stationary application.
- The SOFC is flexible to use many types of fuel, such as methane, methanol, ethanol, or gasoline. This can be achieved, for example, by partial oxidation of methane to syngas (Ishihara., 1999) or selective oxidation of methane to ethane, ethylene and carbon monoxide (Tagawa *et al.*, 1999)

The SOFC types can be characterized by types of mobile ion transporting through an electrolyte. There are two types of SOFC; i.e., SOFC with proton conducting electrolyte (SOFC-H⁺) and SOFC with oxygen ion conducting electrolyte (SOFC-O²⁻).

The electrochemical reactions in the SOFC-H⁺



The electrochemical reactions in the SOFC-O²⁻



2.4 Fuel Cell Performance

The electrochemical reaction is occurred by the reaction between fuel and oxidizing agent. The electromotive force (*EMF* or E^0) is theoretical cell voltage. The *EMF* is calculated from:

$$E^0 = \frac{\Delta G}{nF} \quad (2.11)$$

where ΔG is Gibb's free energy, n number of electrons passing around the circuit per mole of fuel and F Faraday's constant which is equal to 96485.34 C/mol.

The actual cell potential (V) is always less than the theoretical voltage (E^0), because of the presence of several overpotentials.

$$V = E^0 - \eta_{act} - \eta_{ohm} - \eta_{conc} \quad (2.12)$$

2.4.1 Ohmic Overpotential (η_{Ohm})

Ohmic overpotentials are caused by resistance to conduction of ions, (through the electrolyte) electrons, (through the electrode) current, and from contact resistance between cell components. This voltage drop is important in all types of cells and is essentially linear and proportional to current density (i). The ohmic overpotential can be calculated by Ohm's law.

$$\eta_{Ohm} = iR \quad (2.13)$$

The resistance of the materials can be calculated from its resistivity which is the function of temperature (Bessette II *et al.*, 1995).

$$R = \frac{\rho \delta}{A} \quad (2.14)$$

2.4.2 Activation Overpotential (η_{Act})

Activation overpotential is controlled by the electrode kinetics at the electrode surface. This polarization is directly related to the activation barrier that must be overcome by the reacting species in order for the electrochemical reaction to occur. The electrode reaction rate at high temperatures is fast, leading to low activation polarization as commonly observed in SOFC.

2.4.3 Concentration Overpotential (η_{Conc})

Concentration overpotential occurs when the fuel is consumed at the electrode–electrolyte interface, and the gas concentration decreases at the reaction sites. Concentration polarization becomes an important loss at high current densities and small fuel concentrations.

2.5 Palladium Membrane

Palladium was first identified as a highly hydrogen permeable material in the 19th century. Palladium purifiers provide <1 ppb purity with any inlet gas quality. Impurities removed include O₂, H₂O, CO, CO₂, N₂ and all hydrocarbons including methane (CH₄). Normal life expectancy of a palladium membrane purifier is about 5 years and no routine maintenance required.

2.5.1 Mechanism of Hydrogen Permeation Through Palladium Membrane

The mechanism of hydrogen diffusion (Fig. 2.3) involves a series of steps: (1) adsorption, (2) dissociation, (3) ionization, (4) diffusion, (5) recombination and (6) desorption. Several molecules of hydrogen and nitrogen atoms are on the metal surface. Within the metal, hydrogen loses its electron to the palladium structure and diffuses through the membrane as an ion (or proton). At the exit surface the reverse process occurs. Only hydrogen appears to possess the ability to diffuse through palladium or palladium alloys. Assuming no pinholes or micro-cracks, the hydrogen issuing from the low-pressure side of a membrane may be looked upon as a standard of absolute purity. Attempts to detect the presence of impurities show only traces in the parts-per-billion range.

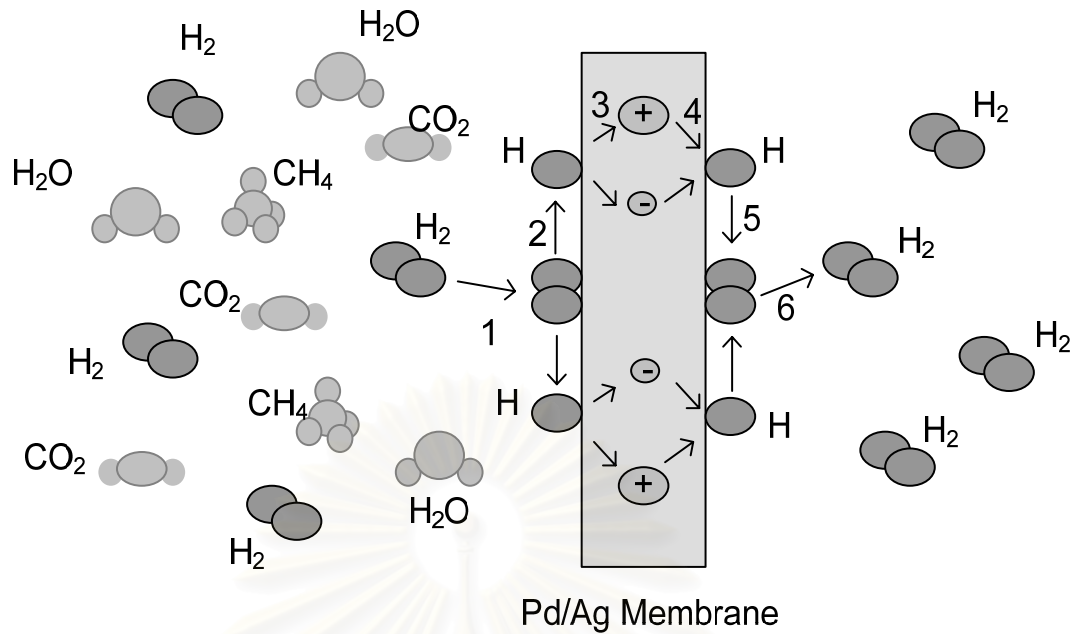


Fig. 2.3 Mechanism of hydrogen diffusion in palladium membrane

The ability of hydrogen transfer through palladium membrane is typically quantified in term of permeability, performance of flux. The *flux* of hydrogen through palladium membrane is the product of the diffusion coefficient and concentration gradient, with the flux of hydrogen atoms being twice that of hydrogen molecular:

$$N_H = 2N_{H_2} = -D_M \frac{\Delta n_H}{\delta} \quad (2.15)$$

In assumption, the surface reaction is considered to be very fast and dissolved hydrogen atoms at the surface of the palladium are in equilibrium with the hydrogen gas on either side of membrane. The concentration of hydrogen atoms in the palladium can be related to the hydrogen partial pressure via the *Sievert's equation*. The exponent of 0.5 reflects the dissociation of the gaseous hydrogen molecule into two hydrogen atoms that diffuse into the metal, where an ideal solution of hydrogen atoms in palladium is formed:

$$n_H = K_s p_{H_2}^{0.5} \quad (2.16)$$

The hydrogen permeability of palladium corresponds to the constant in Eq. 2.15 and 2.16. It is one half of product of the diffusion coefficient and the *Sieverts* constant.

$$k = \frac{1}{2} D_M K_s \quad (2.17)$$

The temperature dependence of permeability values was calculated with an *Arrhenius* –type relation Eq. 2.18

$$k = Q_0 \exp\left(-\frac{E}{RT}\right) \quad (2.18)$$

Therefore, the hydrogen flux is inversely proportional to the membrane thickness and directly proportional to the product of the hydrogen permeability and hydrogen partial pressure gradient across the membrane. Combining these expressions:

$$N_{H_2} = \frac{Q_0}{\delta} \exp\left(-\frac{E_D}{RT}\right) (P_{H_2,r}^{0.5} - P_{H_2,p}^{0.5}) \quad (2.19)$$

where: N_{H_2} is molar flux of hydrogen

Q_0 is pre-exponential constant for membrane permeability

E_D is activation energy for diffusion through membrane

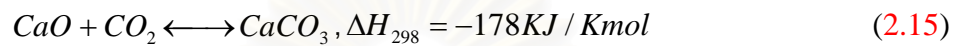
δ is thickness of membrane

Table 2.2 Regressed parameter for the diffusion of hydrogen through Pd membrane

	$Q_0(\text{mol m}^{-1} \text{s}^{-1} \text{Pa}^{-0.5})$	$E_D (\text{kJ mol}^{-1})$	Thickness (μm)	Source
Palladium	4.40×10^{-7}	15.7	10	Holleck (1970)

2.6 CaO-CO₂ Acceptors

The methane steam reforming reaction is a main reaction to produce hydrogen. Carbon dioxide is a key product when attempting to shift the reaction to generate high amount of hydrogen. CaO can be used to capture CO₂ by the carbonation reaction (Eq. 2.15).



The methane steam reforming reaction collaborated with carbonation reaction (Eq. 2.15) become (Eq. 2.16).



The overall reaction (Eq. 2.15) can produce hydrogen more than 95% (Balasubramanian *et al.*, 1999).

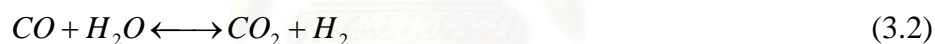
CHAPTER III

LITERATURE REVIEWS

In this chapter, the literature of SOFC system is reviewed. The chapter consists of the reviews of methane steam reforming, SOFC, Non-uniform potential operation, Pd-membrane and CO₂ acceptor.

3.1 Methane Steam Reforming

Steam reforming is a mature technology, practiced industrially on a large scale for hydrogen production. Methane steam reforming (Eq. 3.1) and water gas shift reaction (WGSR) (Eq. 3.2) are carried out over supported nickel catalyst, normally above 500°C (Dicks, 1996).



The coke formation destroys the catalyst structure and decreases its activity. Therefore, the industrial methane steam reaction is usually run under a steam to carbon ratio of 1.4 or higher, to maintain the catalyst activity. Several works concern the model descriptions of equilibrium conversion (Hufton *et al.*, 1999) and (Ding *et al.*, 2000). Al-Qahtani (1997) proposed that effect of ageing on the steam reforming catalyst performance reduced the porosity and the nickel content. These reductions deactivated the catalyst which was indicated by the increment in the operating temperatures, pressure drop and equilibrium approach.

Several works determined the kinetics of the reaction. It is very fast at high temperatures between 1173 and 1273 K and may be affected by mass transfer phenomena (Achenbach *et al.*, 1994). Levent *et al.* (1998) proposed that at high temperature, the volume of the catalyst particle is not limiting in methane reforming,

but an increase in exterior surface area of the catalyst will be effective in increasing the rate of reforming.

Simpson A.P. and Lutz A.E. (2007) studied in the methane steam reforming, evaluated by using exergy analysis. The MSR model used the equilibrium model modified with heat integration. They found that the efficiency increased with excess steam ($CH_4:H_2O = 1:3.2$) and decreased with rising operating pressure (>10 atm). Research and development of the MSR system should be focused on reducing exergy destruction within the reformer and heat exchangers, as well as utilizing the exhaust stream exergy.

Methane steam reforming was investigated on a fluidized bed membrane reactor with in situ or ex situ hydrogen and/or CO_2 removal for production of pure hydrogen by using both of chemical equilibrium and kinetic model (Chen *et al.*, 2008). The results would occur the sorption enhancement could be coupled with membranes. The carbonation is exothermic, the sorbents could also assist with supplying the heat needed for the endothermic reforming reactions. Additionally to improving the yield of hydrogen, the process heat could then be supplied to a sorbent regenerator. Furthermore, this option could facilitate sequestration of CO_2 , the principal greenhouse gas. While sorbent-enhancement is promising, several practical issues associated with sorbent enhancement of steam methane reforming need to be resolved if this option is to have significant impact, especially if the catalyst and sorbent are to co-exist in a sorbent-enhanced, membrane-assisted reformer.

Pedernera *et al.* (2007) studied the effect of hydrogen removal on carbon formation in a membrane reactor (with nickel supported catalyst) for steam and CO_2 methane reforming. The risks of carbon deposition consist of the CO_2 composition in feed, increasing permeated hydrogen and increasing operation temperature. The proposed model is a helpful tool to predict the location where carbon formation is probable in the conventional and membrane reactors for methane reforming, not only along the catalyst tube but also within the Ni catalyst.

Patel and Sunol (2007) investigated modeling and simulation of methane steam reforming in a thermally coupled membrane reactor. The first channel is a

burner, the second channel is a reformer and the third channel selectively removes the hydrogen by permeation through the palladium membrane. Simulations are performed for different inlet sweep gas velocities for the co-current and the countercurrent flow of the sweep gas. It is observed that the countercurrent flow gives increased methane conversion and higher hydrogen recovery yield compared to the co-current flow arrangement for all the sweep gas flow rates due to the higher driving force for hydrogen permeation. Also, with increase in sweep gas flow rate, methane conversion and hydrogen recovery yield increase. However, after the sweep gas flow rate is sufficiently increased, partial pressure of hydrogen in the sweep gas does not reduce with further increase in the sweep gas flow rate, so methane conversion and hydrogen recovery yield remain unaffected.

3.2 Solid Oxide Fuel Cell (SOFC)

Mathematical modeling is an essential tool for the design of SOFC system. For intermediate temperature direct internal reforming (IT DIR-SOFC); cathode activation overpotentials represent the major sources of voltage loss for co-flow operated at steady state condition (Aguiar *et al.*, 2004). Comparison of steady state and dynamic models at same condition show good agreement between both models in terms of the overall performance. However the discrepancies between the two models increase, especially in the fuel channel when higher current density values are assigned to the cell (Iora *et al.*, 2005). Considering a steady state model of IIR-SOFC (indirect internal solid oxide fuel cell), the results have shown that a local cooling of heat, undesirable for ceramic fuel cells, appears close to the reformer entrance. Increasing the operating pressure is shown to be an effective way of reducing both the local cooling (Aguiar *et al.*, 2002). For internal reformer, the operating conditions such as fuel recirculation, fuel inlet temperature, air circulation and air inlet temperature have considerable effects on the exhaust temperature but a slight effect on the efficiency (Nagata *et al.*, 2000). A simulation model for the Integrated Planar Solid Oxide Fuel Cell (IT-SOFC) show that activation overpotential is the major source of voltage drops and vary with current density and anode thickness but inverse to hydrogen molar fraction (Costamagna *et al.*, 2004).

Hernandez-Pacheco et al. (2005) developed the model for an SOFC operated with different composition of synthesis gas from a gasification process. The model was integrated with MathematicaTM. The repeating elements method was used in this study. The developed electrochemical model consisted of three polarizations (i.e. activation, ohmic and concentration loss). Butler-Volmer and Dusty's gas model were used for predicting activation loss and concentration loss, respectively. The reaction rate from Achenbach was also used for mass balance equation. The developed model was then tested and compared with a benchmark developed by IEA when 30% pre-reforming gas was used as fuels. The developed model yields 81.5% which was close to the IEA benchmark operating condition of 85%. It was shown that the methane was consumed quickly via steam reforming reaction at the entrance of the channel while the electrochemical reaction took place beyond the entrance and resulted in the low temperature at the entrance and the high temperature at the end of channel. The current density increased along the channel; however, it dropped sharply at the end of channel because of high concentration and activation polarization. Lastly, the influence of different syngas composition on SOFC performance was investigated. The results found that high concentration of hydrogen yielded high performance while high steam to fuel ratio can suppress coke formation.

Demin and Tsiakaras (2001) showed that efficiency of SOFC with hydrogen conducting (SOFC-H⁺) is higher than SOFC with oxygen conducting (SOFC-O²⁻). It was also estimated that SOFC-H⁺ efficiency at 1000 K is about 70% when it runs at 60% of its maximum power, whereas the practically reachable SOFC-O²⁻ efficiency under the above mentioned conditions is less than 55%. Then they used ethanol as fuel and found that efficiency of SOFC is about 20% less than the maximum SOFC system efficiency in the previous case. When temperature is increased, SOFC system efficiency is decreased (Tsiakaras and Demin, 2001). In some cases, ethanol can be operated at low temperature (933-1073 K) with complete oxidation (Galvia *et al.*, 2002). The products from that process at higher temperature (1073 K) facilitated synthesis gas production. Thermodynamic analysis of methane fed SOFC-H⁺ system is preformed. It was stated that the fuel utilization depends on H₂O/CH₄ mole ratio in the feeding fuel mixture and has a mixture at the ratio about 2.6 and maximum efficiency of SOFC-H⁺ system is about 15% higher than of SOFC system based on SOFC-O²⁻ (Demin *et al.*, 2002).

The special case of ion transport in the co-ionic electrolyte was analyzed. It was shown that partial ion current does not correspond to ion transfer numbers. It was established that the maximum achievable efficiency of a hydrogen-fed SOFC based on the co-ionic electrolyte with proton transfer number of 0.5, is 0.78 at 1173 whereas the efficiency is 0.62 when the SOFC works at 70% of its maximum power (Demin *et al.*, 2004).

System efficiencies can be considered into 2 types; i.e. energetic method (1st laws efficiency) and exergetic method (2nd laws efficiency). Both of them are considered for performance analysis. The results obtained from natural gas reforming thermodynamics simulation indicates that SOFC is more efficient than MCFC (Molten Carbonate Fuel Cell) and the carbon dioxide emission of SOFC is lower than MCFC one (Matelli and Bazzo, 2004). Energy conversion efficiency of ethanol into electricity was maximized considering a SOFC power plant with ethanol steam reforming, an after burner, a vaporizer and two heat exchangers based on mathematical model. The exergy analysis was applied to provide design criteria in terms of the temperature of the reforming and preheating (Douvartzides *et al.*, 2003). In the same system, methane-fed SOFC presents higher 1st law efficiency and 2nd law efficiency than ethanol-fed SOFC (Douvartzides *et al.*, 2004; Bedringas *et al.*, 1997).

3.3 Non-Uniform Potential Operation (NUP)

The use of non-uniform potential operation concept for fuel cells in which the cell voltage is allowed to vary along the cell length is another interesting approach. However, until now only some works have focused on the potential benefits of this approach. It was demonstrated that an improvement in electrical efficiency of about 1% could be achieved by splitting the cell of a molten carbonate fuel cell (MCFC) into 2 sections (Standart, 1998). Selimovic and Plasson (2002) examined performances of networked solid oxide fuel cell (SOFC) stacks combined with a gas turbine cycle. Two multistage configurations, i.e. (i) both anode and cathode flows were serially connected and (ii) only the anode flow was serially connected while the cathode flow was parallel connected, were considered. A significant increase of

system efficiency of about 5% was reported for the former configuration mainly by an improved thermal management.

The similar multistage configurations were also considered for a combined heat and a 250kW power MCFC plant (Au *et al.*, 2003). Detailed flowsheet calculations showed that the improvement in efficiency was about 0.6% for the former configuration, and 0.8% for the latter configuration. And they found that the intricate interaction between the fuel cell stack and the rest of the system. Improvement in fuel cell conversion not only increases the fuel cell stack output but it also reduced auxiliary power consumption by reduced cooling requirement. Less cooling translates to lower cathode mass flow, which increases oxidant utilization and hinders reaction kinetics.

The concept was also extended to PEMFCs divided into many stages (or stacks) of equal size (Senn and Poulikakos, 2005). It was demonstrated that the non-uniform cell potential operation allowed for enhanced maximum power densities compared to the traditional concept involving a uniform cell potential distribution. The improvement of maximum power density within 6.5% was reported. In practical applications, the proposed concept could be realized using segmented current collector plates which were originally developed to perform locally resolved current density measurements.

3.4 Pd Membrane

A palladium membrane is well-known as a highly selective membrane for hydrogen separation. The ability of hydrogen transfer through the membrane is typically quantified in term of permeability. The hydrogen flux (N_{H_2}) is inversely proportional to the membrane thickness (δ) and directly proportional to the product of the hydrogen permeability (Q_0) and the driving force (the difference in the square root of hydrogen partial pressure across the membrane).

$$N_{H_2} = \frac{Q_0}{\delta} \exp\left(\frac{-E_D}{RT}\right) (p_{H_2,r}^{0.5} - p_{H_2,p}^{0.5}) \quad (3.4)$$

The hydrogen permeability of palladium increases with temperature because the endothermic activation energy for diffusion dominates the exothermic adsorption of hydrogen on palladium. Buxbaum, *et al.* (2002) found that conversion of methanol steam reforming in palladium membrane reactor was decreased because of increasing reforming pressure but percentage of hydrogen recovery was increased. If oxygen is added to the hydrogen supply upstream side, hydrogen permeation will cease due to the way efficient catalytic formation of water on the surface of the palladium membrane. Adding oxygen on the other side, permeated hydrogen will react with oxygen to form water, lowering the hydrogen partial pressure on the downstream side close to zero and consequently the effective hydrogen permeation rate will increase. (Amanduson *et al.*, 1999)

Latter *et al.*, 2004 studied in benefit of Pd membrane in polymer exchange membrane (PEM) fuel cell system. They found that the main advantages of a palladium membrane reactor are (i) a reduction in the fuel processor volume, (ii) a small improvement in the overall system efficiency due to elimination of hydrogen losses in the PROX step and (iii) the use of a steam sweep for the permeate provides a pre-humidified anode feed gas.

The Pd-membrane reactor with a PEMFC inside into a micro-CHP unit was investigated (Campanari *et al.*, 2008). They proposed that the innovative membrane reforming solution yields several advantages in terms of electric efficiency and plant layout simplicity, suggesting interesting potential applications and the possibility to achieve relevant energy savings when applied to typical residential loads.

Pd-Ag thin wall tubes packed with a Ru-based, Pt-based and Ni-based catalyst had been investigated for producing pure hydrogen by ethanol steam reforming at 673-723 K (Tosti *et al.*, 2008; Tosti *et al.*, 2008). At low $H_2O:C_2H_5OH$ feed flow ratio, the hydrogen yield follows this sequence $Ru > Ni > Pt$, while for higher $H_2O:C_2H_5OH$ feed flow ratios the performance sequence is $Ru > Ni = Pt$. The best result in terms of hydrogen yield is 82% attained with the Ru-based catalyst at 723 K and 200 kPa in co-current mode and $H_2O:C_2H_5OH = 13:1$.

Brunetti *et al.* (2007) studied the water gas shift (WGS) reaction is an important step of hydrogen production in a Pd-alloy membrane reactor. Pressure ranging 200–1500 kPa which allows a good H₂ recovery index (up to 95%) and a retentate stream rich (up to 80%) in CO₂. In addition to, not only a pure H₂ stream in the permeate side but also a CO₂ concentrated retentate stream easily to be recovered

3.5 CaO-CO₂ Acceptor

Carbon dioxide is major component of greenhouse gases, responsible for global warming. So the reduced CO₂ emission is essential for our environment. Thus, carbonation reaction of calcium oxide (CaO) can capture CO₂ from other gases. The adding CaO can separate CO₂ from gaseous phase. The added CaO in commercial methane steam reformer catalyst can produce >95% H₂ in laboratory-scale (Balasubramanian *et al.*, 1999). On ethanol steam reforming, the results (>95% H₂) of advantage of CaO are similarity the results of methane steam reforming (Comas *et al.*, 2004).

The CO₂-capture capacity of CaO-carbonation is larger amount than hydrotalcite-base sorbent (Ding and Alpay, 2000; Xiu *et al.*, 2002). However, when the CaO-carbonation becomes to CaCO₃, the activity of CaO-carbonation is decrease. There are many researchers proposed the way to recycle CaO with integrated calcinations unit (Abanades, 2002; Berelli *et al.*, 2005). Abanades (2002) reported after 14 cycles of carbonation-calcination the conversion of CaO-carbonation decrease to 20% (Abanades, 2002). The carbonation reaction integrated with calcination reaction was studied (Berelli *et al.*, 2005). The results show the produced H₂ ~99% and zero CO₂ emission.

In addition, CaO acceptor can shift equilibrium of reaction, producing more products. There are many researchers studied chemical reaction with in situ CaO-CO₂ capture. Coal/H₂O/CaO gasification system was considered for hydrogen production (Wang *et al.*, 2006). Methane steam reforming reaction (MSR) contained by CaO-carbonation showed beneficial in CO₂ acceptor and hydrogen production at 1023 K (Lee *et al.*, 2004). The simulation of in-situ carbonation of CaO in MSR was studied

(Lee *et al.*, 2006). Lee has been proposed the kinetics of the carbonation of CaO (Lee *et al.*, 2006 and Lee, 2004).

Although, CaO have been efficient for CO₂-accepture, but main problem of CaO-CO₂ capture is CaCO₃, inactive spice. Therefore, carbonation-calcination cycle of CaO was considered by many authors. Gupta H. and Fan L.S. were considered the reaction based on cycle of separated carbon dioxide (CO₂) with CaO from flue gas (Gupta and Fan, 2002). They studied 2-3 cycle of carbonation-calcination. Consequently, it did not show effect of sintering on CaO sorbents at 700 °C. The multi cycles of carbonation-calcination were studied on the conversion of CaO vs. a number of cycles. When the cycle numbers rise, the conversion of CaO is decreased (Iyer *et al.*, 2004; Grasa *et al.*, 2007; Abanades, 2002). Abanades (2002) has been proposed the relation of maximum capture efficiency of CaO.



สถาบันวิทยบริการ
จุฬาลงกรณ์มหาวิทยาลัย

CHAPTER IV

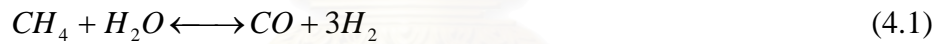
MODELING

This chapter provides details on mathematical models of methane steam reforming (thermodynamic equilibrium and kinetic model), electrochemical of SOFC, Pd-membrane reactor and CaO-CO₂ acceptor. A thermodynamic equilibrium is undertaken for both external methane steam reformer and internal reforming SOFC.

4.1 Calculation of the Converted Mole of Methane Steam Reforming

4.1.1 Thermodynamic Equilibrium Method

The methane steam reforming to produce hydrogen can be represented by Eqs. 4.1-4.3. The major reactions taking place in the reactor are methane steam reforming (Eq. 4.1), water gas shift reaction (Eq. 4.2) and reverse methanation of CO₂ (Eq. 4.3).



The methane steam reforming is generally operated in an external reformer. However, the SOFC can occur internal reforming; the hydrogen produced is consumed by the electrochemical reaction with oxygen ion, producing water and electricity. The number of moles of each component is given by the following expressions:

$$n_{CH_4} = a - x_1 \quad (4.4)$$

$$n_{CO} = d + x_1 - x_2 \quad (4.5)$$

$$n_{CO_2} = f + x_2 \quad (4.6)$$

$$n_{H_2} = e + 3x_1 + x_2 - c \quad (4.7)$$

$$n_{H_2O} = b + c - x_1 - x_2 \quad (4.8)$$

$$n_{tot} = \sum_i n_i = a + b + d + e + f + 2x_1 \quad (4.9)$$

where: n_i is mol of substance i

a is inlet mole of methane

b is inlet mole of water

c is extent of the electrochemical reaction of hydrogen (0, for external reformer)

d is inlet mole of carbon monoxide (0, for external reformer)

e is inlet mole of hydrogen (0, for external reformer)

f is inlet mole of carbon dioxide (0, for external reformer)

x_i is the converted moles associated to the reactions (4.1) to (4.2), respectively

The equilibrium constants (K_i) whose values can be determined from the change in Gibb's free energy of the reaction can be expressed as follows (more details are given in Appendix B):

$$K_1 = \frac{P_{CH_4} P_{H_2O}}{P_{CO} P_{H_2}^3} \quad (4.10)$$

$$K_1 = \frac{\left(\frac{a - x_1}{a + b + d + e + f + 2x_1} \right) \left(\frac{b + c - x_1 - x_2}{a + b + d + e + f + 2x_1} \right)}{\left(\frac{d + x_1 - x_2}{a + b + d + e + f + 2x_1} \right) \left(\frac{e + 3x_1 + x_2 - c}{a + b + d + e + f + 2x_1} \right)^3} \quad (4.11)$$

$$K_2 = \frac{P_{H_2} P_{CO_2}}{P_{CO} P_{H_2O}} \quad (4.12)$$

$$K_2 = \frac{\left(\frac{e + 3x_1 + x_2 - c}{a + b + d + e + f + 2x_1} \right) \left(\frac{f + x_2}{a + b + d + e + f + 2x_1} \right)}{\left(\frac{d + x_1 - x_2}{a + b + d + e + f + 2x_1} \right) \left(\frac{b + c - x_1 - x_2}{a + b + d + e + f + 2x_1} \right)} \quad (4.13)$$

System of non-linear equations was solved by developing a MATLAB program using the Newton's method as a solving algorithm (See Appendix C).

4.1.2 Kinetic Model

Mathematical models of methane steam reforming were reported by Xu and Froment (1989). The kinetic rate expressions on Ni/MgAl₂O₄ catalyst were derived based on the Langmuir-Hinshelwood reaction mechanism. The rate expressions for reactions (4.1)-(4.3) are given by the following expressions:

$$r_1 = \frac{k_1}{P_{H_2}^{2.5}} \left(P_{CH_4} P_{H_2O} - \frac{P_{H_2}^3 P_{CO}}{K_1} \right) / (DEN)^2 \quad (4.14)$$

$$r_2 = \frac{k_2}{P_{H_2}} \left(P_{CO} P_{H_2O} - \frac{P_{H_2} P_{CO_2}}{K_2} \right) / (DEN)^2 \quad (4.15)$$

$$r_3 = \frac{k_3}{P_{H_2}^{3.5}} \left(P_{CH_4} P_{H_2O}^2 - \frac{P_{H_2}^4 P_{CO_2}}{K_3} \right) / (DEN)^2 \quad (4.16)$$

$$\text{where } DEN = 1 + K_{CO} P_{CO} + K_{H_2} P_{H_2} + K_{CH_4} P_{CH_4} + \frac{K_{H_2O} P_{H_2O}}{P_{H_2}} \quad (4.17)$$

$$k_i = A_i \exp\left(\frac{-E_i}{RT}\right); i = 1, 2, 3 \quad (4.18)$$

$$K_j = B_j \exp\left(\frac{-\Delta H_j}{RT}\right); j = CO, H_2, CH_4, H_2O \quad (4.19)$$

The kinetic parameters for the methane steam reforming are summarized in Table 4.1

Table 4.1 Kinetic parameters for methane steam reforming (Xu and Froment, 1989).

Parameter	Pre-exponential factor (A or B)	E or ΔH (kJ.mol ⁻¹)
k ₁	4.225x10 ¹⁵ (mol atm ^{0.5} (g h) ⁻¹)	240.10
k ₂	1.955x10 ⁶ (mol (g h) ⁻¹)	67.13

k_2	$1.020 \times 10^{15} \text{ (mol atm}^{0.5} \text{ (g h)}^{-1})$	243.9
K_{CO}	$6.65 \times 10^{-4} \text{ (atm}^{-1})$	-38.28
K_{H_2}	$1.77 \times 10^5 \text{ (-)}$	88.68
K_{H_2O}	$6.12 \times 10^{-9} \text{ (atm}^{-1})$	-82.90
K_{CH_4}	$8.23 \times 10^{-5} \text{ (atm}^{-1})$	-70.65

The rates of consumption or formation of specie i are calculated by following expression:

$$r_{CH_4} = \frac{dn_{CH_4}}{dt} = -(r_1 + r_3) \quad (4.20)$$

$$r_{H_2O} = \frac{dn_{H_2O}}{dt} = -(r_1 + r_2 + 2r_3) \quad (4.21)$$

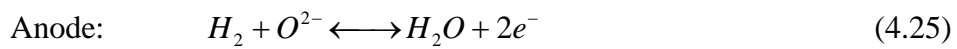
$$r_{H_2} = \frac{dn_{H_2}}{dt} = (3r_1 + r_2 + 4r_3) \quad (4.22)$$

$$r_{CO_2} = \frac{dn_{CO_2}}{dt} = (r_2 + r_3) \quad (4.23)$$

$$r_{CO} = \frac{dn_{CO}}{dt} = (r_1 - r_2) \quad (4.24)$$

4.2 Calculation of the SOFC Performance

In the SOFC stack, hydrogen and CO can react electrochemically with oxygen. However, it is assumed that the CO electro-oxidation is neglected. The electrochemical reactions of hydrogen and oxygen take place according to Eqs. (4.25) and (4.26). It was estimated earlier that about 98% of current is produced by H₂ oxidation in common situations (Khaleel *et al.*, 2004). This is due to the fast rate of water gas shift reaction at an SOFC operating temperature.



4.2.1 Electromotive Force (E_0)

Electromotive force (E_0) of the cell is a difference of potentials between both of the cell electrodes. It can be represented as follows:

$$E_0 = |\varphi_C - \varphi_A| \quad (4.27)$$

where: φ_C and φ_A are potentials of the cathode and the anode, respectively. The electrode potential can be calculated from Nernst equation which can be expressed as follows:

$$\varphi = (RT/(4F)) \ln p_{O_2} \quad (4.28)$$

where: R is the universal gas constant, T is the absolute temperature and F is the Faraday's constant.

From Eqs. 4.27 and 4.28, the electromotive force can be expressed as follows:

$$E_0 = \frac{RT}{4F} \ln \frac{p_{O_2,c}}{p_{O_2,a}} = -\frac{\Delta G}{2F} - \frac{RT}{2F} \ln \frac{P_{H_2O,a}}{P_{H_2,a} P_{O_2,c}^{0.5}} \quad (4.29)$$

The partial pressure of oxygen in the anode chamber is calculated from its mole fraction while the partial pressure of oxygen in the anode chamber is given by:

$$p_{O_2,a} = \left(\frac{P_{H_2O,a}}{K_{H_2O} P_{H_2,a}} \right)^2 \quad (4.30)$$

where: p_i is the partial pressure, K is the equilibrium constant of the hydrogen oxidation reaction.

4.2.2 Overpotentials

The actual cell potential (V) is always less than the theoretical voltage (E^0), because of the presence of several overpotentials.

$$V = E_0 - \eta_{Ohm} + \eta_{Act,A} + \eta_{Act,C} + \eta_{Conc,A} + \eta_{Conc,C} \quad (4.31)$$

For this study, ohmic and activation overpotentials were considered in this study while concentration overpotential was neglected.

Ohmic Overpotential:

The resistance of each material can be calculated from its resistivity which is the function of temperature (Bessette *et al.*, 1995).

$$\eta_{Ohm} = iR \quad (4.32)$$

$$R = \rho\delta \quad (4.33)$$

where: δ is thickness (m).

$$\rho_j = a_j \exp\left(\frac{b_j}{T}\right) \quad (4.34)$$

Table 4.2 summarizes the cell components and their parameters used in this study (Chan *et al.*, 2002).

Table 4.2 Resistivity and thickness of cell component.

Material used	Ni-YSZ/YSZ/LSM-YSZ
Anode thickness (μm)	150
Anode Ohmic resistance constant	$a=0.0000298, b=-1392$
Cathode thickness (μm)	2000
Cathode Ohmic resistance constant	$a=0.0000811, b=600$
Electrolyte thickness (μm)	40
Electrolyte Ohmic resistance constant	$a=0.0000294, b=10350$

Interconnect thickness (μm)	10
Interconnect Ohmic resistance constant	$a=0.001256, b=4690$

Activation overpotential:

A comparison between these correlations and the Butler–Volmer equation reveals that the empirical correlations were reasonably accurate between 1073 and 1473 K. At higher temperatures, the empirical expressions gave polarization values much smaller than the Butler–Volmer equation, which was expected based on the assumptions used for these correlations. However, at lower and higher temperatures ($T \leq 1173$ K and $T \geq 1473$ K), the numerical values reported unrealistic results and cannot be used for any practical purpose. Thus Achenbach correlation has accurate data at 1173 K (Pacheco *et al.*, 2004).

The Achenbach's correlations at an anode and a cathode are presented in Eqs. (4.35) and (4.36), respectively. These expressions are employed in the study described in Chapter 5.

$$\eta_{Act,C} = i \cdot R_{Act,C} = i \cdot \left(\frac{4F}{RT} r_C \left(\frac{p_{O_2}}{p} \right)^m \exp\left(\frac{-E_C}{RT}\right) \right)^{-1} \quad (4.35)$$

$$\eta_{Act,A} = i \cdot R_{Act,A} = i \cdot \left(\frac{2F}{RT} r_A \left(\frac{p_{H_2}}{p} \right)^m \exp\left(\frac{-E_A}{RT}\right) \right)^{-1} \quad (4.36)$$

Table 4.3 Summary of activation polarization parameters (Hernandez-Pacheco *et al.*, 2004).

	k (A m^{-2})	$E_{A,pol}$ ($\text{kJ mol}^{-1}\text{K}^{-1}$)	m (-)
Cathode	14.9×10^9	160	0.25
Anode	0.213×10^9	110	0.25

The Butler–Volmer’s correlations at an anode and a cathode are presented in Eqs. (4.37) and (4.40). These expressions are employed in the study described in Chapters 6 and 7.

$$\eta_{Act} = \frac{2RT}{n_e F} \sinh^{-1} \left(\frac{i}{i_0} \right) \quad (4.37)$$

$$i = i_0 \left[\exp \left(\frac{\alpha n_e F \eta_{Act}}{RT} \right) - \exp \left(- \frac{(1 - \alpha) n_e F \eta_{Act}}{RT} \right) \right] \quad (4.38)$$

where: $\alpha = 0.5$

$$i_{0,A} = 5.5 \times 10^8 \left(\frac{P_{H_2}}{p} \right) \left(\frac{P_{H_2O}}{p} \right) \exp \left(\frac{-100 \times 10^3}{RT} \right) \quad (4.39)$$

$$i_{0,C} = 7.0 \times 10^8 \left(\frac{P_{O_2}}{p} \right)^m \exp \left(\frac{-120 \times 10^3}{RT} \right) \quad (4.40)$$

4.2.3 SOFC Performances

For SOFC performances, power density (P_{dens}), current (I), SOFC area (A_{SOFC}), electrical power (W_{elec}) and electrical efficiencies (η_{elec}) are expressed in this section.

$$\text{Power density: } P_{dens} = iV \quad (4.41)$$

$$\text{Current: } I = n_{H_2,consumed} * 2F \quad (4.42)$$

$$\text{SOFC area: } A_{SOFC} = \frac{I}{i} \quad (4.43)$$

$$\text{Electrical power: } W_{elec} = IV \quad (4.44)$$

$$\text{Electrical efficiencies: } \eta_{elec} = \frac{W_{elec}}{n_{CH_4} * LHV_{CH_4}} \quad (4.45)$$

where: $n_{H_2,consumed}$ is the molar flow rate of hydrogen consumed in the electrochemical reaction. n_{CH_4} is the molar flow rate of methane. LHV_{CH_4} is lower heating value of methane (820.6 kJ.mol⁻¹).

4.3 Pd Membrane Reactor

A palladium membrane is well-known as a highly selective membrane for hydrogen separation. The ability of hydrogen transfer through the membrane is typically quantified in term of permeability. The hydrogen flux (N_{H_2}) is inversely proportional to the membrane thickness (δ) and directly proportional to the product of the hydrogen permeability (Q_0) and the driving force (the difference in the square root of hydrogen partial pressure across the membrane).

$$N_{H_2} = \frac{Q_0}{\delta} \exp\left(\frac{-E_D}{RT}\right) (P_{H_2,r}^{0.5} - P_{H_2,p}^{0.5}) \quad (4.46)$$

In order to achieve a high hydrogen flux, a thin film of palladium membrane is generally coated on a porous support with good mechanical property. In addition, the driving force is enhanced by installing a compressor and/or a vacuum pump. The required power (P_{pump}) for the compressor and vacuum pump can be calculated by using the Aspen Plus program (Appendix D). In this study, the efficiencies of both the compressor and the vacuum pump are assumed to be 85%.

A membrane reactor (MR) is a reaction system where separation unit and chemical reactors are combined together. The use of a palladium membrane reactor (Pd-MR) is a promising approach for methane steaming reforming (MSR). As the reactions are limited by equilibrium; the separation of hydrogen product via the selective palladium membrane can increase the conversion of methane and achieve a high-purity hydrogen product at the same time. To calculate the palladium membrane area, the membrane was divided into small increments represented by $dz_{Pd,i}$. The corresponding hydrogen recovery ($H_{2,permeate,i}$) at each element can be computed by Eq. 4.47 and the total hydrogen recovery ($H_{2,permeate}$) obtained from the membrane reactor was the summation of hydrogen recovery at each element (Eq. 4.48). The length of the membrane reactor ($z_{Pd,total}$) was extended until the hydrogen recovery reaches the target value ($H_{2,require}$) (Eq. 4.49). The final membrane area which

corresponds to the target hydrogen recovery represents the required membrane area (A_{Pd}) for the operation (Eq. 4.50).

$$H_{2,permeate_i} = 2 \cdot \pi \cdot r_{ext} \cdot dz_{Pd,i} \cdot N_{H_2,i} \quad (4.47)$$

$$H_{2,permeate} = \sum_{i=1}^n H_{2,permeate_i} \quad (4.48)$$

$$z_{Pd,total} = \sum_{H_{2,permeate}=0}^{H_{2,permeate}=H_{2,require}} dz_{Pd,i} \quad (4.49)$$

$$A_{Pd} = 2 \cdot \pi \cdot r_{ext} \cdot z_{Pd,total} \quad (4.50)$$

4.4 CaO-CO₂ Acceptor

Carbonation reaction of calcium oxide (CaO) can capture carbon dioxide (CO₂) and convert CaO to calcium carbonate (CaCO₃). Calcination of CaCO₃ can reverse to CaO. It can be used in a CO₂ separator, when operated carbonator and calciner together. Schematic diagram of a carbonation-calcination cycle is illustrated in Fig. 1. Fresh CaO (F_0) is added to the cycle systems. The carbonation conversion depends on the number of cycle (Eq. 4.51). This cycle can operate for CO₂ separation from reformed gases. The carbonation conversion ($x_{c,N}$) is a function of the number of cycles (Abanades, 2002)

$$x_{c,N} = f^{N+1} + b \quad (4.51)$$

where: $f = 0.782$ and $b = 0.174$ (correlation coefficient is 0.982).

The CO₂ capture efficiency (Eq. 4.52) is defined by mass balance shown in Fig. 4.1.

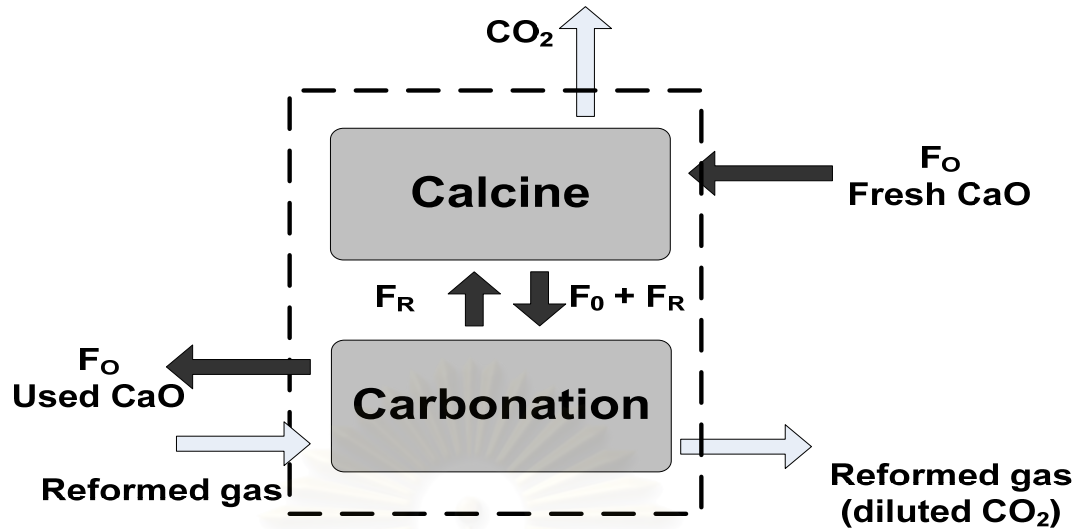


Fig. 4.1 Schematic diagram of a CaO-CO₂ acceptor system.

$$E_C = \frac{(F_R + F_0) \cdot \bar{x}_c}{F_0 + F_{CO_2}} \quad (4.52)$$

The average carbonation conversion (\bar{x}_c) is presented:

$$\bar{x}_c = \sum_{k=1}^{\infty} r_k \cdot x_{c,k} \quad (4.53)$$

where: r_k is mass fraction of particles at k times.

If the carbonation-calcination was circulated N times, the mass fraction of particles can be expressed by the following correlation:

$$r_1 = \frac{F_0}{F_0 + F_R} \quad (4.54)$$

$$r_2 = \frac{r_1 \cdot F_R}{F_0 + F_R} \quad (4.55)$$

•

$$r_N = \frac{F_0 \cdot (F_R)^{N-1}}{(F_0 + F_R)^N} \quad (4.56)$$

From Eqs. 4.51, 4.53 and 4.56, the average carbonation conversion (\bar{x}_c) is obtained:

$$\bar{x}_c = \sum_{k=1}^{\infty} \left(\frac{F_0 \cdot (F_R)^{k-1}}{(F_0 + F_R)^k} \right) \cdot (f^{k+1} + b) \quad (4.57)$$

$$\text{From: } \sum_{k=1}^{\infty} X^k = \lim_{X \rightarrow 1} \frac{1 - X^{k+1}}{1 - X} = \frac{1}{1 - X} \quad (4.58)$$

From Eqs. 4.57 and 4.58, the average carbonation conversion (\bar{x}_c) can be expressed as:

$$\bar{x}_c = \frac{f \cdot F_0}{F_0 + F_R(1 - f)} + b \quad (4.59)$$

Abanades (2002) developed an expression for the maximum capture efficiency of CO₂ as shown below:

$$E_C = \frac{F_R + F_0}{F_0 + F_{CO_2}} \cdot \left(\frac{f \cdot F_0}{F_0 + F_R(1 - f)} + b \right) \quad (4.60)$$

where F_0 is fresh feed of CaO. F_R is feed recycle of CaO. F_{CO_2} is feed of CO₂.

The circulating fluidized bed was chosen for this CaO carbonation-calcination operation. The constraint of circulating fluid bed is that gas velocity (v) must more than gas terminal velocity (v_t), ($v \geq v_t$) (Eq. 4.61). Pressure drop along reactor was calculated by Eq. 4.62 (Walas, 1988).

$$v_i = \frac{g(\rho_p - \rho_f)d_p^2}{18\mu} \quad (4.61)$$

$$\frac{\Delta P}{L} = \rho_p(1 - \varepsilon)g + \rho_f \varepsilon g + \frac{2f_g \rho_f u_f^2}{D} + \frac{2f_s \rho_p (1 - \varepsilon)u_p^2}{D} \quad (4.62)$$

4.5 Economic Analysis

Economic analysis was carried out to compare the costs of the SOFC systems incorporated with palladium membrane reactors of different operation modes with that of the system with the conventional reformer. The total capital cost includes the costs of compressor, vacuum pump, SOFC stack (1500 \$/m²) (Riensch *et al.*, 1998) and Pd membrane (746 \$/m²) (Criscuolo *et al.*, 2001). The compressor cost and vacuum pump cost (\$) were described by the following expressions, Eqs. 4.63 and 4.64, respectively (Walas, 1988).

$$\text{Cost of compressor (\$)} = 1.49 \cdot HP^{0.71} \times 10^3 \quad (4.63)$$

where: $10 < HP < 800$

$$\text{Cost of vacuum pump (\$)} = 2.59 \cdot X^{1.03} \times 10^5 \quad (4.64)$$

where: $0.01 < X < 0.52$ (lbs H₂/h)/(suction Torr)

4.6 Simulation of SOFC System by Using *MATLAB*TM

The flowchart of program used in Chapter 5 to 7 is simulated by *MATLAB*TM, respectively. Fig. 4.2 show flowchart of NUP-SOFC. Firstly, the parameters CH₄ and H₂O mole flow rate, final fuel utilization ($U_{f,final}$), operating voltage at each stage (V_i) and a number of stages were set into program. The composition of methane steam reforming (MSR) was calculated by equilibrium composition, first loop refer to external methane steam reformer and N^{th} loop refer to internal reformer–SOFC (IR-

SOFC). EMF and overpotential were calculated, at $U_{f,i}$. Until $U_{f,I} = U_{f,final}$ and $Stage_i = Stage$, the NUP-SOFC was calculated performance and compared with UP-SOFC.

Flowchart of MR-SOFC shows in Fig. 4.3. Initially, parameter input to simulation program. Then program will switch to membrane reactor or conventional reactor. The conventional methane steam reformer was calculated by kinetic model of methane steam reforming. The Pd-membrane reactor of steam reforming was calculated by modified kinetic model with hydrogen permeation model. After that performance of SOFC system was calculated. Fig. 4.4 shows flowchart of CaO-SOFC. In this section, kinetic model still was selected. Program select operating mode. In Before-SOFC mode, reformed gas was captured with CaO-CO₂ acceptor before fed to SOFC system. Then performance of SOFC was calculated.



สถาบันวิทยบริการ
จุฬาลงกรณ์มหาวิทยาลัย

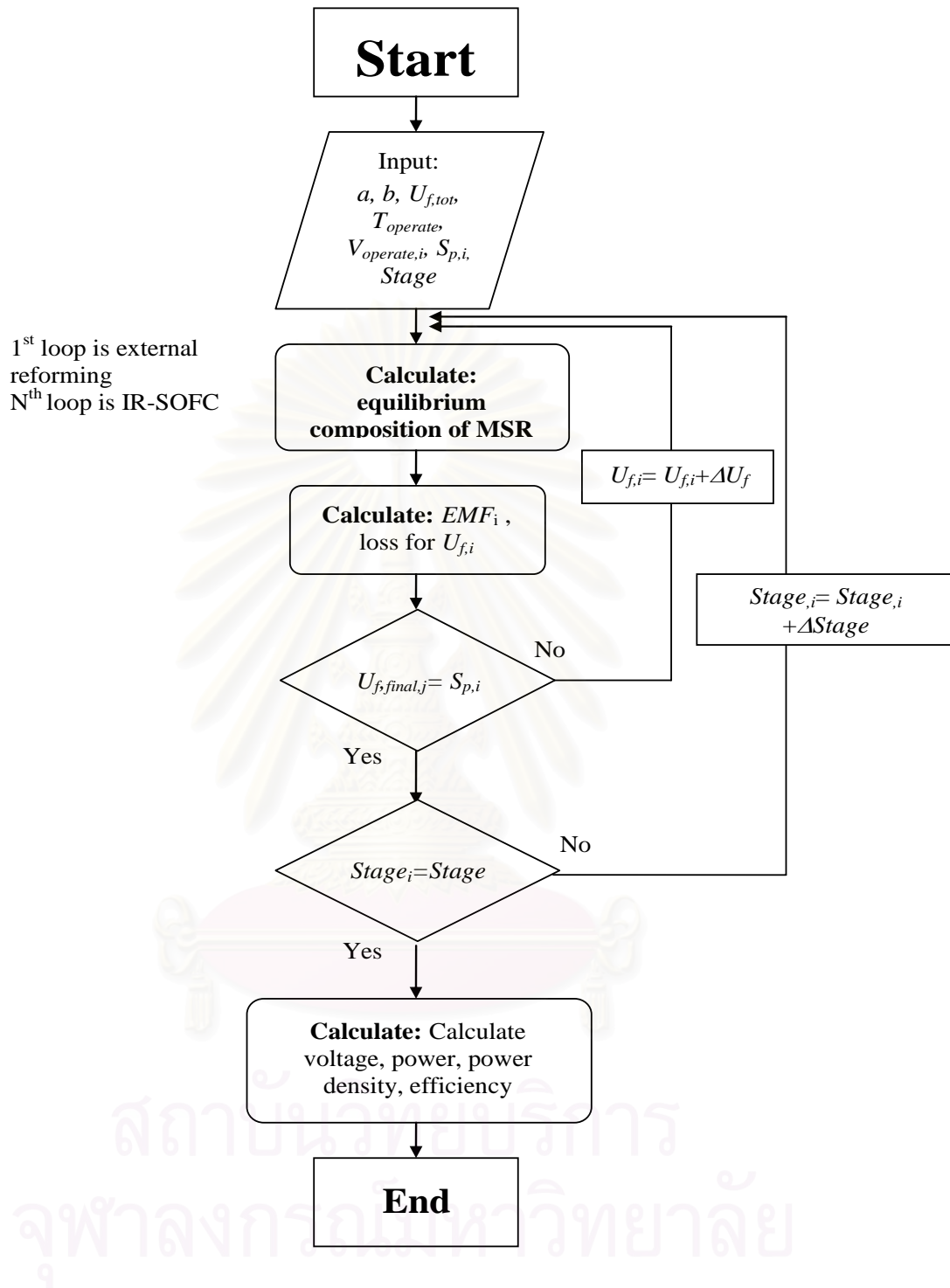


Fig. 4.2 Flowchart of non-uniform potential operation of solid oxide fuel cell.

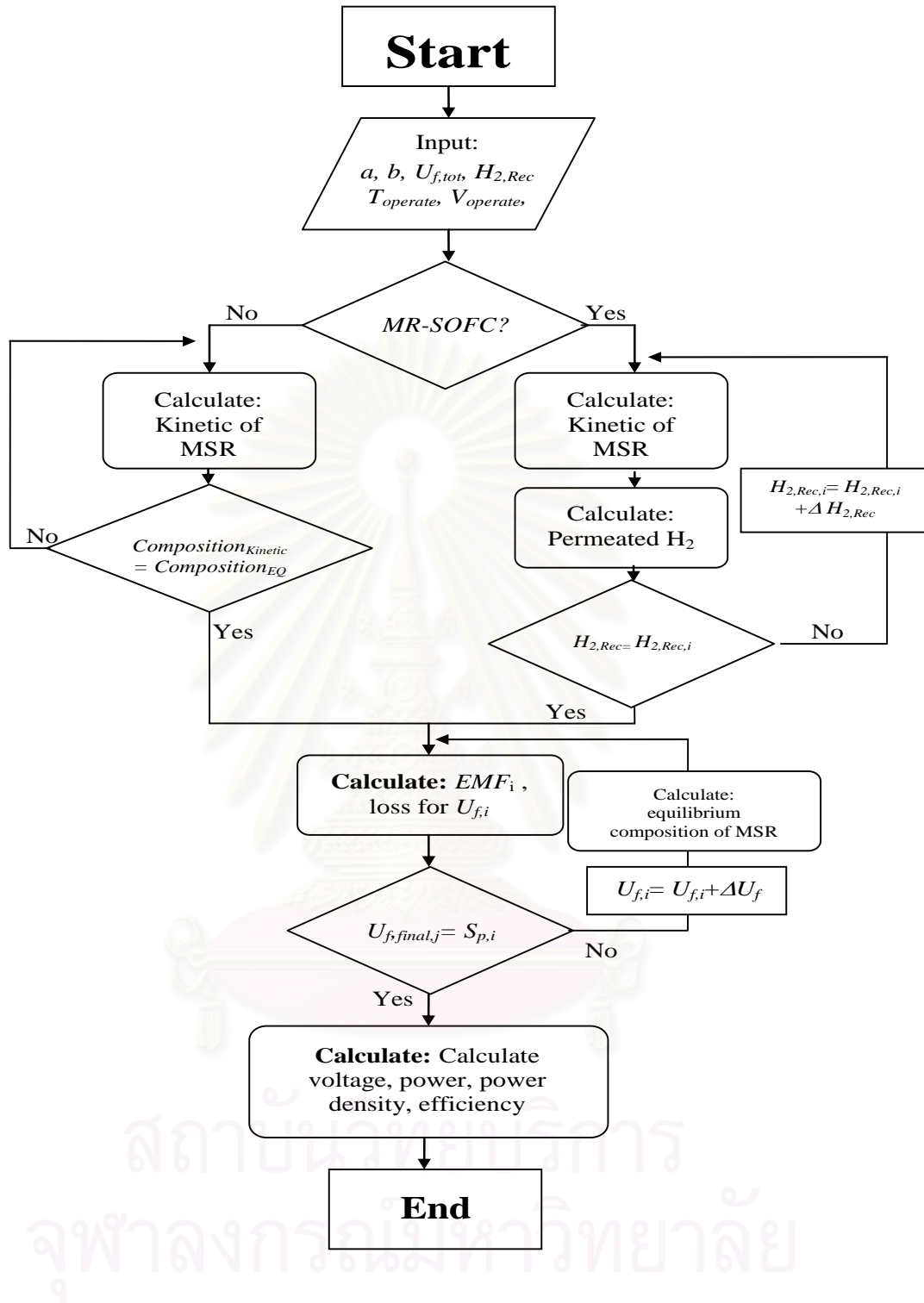


Fig. 4.3 Flowchart of SOFC incorporated with Pd-membrane reactor.

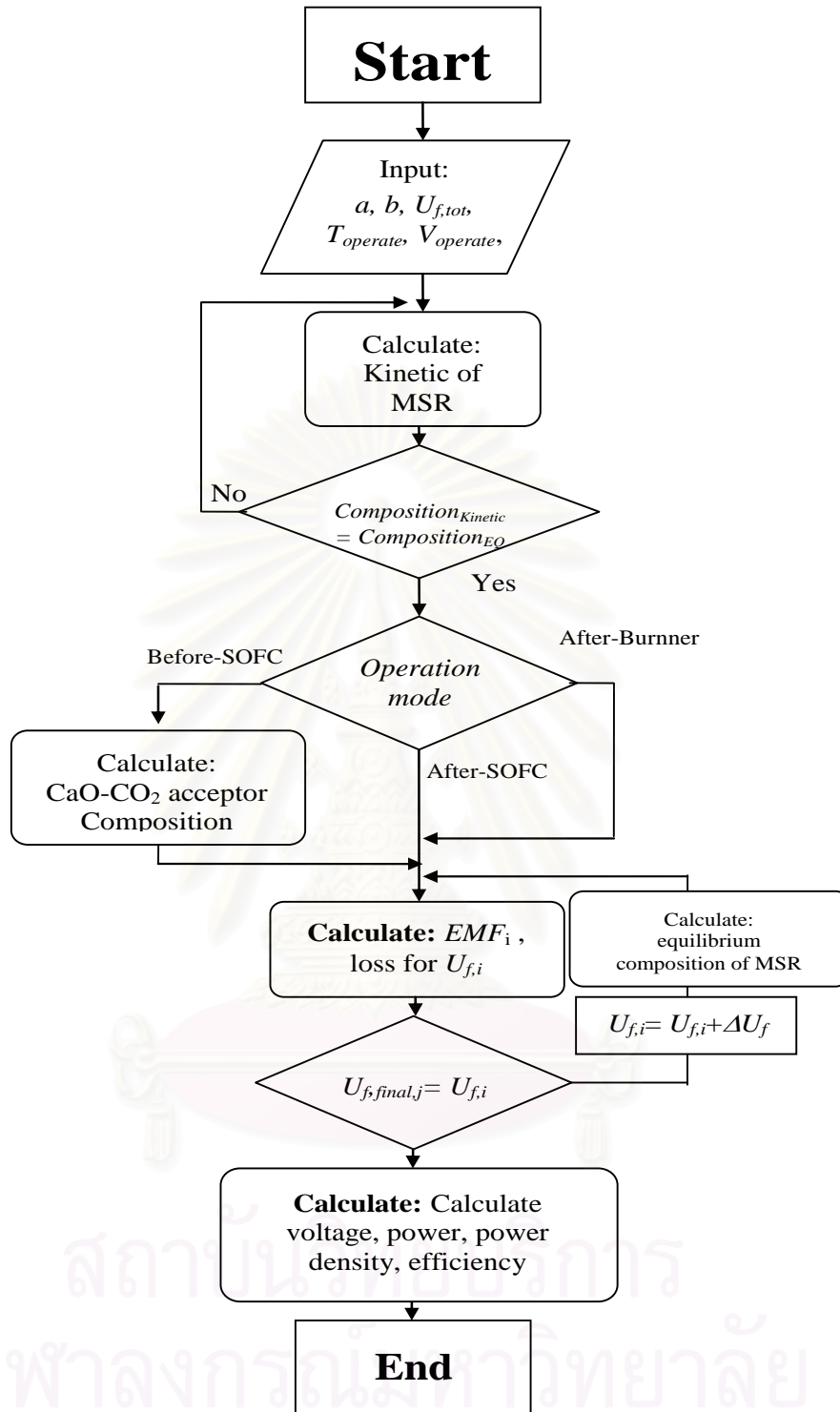


Fig. 4.4 Flowchart of SOFC incorporated with CaO-CO₂ acceptor.

CHAPTER V

IMPROVEMENT OF SOLID OXIDE FUEL CELL PERFORMANCE BY USING NON-UNIFORM POTENTIAL OPERATION

In this chapter, the concept of non-uniform potential operation implemented to SOFCs fed by methane was investigated in an effort to optimize cell operating voltages and sizes so that a maximum power density could be achieved without a reduction of electrical efficiency. Values of power density of a simple SOFC with a cell divided into 2 sections whose operating voltages and sizes were allowed to vary were compared to those of a typical SOFC with uniform cell potential at various electrical efficiencies. Additionally, the effect of number of cell section on the obtained performance was determined.

5.1 Results and Discussion

The schematic diagram of an SOFC with non-uniform potential operation (SOFC-NUP) is illustrated in Fig. 5.1 Compositions of fuel and air streams change along the cell channel according to changes in value of fuel utilization defined as the mole of hydrogen electrochemically consumed divided by the theoretical mole of hydrogen generated from complete reforming of the methane feed. In section k , the fuel utilization changes from $U_{f,k-1}$ to $U_{f,k}$, and the cell is operated at a constant potential of V_k within the section. In practice, the non-uniform cell potential can be realized by using segmented current collectors for a single-cell SOFC or it can be carried out in a series of SOFC stacks operated at different stack potentials. The section split of section k ($S_{p,k}$) is defined by

$$S_{p,k} = \frac{U_{f,k} - U_{f,k-1}}{U_{f,final}} \quad (5.1)$$

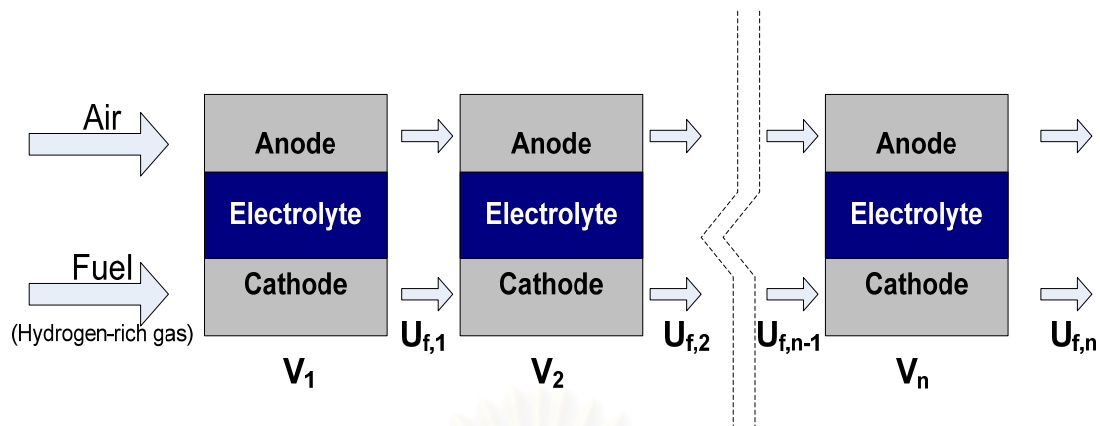


Fig. 5.1 Schematic diagram of SOFC-NUP.

Fig. 5.2 shows the performances of a typical SOFC with uniform potential operation (SOFC-UP). Each line represents the results at a constant value of fuel utilization (U_f). It should be noted that because concentration polarization becomes an importance loss at high current densities and small fuel concentration ($U_f \geq 80\%$) (Hernandez-Pacheco *et al.*, 2005), the simulations were performed only in the ranges of high voltage (low current density) and fuel utilizations (U_f) of lower than 80%. In order to validate the model, the results from a previous literature (Achenbach, 1994) at a condition close to this work have been included in Fig. 5.2 for comparison. This figure has shown the results at high voltage rather close to our results. Although the ohmic polarization equation employed in their calculations and some operating conditions are different from our work; i.e., $U_f = 85\%$, air ratio = 7 (2), non-isothermal reactor (isothermal reactor) and $\text{CH}_4/\text{H}_2\text{O} = 2.5$ (2.2), the performances of the SOFC are within the same order. Note that the values shown in the blanket represent our simulation conditions. From Fig. 5.2, regarding the electrical efficiency, it is favourable to operate the SOFC at high voltage in order to obtain high efficiency. However, when taking into account the power density, operation at a high value of voltage is not practical due to the achievement of low power density. Therefore, in practice, suitable operating voltage and fuel utilization should be carefully selected. Some workers suggested operating the cell at 70% of maximum power density (Demin *et al.*, 2004) and fuel utilization of 80-95% (Rostrup-Nielsen *et al.*, 2001, Campanari, 2001, Riensche *et al.*, 1998, Criscuoli *et al.*, 2001). In the present work, the fuel utilization (U_f) of 80% was considered and SOFC with non-uniform potential

operation (SOFC-NUP) was investigated with the aim to improve the power density without lowering the electrical efficiency.

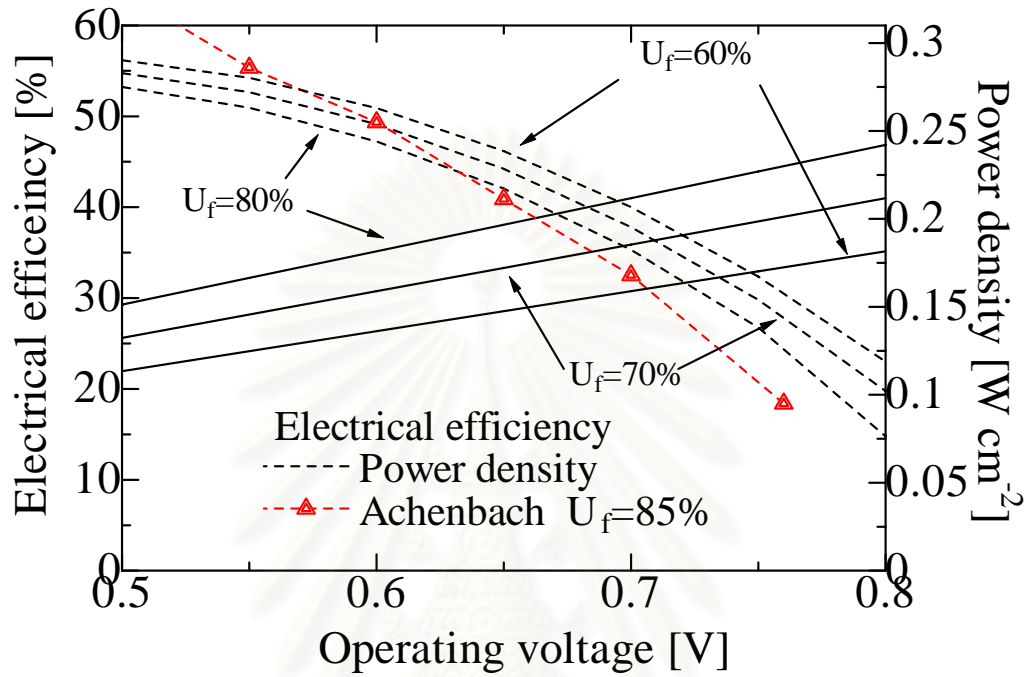


Fig. 5.2 Performance characteristic curves of typical SOFC-UP (H_2O/CH_4 ratio = 2.2 and $T_{SOFC} = 1173$ K).

Fig. 5.3 shows the relationship between power density and electrical efficiency of a simple SOFC-NUP with a cell divided into 2 sections of equal range of fuel utilization ($S_{p,1} = S_{p,2} = 0.5$). V_1 and V_2 represent the operating voltages of sections 1 and 2, respectively. The thick solid line indicates the results of the SOFC-UP. It is indicated that there are some ranges of operation in which the SOFC-NUP offers higher power density than the SOFC-UP without lowering the electrical efficiency (area above of the thick solid line). The improvement becomes significant when the cell is operated at high electrical efficiency. In order to indicate suitable operating voltages which offer the highest average power density, the value of electrical efficiency was specified and the value of V_1 was varied. Then V_2 , which gives the desired value of the electrical efficiency, and its corresponding power density can be calculated. For example, as shown in Fig. 5.4, for an electrical efficiency of 43%, the

values of V_2 are 0.623, 0.673 and 0.723 V for $V_1 = 0.7, 0.75$ and 0.80 V, respectively, and the corresponding values of the power density are 0.178, 0.156 and 0.159 W cm^{-2} , respectively. By varying V_1 , the maximum power density of 0.162 W cm^{-2} is obtained at $V_1 = 0.773 \text{ V}$ and $V_2 = 0.700 \text{ V}$.

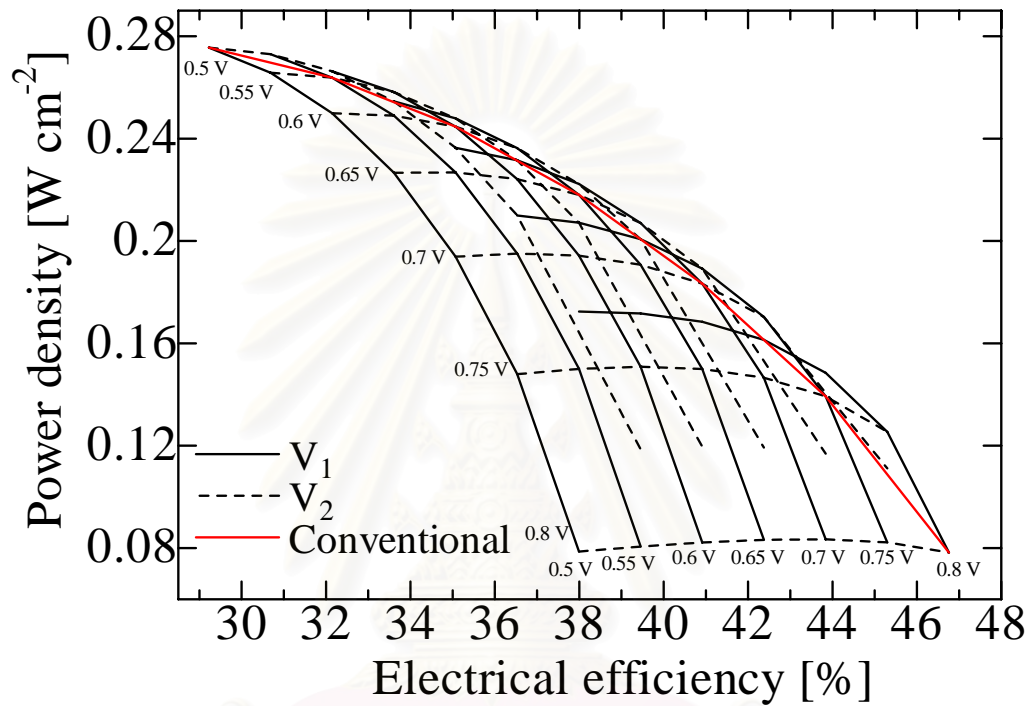


Fig. 5.3 Relationship between power density and electrical efficiency of SOFC-UP and SOFC-NUP ($U_f = 80\%$ and $T = 1173 \text{ K}$; for SOFC-NUP: $n = 2$, $S_{p,1} = 0.5$).

สถาบันวิทยบริการ
จุฬาลงกรณ์มหาวิทยาลัย

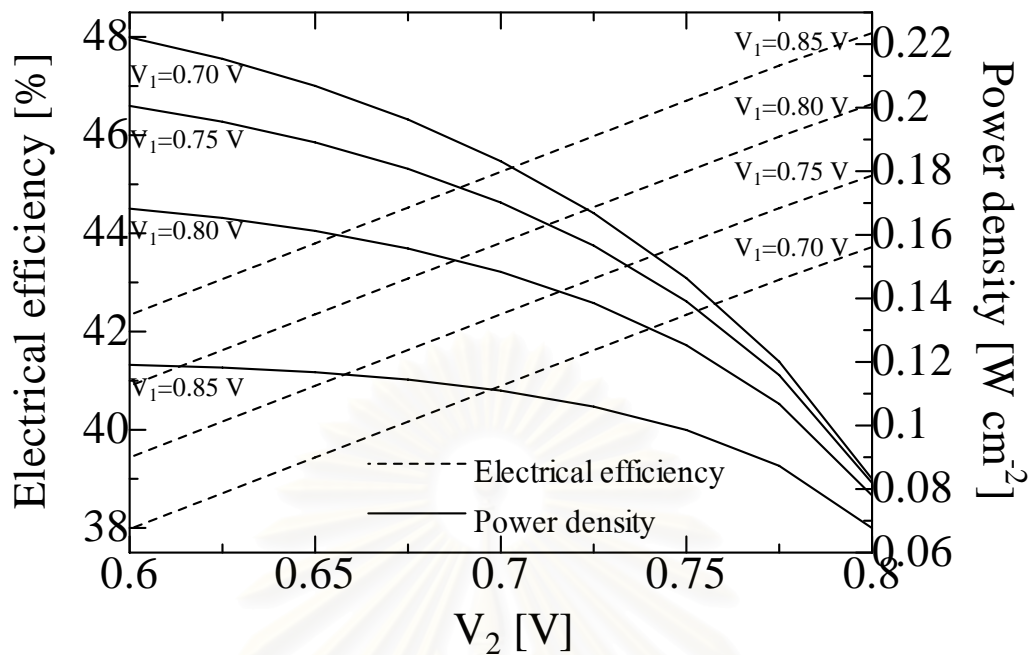


Fig. 5.4 Effect of operating voltages on performance of SOFC-NUP ($n = 2$, $U_f = 80\%$, $T = 1173$ K, $S_{p,1} = 0.5$ and $S_{p,2} = 0.5$).

According to the above study, the section splits were maintained at $S_{p,1} = S_{p,2} = 0.5$. Those values were then adjusted in order to achieve better performance. Fig. 5.5 shows the effect of section split ($S_{p,1}$) on the power density improvement at different values of electrical efficiency. It should be noted that the reported values are based on the operation using optimum voltages for each value of the section split. It was found that the power density improvement as high as 9.2% can be achieved at the electrical efficiency of 45% but the improvement becomes less significant when the SOFC is operated at lower electrical efficiency. In addition, the optimum $S_{p,1}$ for all cases was found to be around 0.55. Table 5.1 summarizes the values of the power density and the corresponding optimum voltages at different electrical efficiency of the SOFC-UP and the SOFC-NUPs with $S_{p,1} = S_{p,2}$ and with the optimum $S_{p,1}$ and $S_{p,2}$. It was found that the results of the SOFC-NUP with the optimum $S_{p,1}$ and $S_{p,2}$ are not significantly different from those of the SOFC-NUP with $S_{p,1} = S_{p,2}$ although the voltages are different.

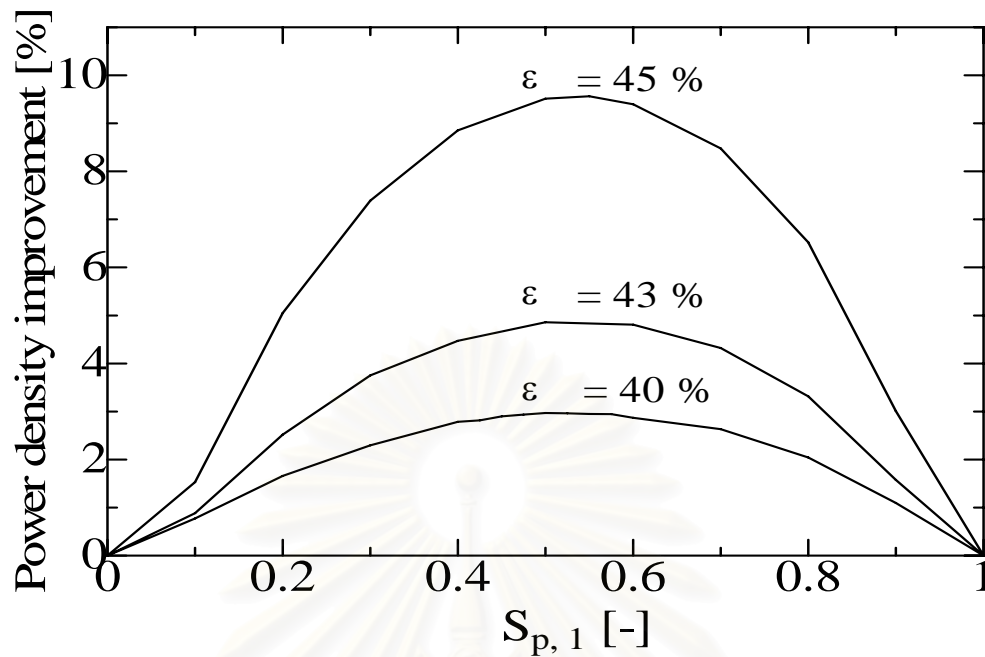


Fig. 5.5 Effect of section split on power density improvement of SOFC-NUP

($n = 2$, $U_f = 80\%$ and $T = 1173$ K).

Table 5.1 Comparison of power density between SOFCs with different number of section and section splits.

Electrical efficiency (%)	Power density (W cm^{-2})			
	$n = 1$	$n = 2$ ($S_{p,1}=S_{p,2}=0.5$)	$n = 2$ ($S_{p,1}=0.55, S_{p,2}=0.45$)	$n = 3$ ($S_{p,1}=S_{p,2}=S_{p,3}=1/3$)
35	0.246 (0.598 V)	0.248 (0.619, 0.571 V)	0.249 (0.631, 0.560 V)	0.250 (0.644, 0.608, 0.544 V)
37	0.229 (0.632 V)	0.232 (0.669, 0.598 V)	0.232 (0.666, 0.594 V)	0.233 (0.682, 0.632, 0.583 V)
40	0.196 (0.683 V)	0.201 (0.721, 0.649 V)	0.201 (0.717, 0.645 V)	0.202 (0.740, 0.666, 0.647 V)
43	0.154 (0.734 V)	0.162 (0.7726, 0.7001 V)	0.162 (0.768, 0.697 V)	0.164 (0.782, 0.736, 0.688 V)
45	0.120 (0.768 V)	0.131 (0.8069, 0.7342 V)	0.131 (0.803, 0.731 V)	0.134 (0.817, 0.772, 0.720 V)

To further enhance the performance of the SOFC-NUP, the number of separated section (n) was increased. Fig. 5.6 shows the effect of the number of section on the power density improvement for three values of electrical efficiency. The section splits of all sections are specified to be at the same value of $S_{p,k} = 1/n$ in order to simplify the calculations. The optimum voltages of the SOFC-NUPs which offer the highest power density for each case were determined by following the procedure described earlier for the case with $n = 2$. It was assumed that the maximum power density achieved from the case with adjustable section splits does not significantly differ from that achieved from the case with equally divided sections. This assumption is valid at least for the case of the SOFC-NUP with $n = 2$ as shown earlier. The calculated results indicate that the obtained maximum power density increases with increasing the number of sections (n). However, the improvement becomes less significant after $n > 3$. The SOFC-NUP with $n = 3$ is likely to be a suitable system for improving the power density without the reduction of electrical efficiency. Table 5.1 also shows the values of the maximum power density and the corresponding voltages at different values of electrical efficiency. At the electrical efficiency of 45%, the power density of the SOFC-NUP with $n = 3$ is 11.7% higher than that of the typical SOFC-UP.

From the above results, it has been demonstrated that the use of the non-uniform potential operation with SOFC is technically feasible. The cell area can be reduced without lowering the electrical efficiency. However, the SOFC-NUP would require more sophisticated cell arrangement, power conditioning system and so on. The system control would inevitably become more complicated. Further investigations are required before implementing this system for commercial use.

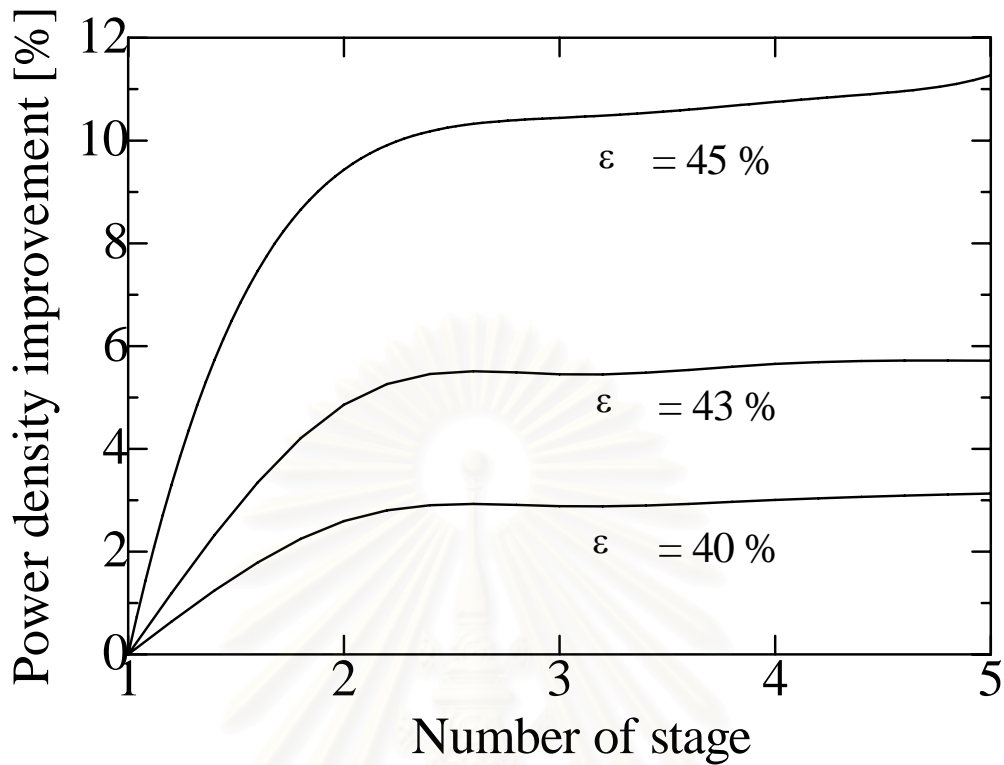


Fig. 5.6 Effect of number of stage on power density improvement of SOFC-NUP ($U_f = 80\%$, $T = 1173$ K and $S_{p,k} = 1/n$).

5.2 Conclusions

An SOFC-NUP can provide higher power density than a typical SOFC-UP without a reduction of electrical efficiency. The optimum SOFC-NUP was determined by allowing the operating voltage and section split of each section to be appropriately adjusted to achieve the highest power density for each level of electrical efficiency. The maximum power density can be further improved by increasing the number of separated section (n) of the cell; however, it became less pronounced after $n > 3$. Although it is obvious that the non-uniform operation can allow the SOFC to be operated at higher performance, further investigation is necessary to determine whether the cost reduction by the reduced stack size would be sufficiently attractive compared to the increases of power conditioning cost and complication of the SOFC.

CHAPTER VI

PERFORMANCE IMPROVEMENT OF SOLID OXIDE FUEL CELL SYSTEM USING PALLADIUM MEMBRANE REACTOR WITH DIFFERENT OPERATION MODES

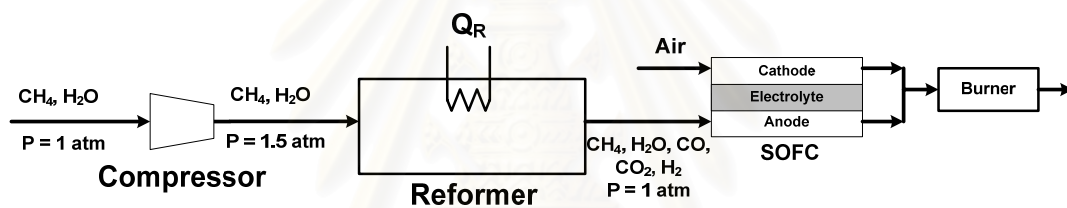
In this chapter, the characteristics of the methane-fuelled SOFC systems integrated with a palladium membrane reactor with different operation modes (i.e., high pressure compressor (MR-HPC), vacuum pump (MR-V) and combined high pressure compressor and vacuum pump (MR-HPC-V)) were investigated. Their economic analysis was compared with that of the SOFC system integrated with a conventional reformer in order to find a suitable operation mode of the membrane reactor for integrating with the SOFC system.

6.1 Results and Discussion

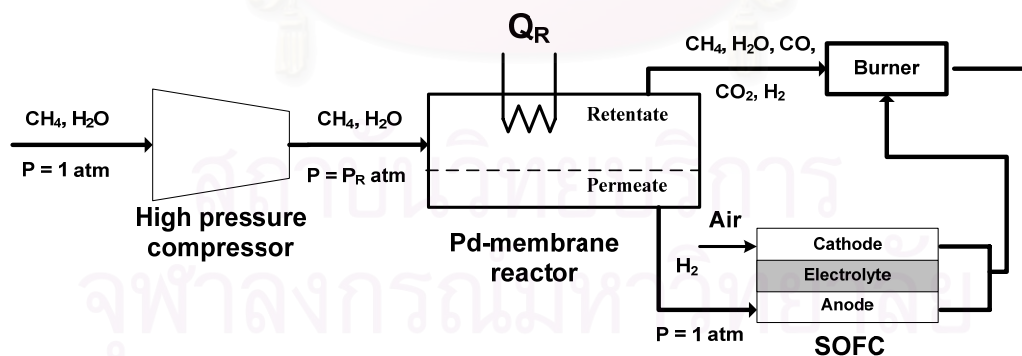
The diagrams of different SOFC systems are illustrated in Fig. 6.1. In a conventional system (Fig. 6.1a.), methane and steam are fed to a reformer where they are converted to CO, CO₂ and H₂. The product gas containing hydrogen at a low concentration is directly introduced to the SOFC stack where electrical power is generated. The SOFC exhaust gases are combusted in a burner whose heat can be utilized for energy-demanding units in the system. When the conventional reformer is replaced by a membrane reactor, pure hydrogen is extracted from the reaction mixture and fed to the SOFC stacks. The term “hydrogen recovery (ξ)” is defined as the mole of hydrogen extracted by the membrane divided by the mole of hydrogen theoretically produced based on the mole of methane feed (4 mol of H₂: 1 mol of CH₄). The term “fuel utilization (U_f)” represents the mole of hydrogen electrochemically consumed within the stack divided by the mole of hydrogen theoretically produced based on the mole of methane feed.

Three operation modes of a membrane reactor are considered in this study. For the membrane reactor with a high pressure compressor (MR-HPC) (Fig. 6.1b.), the pressure of the permeation is kept at 1 atm while the driving force for hydrogen permeation is enhanced by using the high pressure compressor. In the second case (Fig. 6.1c.), the permeation side is kept at below atmospheric pressure by using a vacuum pump. It is noted that the low pressure compressor is still required at the inlet of the conventional reformer and the membrane reactor in order to feed the reactants to the system. In the last configuration (Fig. 6.1d.), both the high pressure compressor and the vacuum pump are used. In all SOFC systems with the membrane reactor, the residue gas in the reaction gas mixture and the exhausted gas from the SOFC stacks are combusted in the burner similar to the case with the conventional reformer.

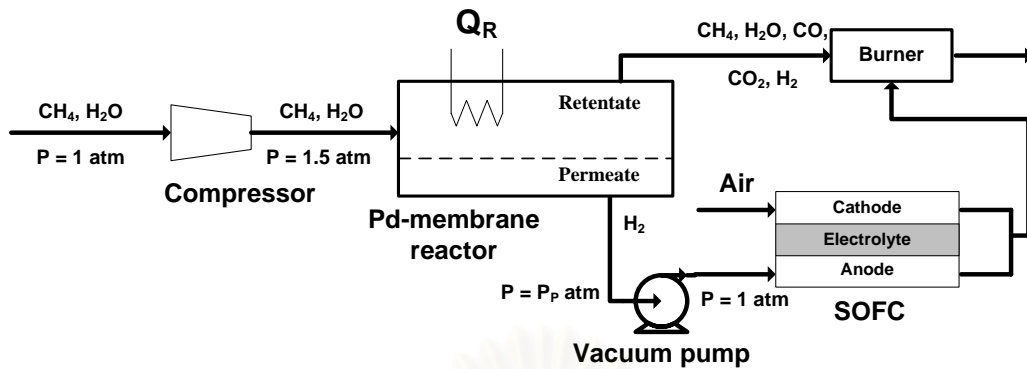
(a)



(b)



(c)



(d)

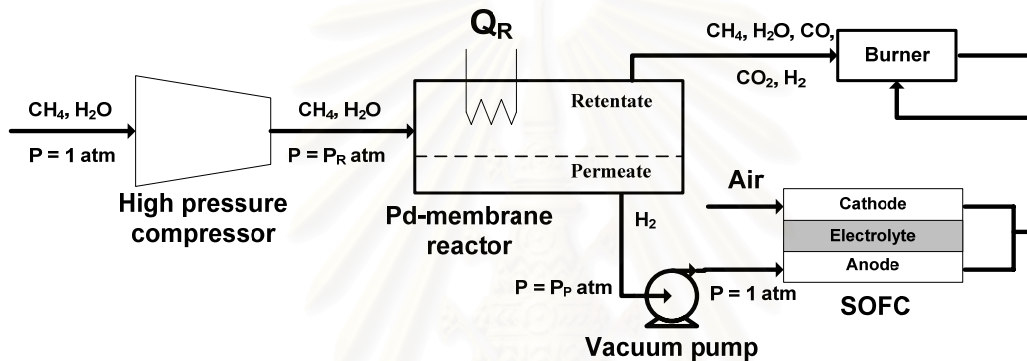


Fig. 6.1 Schematic diagrams of SOFC systems with different operation modes:

(a) conventional reformer, (b) MR-HPC, (c) MR-V, (d) MR-HPC-V.

The study began with the model validation of the methane steam reforming in a conventional reformer. The calculations were based on the condition reported in the literature (Pfafferodt *et al.*, 2005); i.e., $\text{H}_2\text{O}:\text{CH}_4$ ratio = 3, GHSV = 1067 h^{-1} and reformer pressure = 1 atm. As shown in Fig. 6.2, it is obvious that our calculation results are in good agreement with those reported by Shu *et al.*, 1994 for all temperature ranges (723-773 K). The deviations are in the range between 3-5%. Then, the SOFC model was verified. Fig. 6.3 shows the relationship between the power density and current density at three temperature levels; i.e., 1023, 1073 and 1123 K. In the simulation, pure hydrogen was fed to the SOFC and the fuel utilization (U_f) was kept at 80%. Again, our calculations show good agreement with those reported in the previous literature (Hernandez-Pacheco *et al.*, 2005)

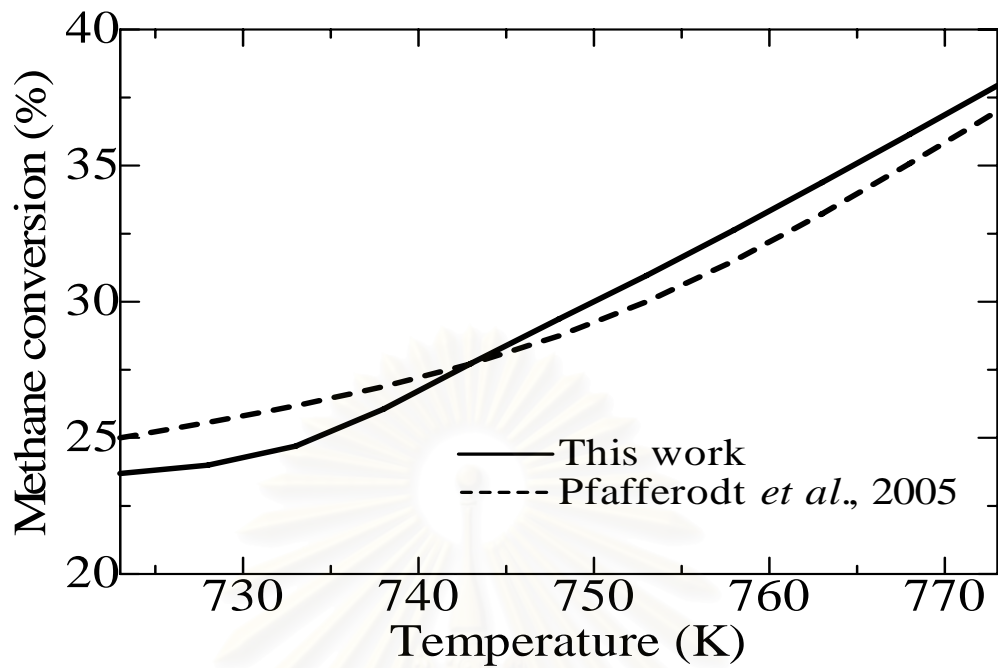


Fig. 6.2 Validation of the reformer model with experimental results from the literature (Pfafferodt *et al.*, 2005) ($P = 1$ atm and $H_2O:CH_4 = 3$).

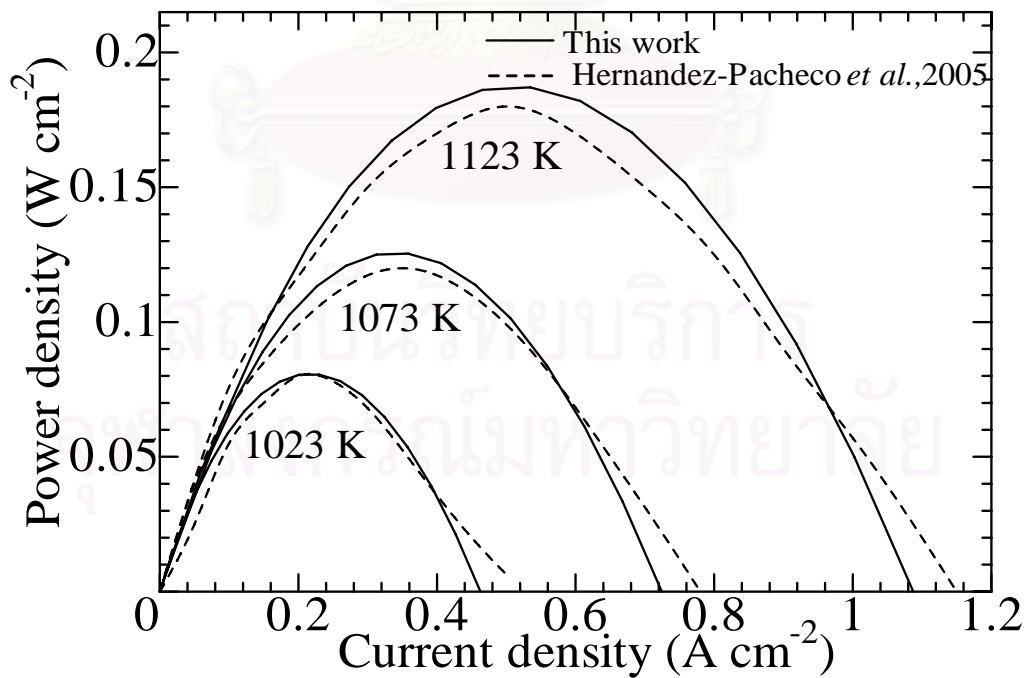


Fig. 6.3 Validation of SOFC model with results from the literature (Hernandez-Pacheco *et al.*, 2005) (Pure H_2 feed and $U_f = 80\%$).

In order to demonstrate the benefit from replacing of the conventional reformer with the membrane reactor, the plots of the power density and electrical efficiency against the current density of different systems are compared (Fig. 6.4). The fuel utilization and operating temperature were kept at 80% and 1073 K, respectively. It is obvious that the SOFC system with the membrane reactor offers higher power density and electrical efficiency than that with the conventional reformer, particularly at higher values of hydrogen recovery (ξ). At $\xi = 95\%$, the increase of the maximum power density of 25% can be achieved. However, when the membrane reactor is operated at too low hydrogen recovery (e.g., $\xi = 80.6\%$), the use of the palladium membrane reactor can not compete the use of the conventional reformer due to the fuel depletion in the anode of the SOFC. Therefore, the membrane reactor has to be operated at a sufficiently high hydrogen recovery (ξ).

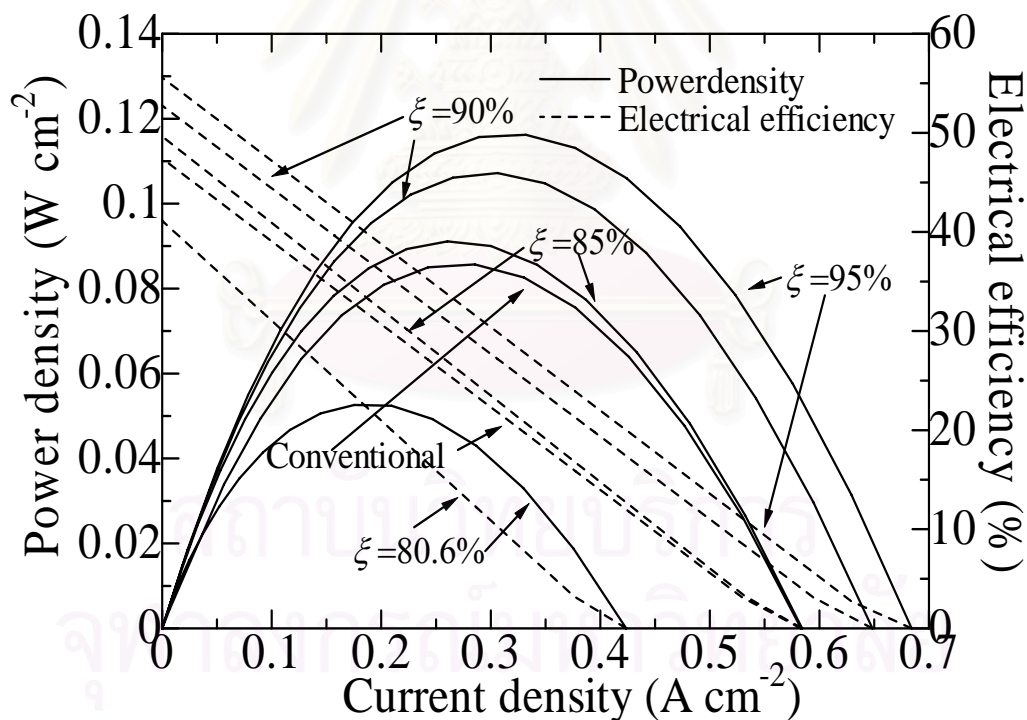


Fig. 6.4 Improvement of SOFC performance by using Pd membrane reactor ($U_f=80\%$ and $T_{SOFC} = 1073$ K).

According to the operation of membrane reactors, various operation modes are possible for enhancing the driving force of hydrogen permeation through the

membrane. The selection of suitable operation mode and operating condition should be based on the consideration of the required membrane area and power consumption. Fig. 6.5 shows the effect of the compressor pressure on the required palladium membrane area and the required power for the case of the membrane reactor with a high pressure compressor (MR-HPC). The pressure in the permeation side was always kept at 1 atm. The results indicate that when the compressor is operated at higher pressures, the membrane reactor requires less membrane area but higher compressor power.

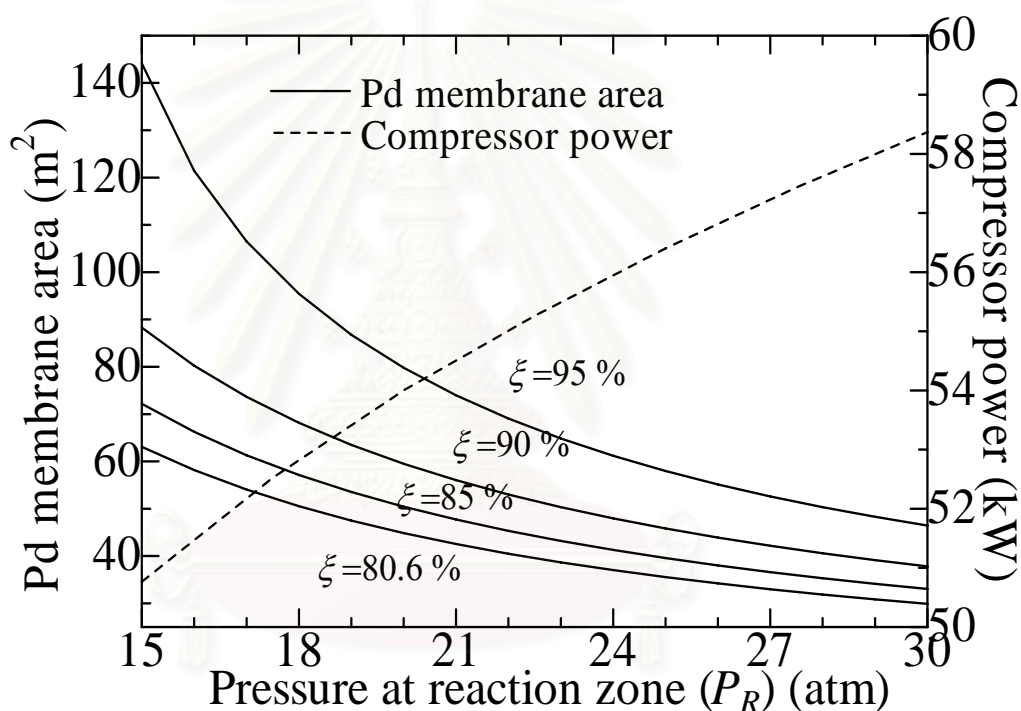


Fig. 6.5 Effect of reaction pressure on required Pd membrane area and compressor power ($T = 773$ K, $P_R = 1$ atm and $H_2O:CH_4 = 3$).

For the membrane reactor with a vacuum pump (MR-V), the results shown in Fig. 6.6 indicate that when the vacuum pump pressure is reduced, the required membrane area decreases initially and then levels off but the overall power consumption for operating the vacuum pump and the low pressure compressor continuously increases. Comparison between the MR-HPC and the MR-V reveals that the MR-V generally requires less membrane area but higher power consumption.

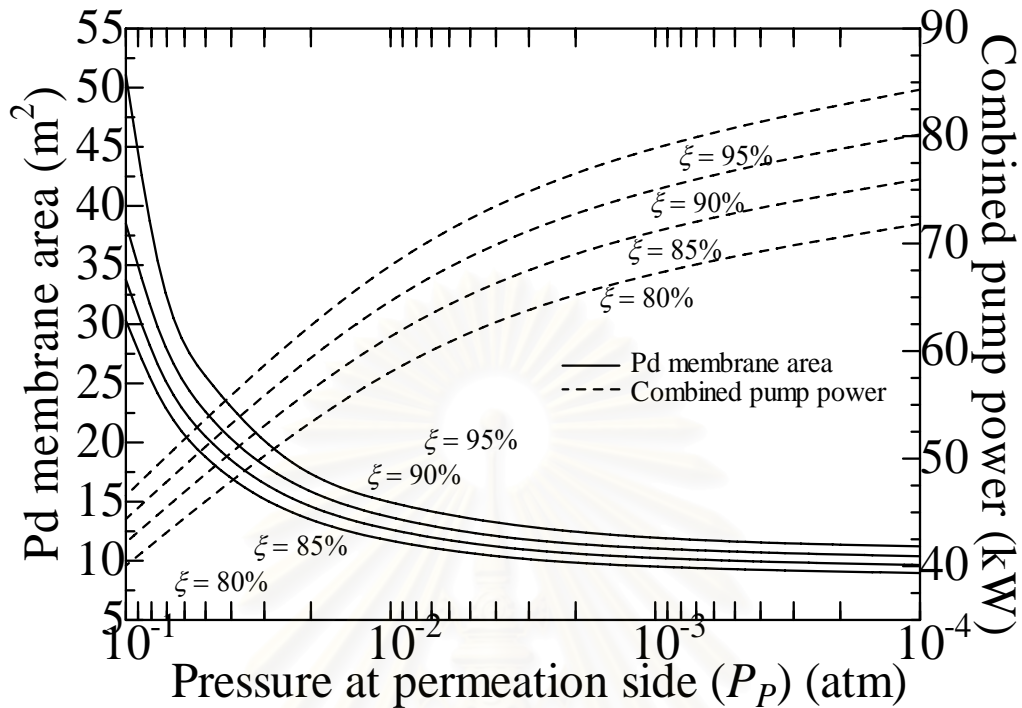


Fig. 6.6 Effect of permeation pressure on required Pd membrane area and vacuum pump power ($T_{SOFC} = 773$ K, $P_p = 1$ atm and $H_2O:CH_4 = 3$).

The other operation mode of the membrane reactor considered in this study is the combination of both high pressure compressor and vacuum pump (MR-HPC-V). Fig. 6.7 shows the effects of the compressor pressure (between 2-5 atm) and the vacuum pump pressure (between 0.01-0.2 atm) on the required membrane area and the power consumption for $\xi = 90\%$. Similar trends as the effects of the compressor pressure and the vacuum pump pressure on the required membrane area and the power consumption are observed. For comparison among the three operation modes, considering the case with the required membrane area of 25 m^2 and the hydrogen recovery of 90%, it is obvious that within the range of pressure studied in the MR-HPC, even with the highest pressure (30 atm), the hydrogen recovery of 90% can not be achieved. For the MR-V, the required vacuum pump pressure and power consumption are about 0.035 atm and 50 kW, respectively. For the MR-HPC-V, the power consumption also depends on the choice of the operating pressure of the high pressure compressor. At $P_R = 2, 3, 4$ and 5 atm, the vacuum pump pressures are 0.088,

0.127, 0.162 and 0.198 atm, respectively while the required power consumptions are 50, 52.5, 54 and 55 kW, respectively. It is therefore obvious for the MR-HPC-V that the load of the vacuum pump can be reduced by using the high pressure compressor.

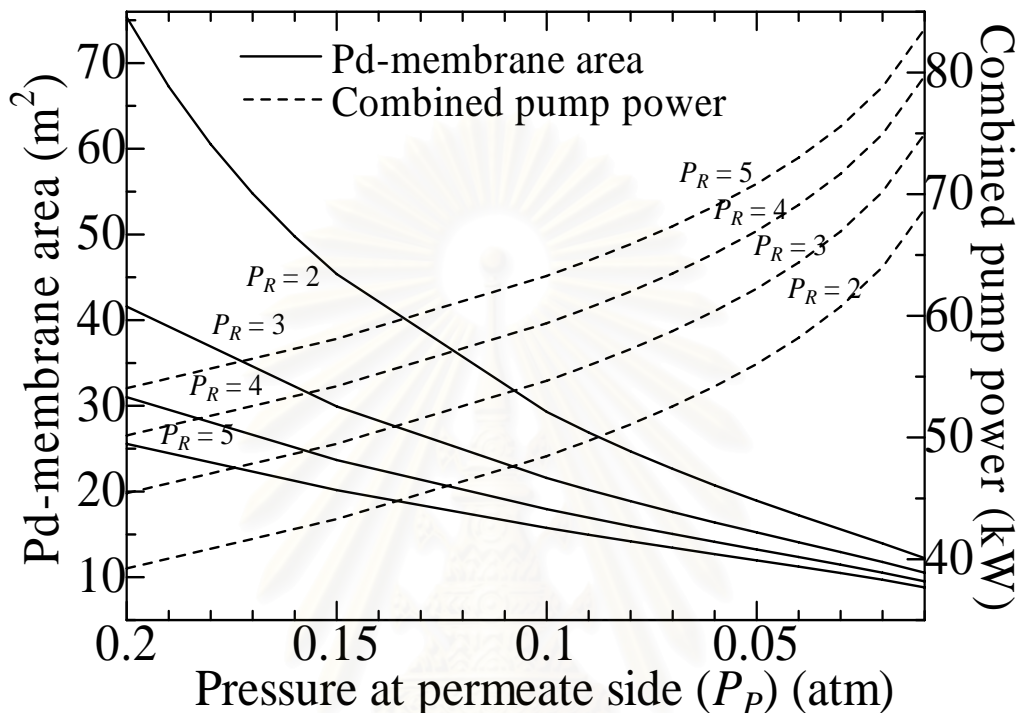


Fig. 6.7 Effect of reaction and permeation pressure on required Pd membrane area and power consumption ($\xi = 90\%$, $T_{SOFC} = 773$ K and $H_2O:CH_4 = 3$).

It is clear from the previous paragraphs that the operation modes of the membrane reactor and the operating condition (pressure) play an important role on the membrane area and the power requirement. The economic analysis is essential for selecting a suitable operation mode of the membrane reactor for the SOFC system. Table 6.1 provides an example of the economic analysis of the SOFC systems with different operation modes. In all systems, the hydrogen recovery (ξ) and the fuel utilization (U_f) were set at 90% and 80%, respectively. The compressor was operated at 30 atm for the MR-HPC while the vacuum pump was operated at 0.035 atm for the MR-V. For the MR-HPC-V, the compressor and the vacuum pump were operated at 5 and 0.135 atm, respectively. The net electrical power was 371.4 kW corresponding to the overall electrical efficiency of 45.3%. However, the actual electrical power to

be generated for the cases with the conventional reformer, MR-HPC, MR-V and MR-HPC-V are 373.7, 429.8, 426.8 and 427.5 kW, respectively. The additional powers are required to operate the compressor and/or vacuum pump in the systems. It should be noted that for all cases the heat obtained from the burner and the SOFC is sufficient to provide to all heat-demanding units in the systems. Regarding the required SOFC area, it is clear that the uses of membrane reactors could reduce the requirement of the overall SOFC area; however, they require additional cost on the palladium membrane and the compressor and/or vacuum pump. The total capital cost of each system could be calculated. The values of the total capital cost followed the order: MR-HPC-V < MR-HP-C < MR-V < conventional. Obviously, based on the same net electrical power output, the total capital costs of the SOFC systems with the membrane reactors were lower than that of the conventional SOFC system. The MR-V was the most expensive among different operation modes due to the expensive vacuum pump. The MR-HPC-V was found to be the most attractive operation mode under this condition.

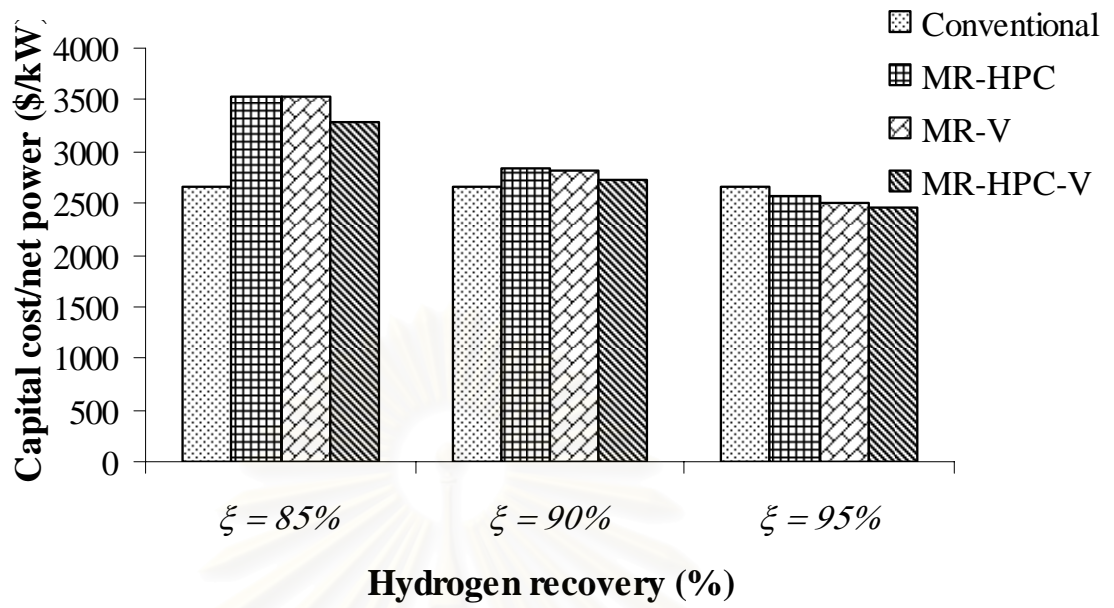
The economic analysis at various values of hydrogen recovery (85, 90 and 95%) and overall electrical efficiency (40.7, 45.3 and 47.7%) were considered and the corresponding values of the total capital cost/net electrical power were calculated for the cases with the conventional reformer, MR-HPC, MR-V and MR-HPC-V. As shown in Fig. 6.8, the total capital cost/net electrical power is dependent on the hydrogen recovery, electrical efficiency and operation mode. In all systems, the values of the total capital cost/net electrical power increases with the increase of the electrical efficiency because the SOFC needs to operate at a lower power density to achieve the high electrical efficiency, resulting in the higher SOFC area and consequently the higher total capital cost. When the system is operated at a higher hydrogen recovery, the value of the total capital cost/net electrical power decreases due to the improved power density of the SOFC as demonstrated earlier in Fig. 6.4. It is observed that for $\eta = 40.7\%$, the replacement of the conventional reformer with the membrane reactor is not attractive at $\xi = 85\%$. However, it becomes quite comparable at $\xi = 90\%$ and attractive at $\xi = 95\%$. At high values of electrical efficiency, the use of membrane reactor offers lower total capital cost/net electrical power than the use of the conventional reformer. Comparison between the different operation modes of the SOFC systems with membrane reactor reveals that the MR-

HPC-V is the most attractive operation mode in all ranges of hydrogen recovery and electrical efficiency.

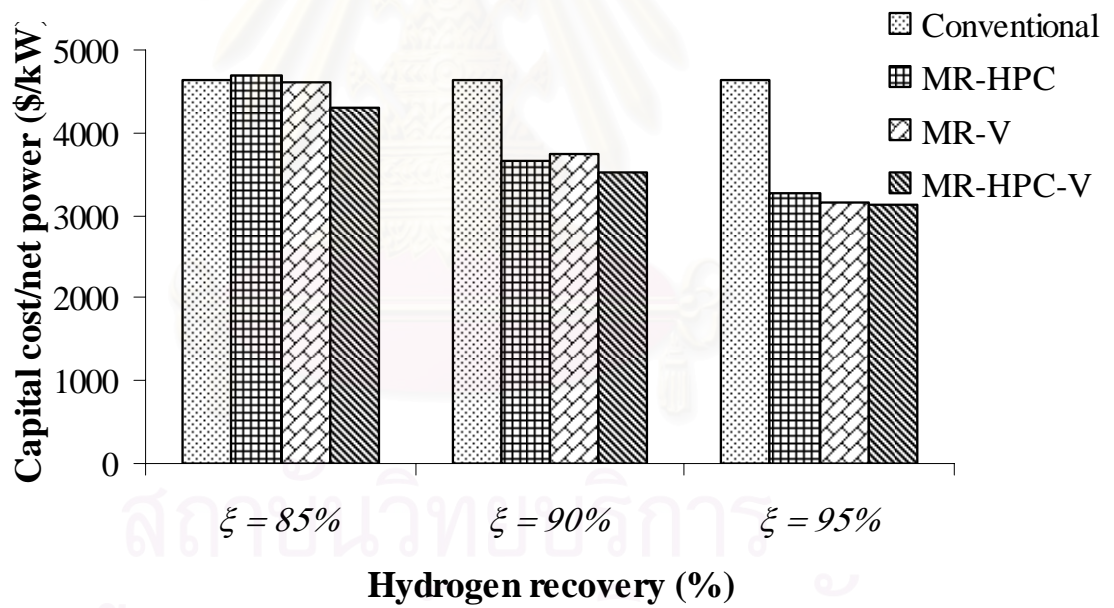
Table 6.1 Economic analysis of the SOFC systems with different operation modes.

	Conventional	MR-HPC	MR-V	MR-HPC-V
Temperature of reformer (K)	923	773	773	773
Fuel utilization (U_f) (%)	80	80	80	80
H ₂ Recovery (%)	-	90	90	90
Operating voltage (V)	0.610	0.696	0.691	0.692
Electrical power (kW)	376.7	429.9	426.8	427.5
Pressure at reaction side				
(P_R) (atm)	1.5	30	1.5	5
Compressor Power (kW)	5.3	58.4	5.3	20.3
Pressure at permeation side				
(P_P) (atm)	-	1.00	0.035	0.135
Vacuum pump power (kW)	-	-	50.	35.9
Net electrical power (kW)	371.4	371.4	371.4	371.4
Efficiency (%)	45.26	45.26	45.26	45.26
Pd membrane area (m ²)	-	38.17	19.12	18.76
SOFC area (m ²)	1143	866.72	877.86	843.34
Cost of Pd membrane				
(746 \$ m ⁻²)	-	28,476	14,260	13,995
Cost of SOFC (1500 \$ m ⁻²)	1,714,500	1,300,080	1,316,790	1,265,010
Saving cost on SOFC (\$)	-	414,420	397,710	449,490
Capital cost of compressor (\$)	5,979	32,194	5,979	17,200
Capital cost of vacuum pump (\$)	-	-	51,700	13,652
Saving cost of SOFC over Pd membrane (\$)	-	385,944	383,450	435,495
Total capital cost (\$)	1,720,479	1,360,750	1,388,729	1,309,857
Total capital cost/electrical energy (\$/kW)	4,568	3,166	3,254	3,064
Total Capital cost /net power (\$/kW)	4,633	3,664	3,739	3,527

(a)



(b)



(c)

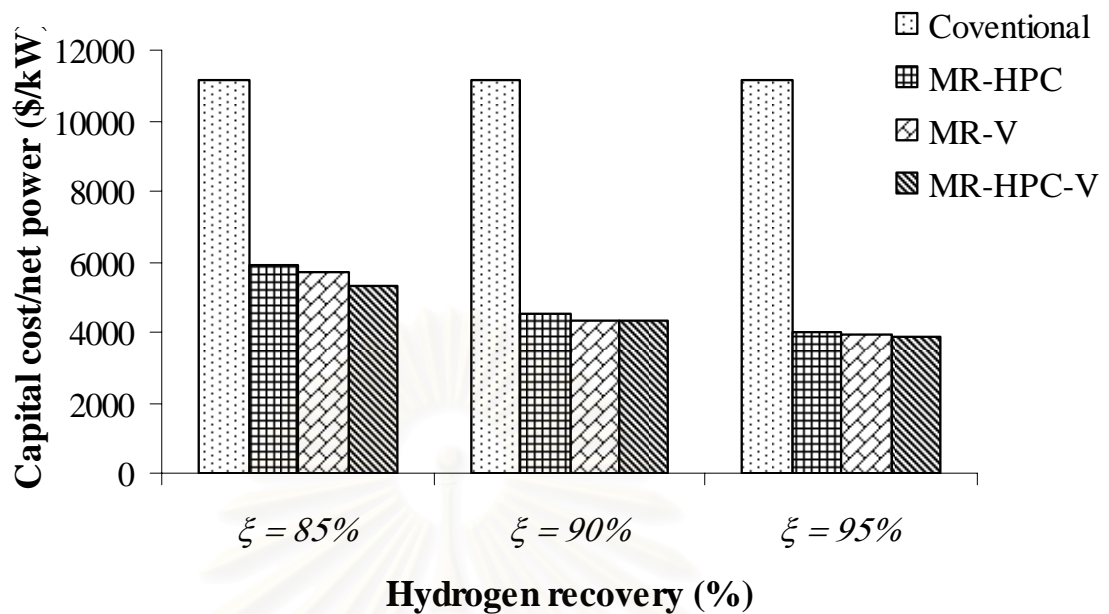


Fig. 6.8 Economic analysis of different SOFC systems: (a) $\eta = 40.7\%$,
 (b) $\eta = 45.3\%$ and (c) $\eta = 47.7\%$ ($U_f = 80\%$ and $T = 1073$ K).

6.2 Conclusion

Performance of the SOFC systems fed by methane was analyzed to investigate the potential benefit from replacing the conventional reformer with the palladium membrane reactor. Obviously, the use of the palladium membrane reactor can improve the power density of the SOFC. Three operation modes of membrane reactors; i.e., MR-HPC, MR-V and MR-HPC-V were considered. The economic analysis of the different systems revealed that the total capital cost/net electrical power is dependent on hydrogen recovery, electrical efficiency and operation mode of the membrane reactor. The use of the palladium membrane reactor becomes attractive over the conventional reformer when the system is operated at high values of electrical efficiency and hydrogen recovery. Finally, it was demonstrated that the MR-HPC-V was the best operation mode for integration with the SOFC system.

Chapter VII

SOLID OXIDE FUEL CELL SYSTEMS INCORPORATED WITH CaO-CO₂ CAPTURE UNIT

Nowadays, global warming is one of the most concerning issues. Carbon dioxide is considered as a major cause of the green house effect problem. Therefore, novel processes which offer low CO₂ emission are desired. An integration of a solid oxide fuel cell (SOFC) with a CaO-CO₂ capture unit is an attractive choice for electrical power generation. Due to high electrical efficiency of SOFC, lower amount of fuel is consumed and therefore lower amount of CO₂ is generated. The use of a CaO-CO₂ capture unit further reduces the amount of CO₂ emitted to the environment. In this study, various SOFC systems integrated with carbonation-calcination systems (SOFC-CaO system) were investigated. The effects of location of CaO-CO₂ acceptor in the SOFC system and other operating parameters were studied in terms of amount of reduced CO₂ emission, SOFC performance and economic analysis.

7.1 Results and Discussion

The schematic diagram of a conventional SOFC system fed by methane (CH₄) is shown in Fig. 7.1. The conventional SOFC system is composed of a reformer, a SOFC and a burner. First, methane and water are fed to the reformer where methane steam reforming reaction (MSR) and water gas shift reaction (WGSR) take place. Then, the reformed gas, mixtures of hydrogen, carbon monoxide, carbon dioxide and unreacted reagents, is fed to the SOFC unit. Oxygen is reduced and permeated through an electrolyte and then reacted with hydrogen at the anode chamber. After that, the exhaust gas is fed to the burner where residue fuels are combusted, providing heat to other parts of the system. In this study, the conventional SOFC system operates at $U_f=90\%$, $T_{ref}=973$ K and $T_{SOFC}=1073$ K. The gas compositions in each streamline are presented in Fig. 7.1. Methane of 1 mol.s^{-1} and water of 3 mol.s^{-1} were fed to the system. The CO₂ flow rates after the reformer, after SOFC and after the burner were 0.4247 , 0.8888 and $0.9393 \text{ mol.s}^{-1}$, respectively. It can be seen that the

amounts of CO_2 are different among the different streams. Therefore, different amount of CO_2 can be captured when the CaO-CO_2 acceptor is installed at different locations in the system.

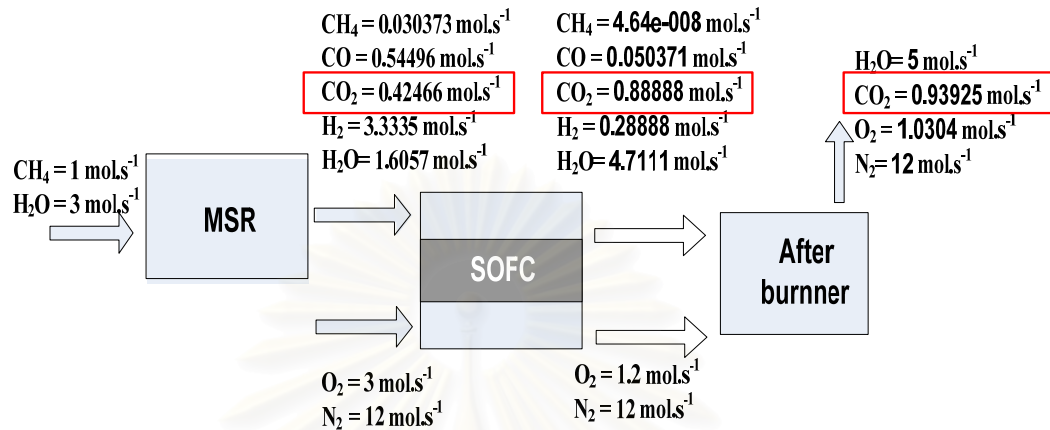
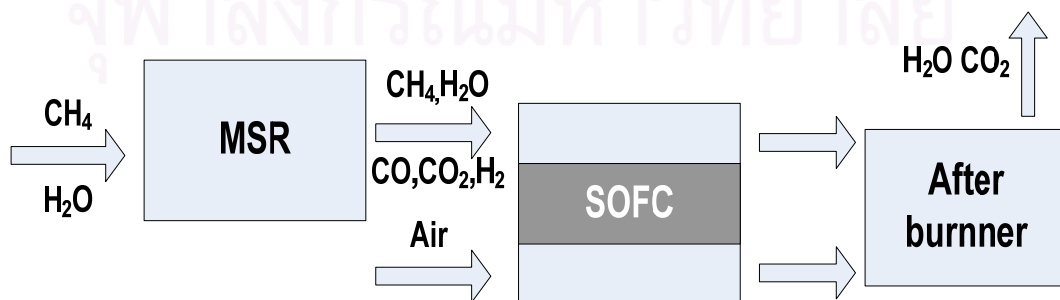


Fig. 7.1 Flow rates of different components in the conventional SOFC system (at $U_f=90\%$, $T_{ref}=973 \text{ K}$ and $T_{SOFC}=1073 \text{ K}$).

The SOFC systems consisting of a reformer, an SOFC and a burner were integrated with carbonation-calcination systems (SOFC-CaO system). Figs. 7.2(a)-(d) show the SOFC systems of different cases; i.e., (a) without the acceptor, (b) the SOFC system incorporated with CaO-CO_2 acceptor before SOFC unit (CaO-Before-SOFC), (c) the SOFC system incorporated with CaO-CO_2 acceptor after SOFC unit (CaO-After-SOFC) and (d) the SOFC system incorporated with CaO-CO_2 acceptor after the afterburner unit (CaO-After-Burner). As mentioned earlier, the amount of CO_2 produced is different among the streams in the system. Hence, the location of CaO -acceptor could affect the performance of SOFC system.



a.)

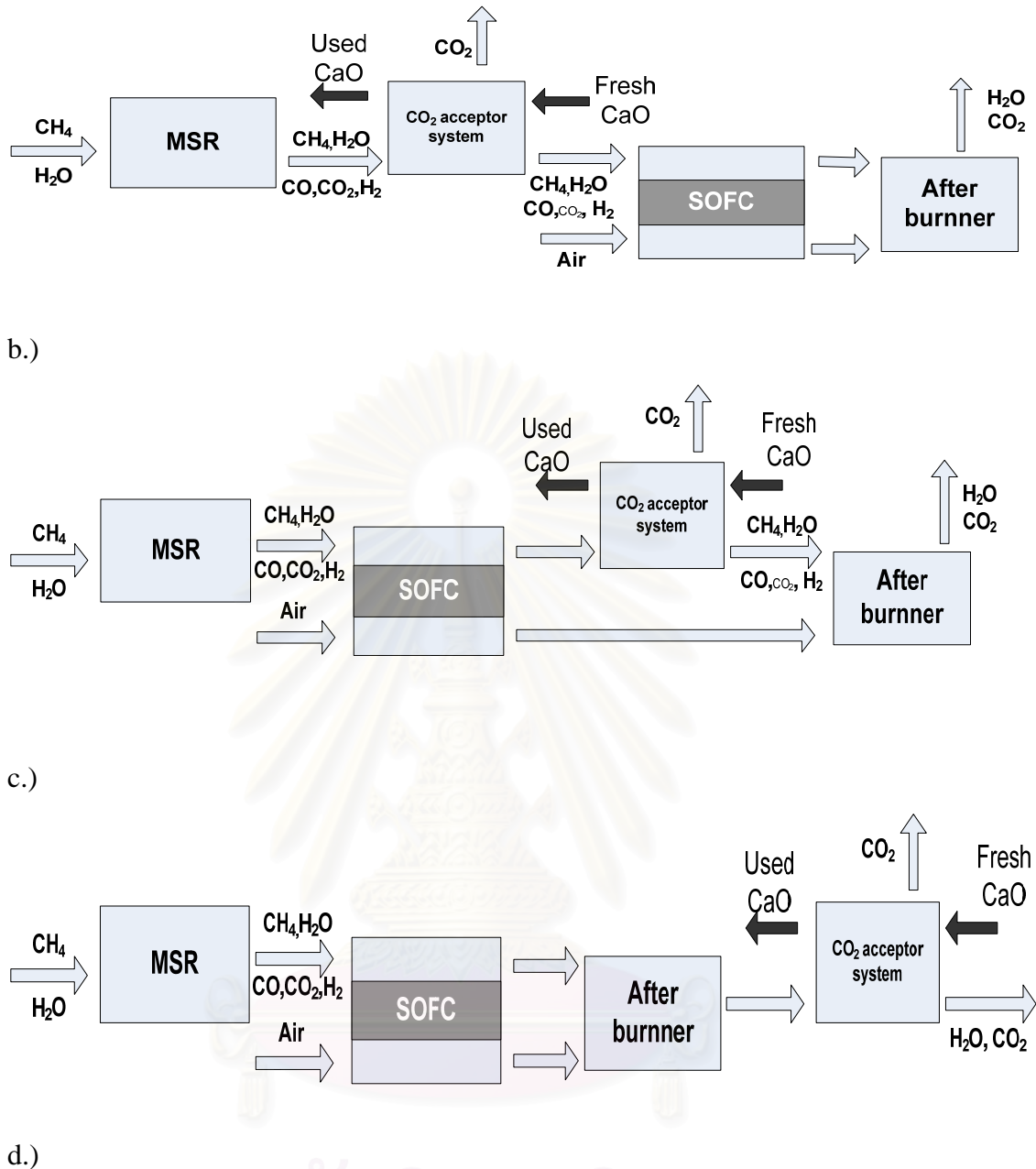
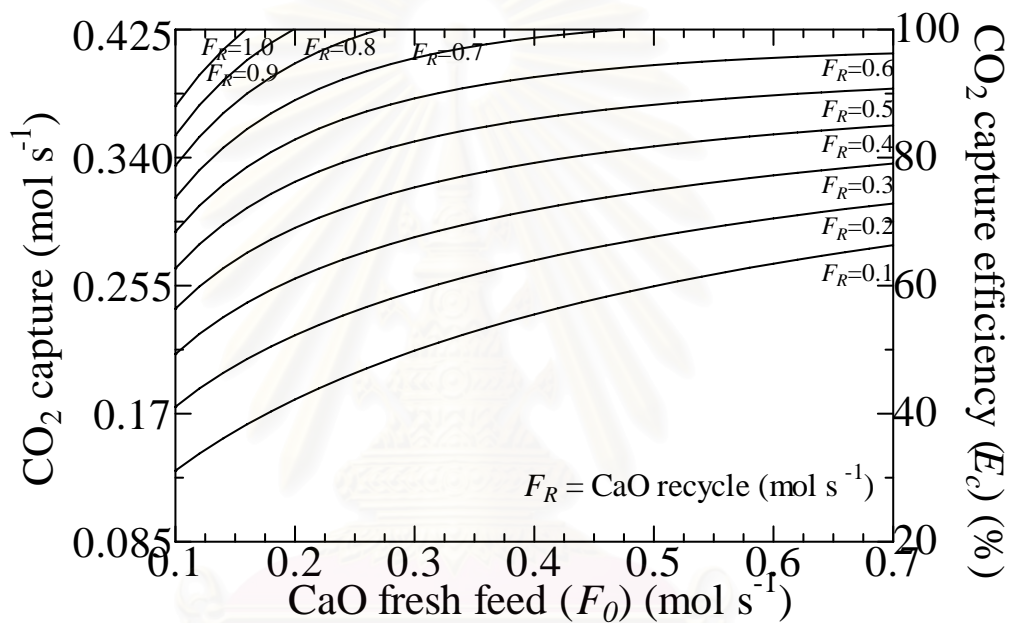


Fig. 7.2 a) Conventional SOFC system, b) CaO-Before-SOFC, c) CaO-After-SOFC and d) CaO-After- burner.

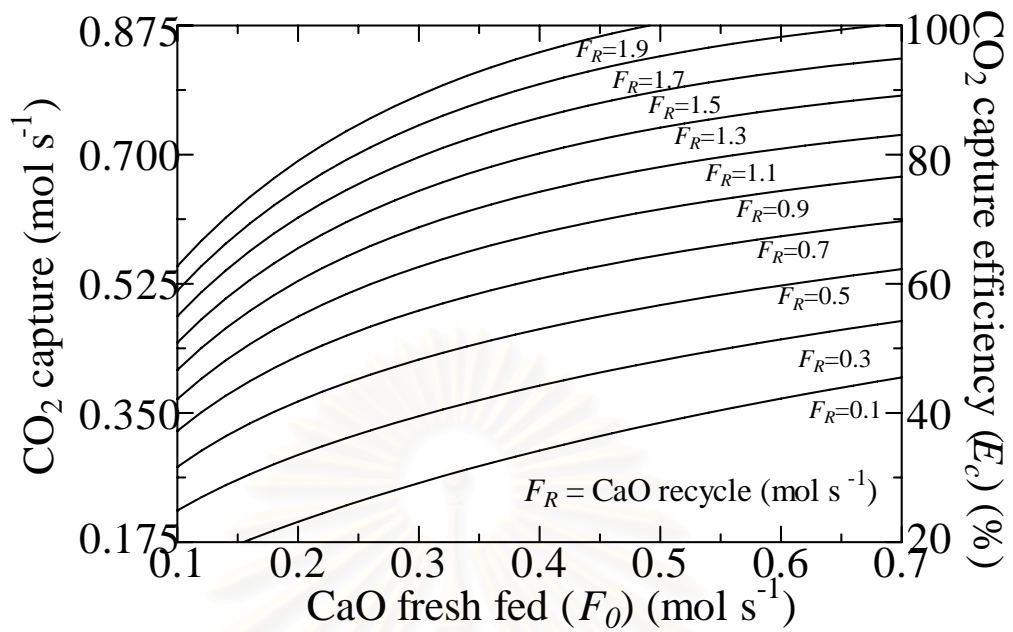
The performance of a CaO-CO₂ acceptor was generally influenced by amount of fresh CaO feed (F_0), recycle rate of CaO (F_R) and the composition of stream inlet to the acceptor. Figs. 7.3 (a)-(d) show the effects of fresh CaO feed (F_0) and recycle rate of CaO (F_R) on maximum CO₂ capture efficiency (E_c) for the CaO-Before-SOFC, CaO-After-SOFC and CaO-After-Burner, respectively. As indicated in Eq. (4.60), the maximum CO₂ capture efficiency (E_c) depended on amount of fresh CaO feed (F_0),

recycle rate of CaO (F_R) and the concentration of CO₂ in the stream inlet. All figures show that CO₂ capture efficiency increased with increasing fresh CaO feed (F_0) and recycle rate of used CaO (F_R). To obtain higher efficiency of CO₂ capture, the value of F_R and F_0 can be adjustable. The maximum CO₂ capture efficiency (E_c) was increased by increasing fresh CaO feed (F_0) or recycle rate of CaO (F_R). For example, if E_c is required as high as 60% capture, the CaO-CO₂ acceptor can operate at $F_0=0.1$ mol s⁻¹ and $F_R=0.556$ mol s⁻¹, or at $F_0=0.2$ mol s⁻¹ and $F_R=0.333$ mol s⁻¹, or at $F_0=0.3$ mol s⁻¹ and $F_R=0.222$ mol s⁻¹, etc.

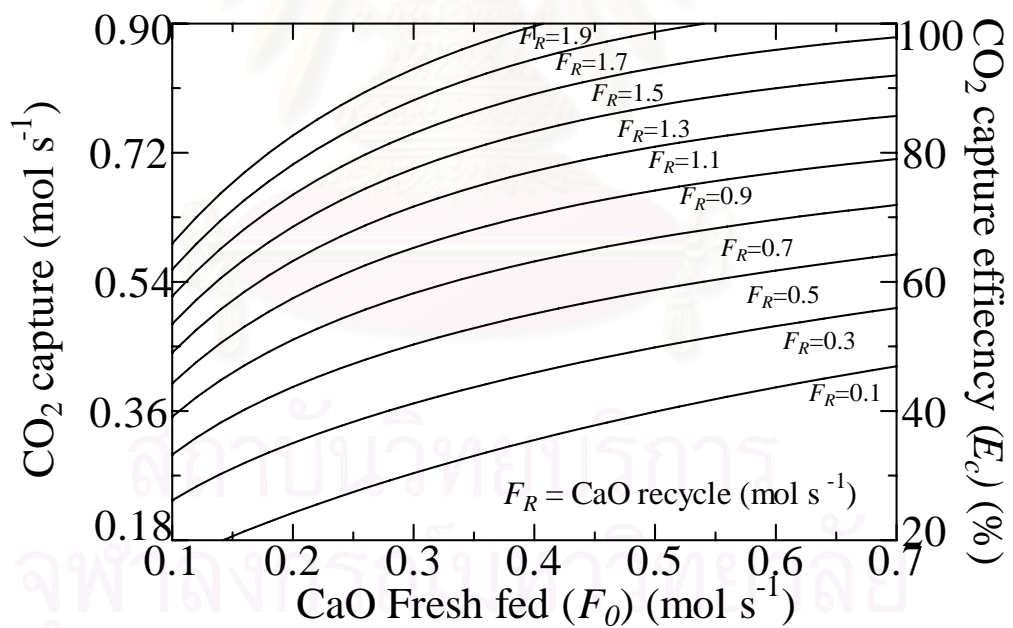


a.)

สถาบันวิทยบริการ
จุฬาลงกรณ์มหาวิทยาลัย



b.)



c.)

Fig. 7.3 Effect of CaO fresh feed (F_0) and CaO recycle rate (F_R) on CO₂ capture efficiency (E_c) a.) CaO-Before-SOFC, b.) CaO-After-SOFC and c.) CaO-After-Bunner. (At $T_{ref} = 973$ K).

Fig. 7.4 shows the partial pressures of produced CO_2 and H_2 in the stream to be fed to the SOFC when operating at various reforming temperatures at the base condition as shown in Table 7.1. The partial pressure of produced CO_2 initially increased and dropped at higher temperatures. This is because methane steam reforming (MSR) is an endothermic reaction while the water gas shift reaction (WGRS) is an exothermic reaction. At higher temperatures, the MSR is the most dominant reaction. The results show the maximum produced CO_2 is at about 873 K and the H_2 partial pressure is highest at 900-1000 K. It should be noted that the conventional line can refer to the feed composition of the anode inlet for the case of CaO-After-SOFC and CaO-After-Burner. The partial pressure of hydrogen before feeding into the SOFC is increased in the case of the CaO-Before-SOFC system whereas those of other CaO-SOFC systems are similar to that of the conventional one. Consequently, the CaO-Before-SOFC system can realize other potential benefits from the increase of H_2 partial pressure, not observed in other SOFC-CaO systems.

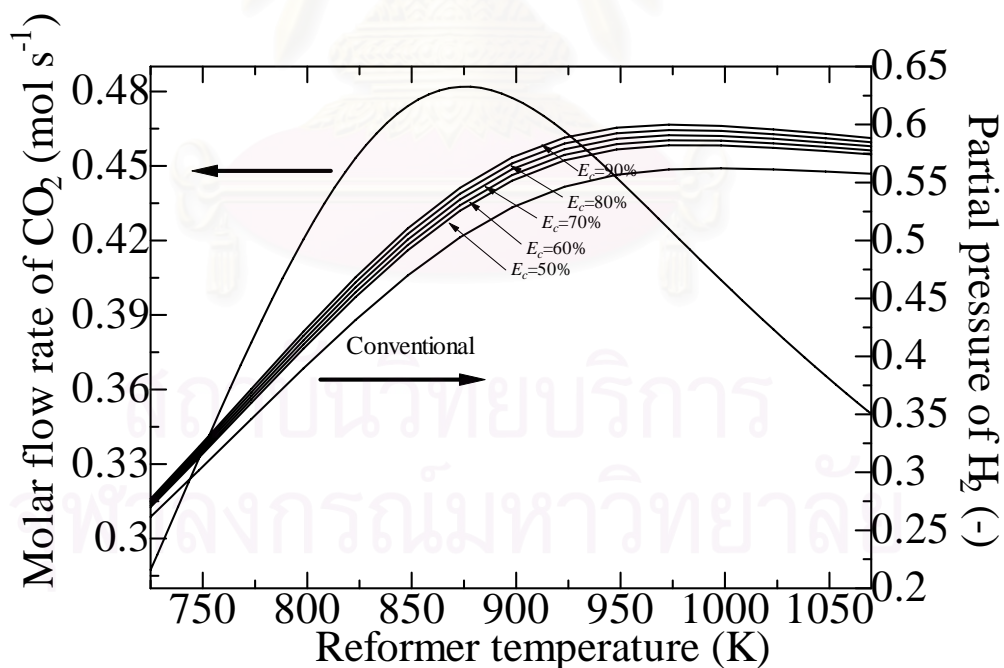


Fig. 7.4 Effect of reforming temperature on produced CO_2 and effect of CO_2 capture efficiency (E_c) on partial pressure of H_2 .

Table 7.1 Standard condition.

Parameter	Value
CH ₄ input	1 (mol/s)
Reforming H ₂ O:CH ₄ ratio	3 (-)
U_f (fuel utilization)	80 (%)
SOFC Temperature	1073 (K)
Input Air:CH ₄ ratio	15 (-)
Conventional reformer temperature	973 (K)
Membrane reactor temperature	773 (K)

To demonstrate the potential benefits from the increase of hydrogen partial pressure, the SOFC performance at various values of fuel utilization (U_f) was illustrated in Fig. 7.5. The reforming temperature (T_{ref}) and SOFC temperature was selected at 973 K and 1073 K, respectively. Solid lines represent the obtained power density of the conventional SOFC system at different values of U_f while dashed lines illustrate the power density of the CaO-Before-SOFC system at different values of E_c ranging from 50% to 90%. Again, the obtained power density from the CaO-After-SOFC and the CaO-After-Burner were the same as that of the conventional one. The results show that the CaO-Before-SOFC system can improve the SOFC performance. This is particularly pronounced at a higher efficiency of CO₂ capture. Figs. 7.6 (a) and (b) show performance improvement of the CaO-Before-SOFC system calculated by an increase of power density obtained from the CaO-Before-SOFC compared to that of the conventional system at 70% of maximum power density and maximum power density, respectively. The SOFC performance increases when increasing the fuel utilization and efficiency of CO₂ capture. At $E_c = 90\%$ and $U_f = 90\%$, the CaO-Before-SOFC can increase performance by 8% and 5.4%, respectively.

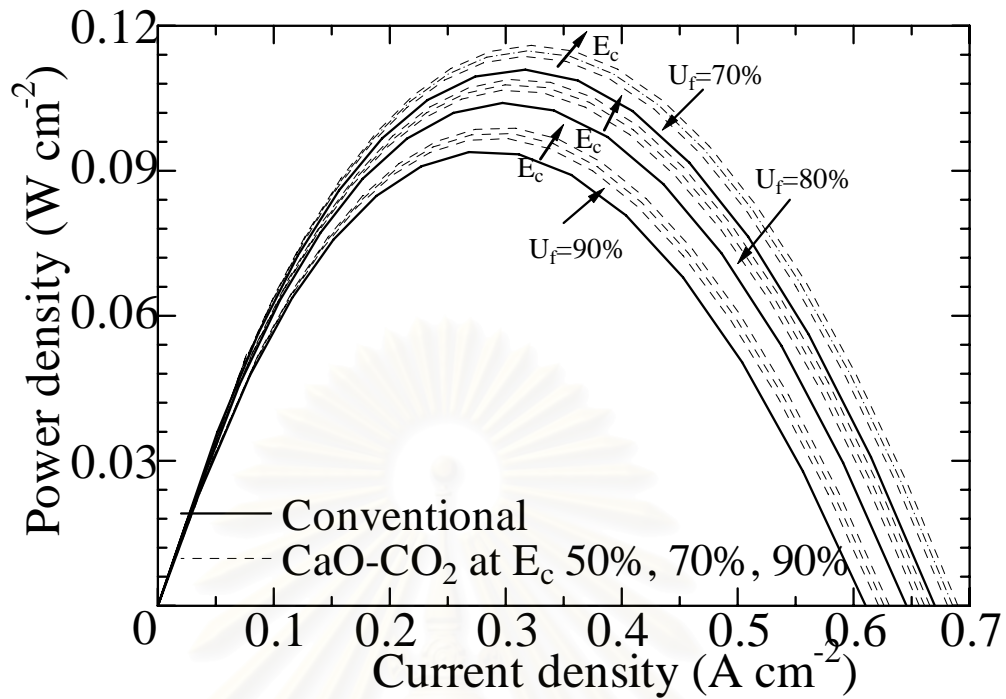
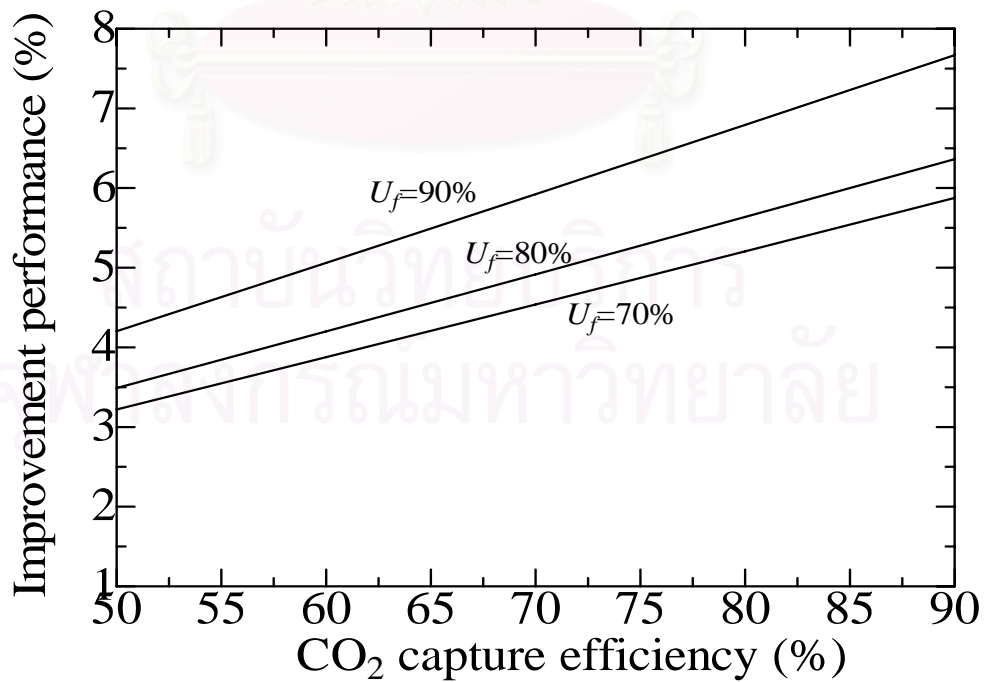
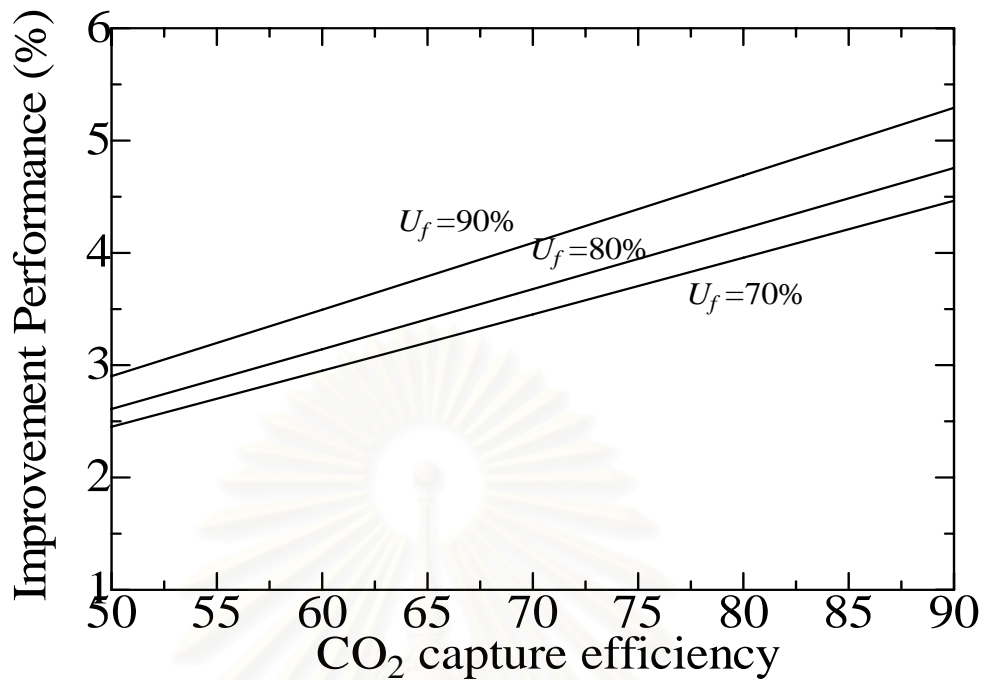


Fig. 7.5 Comparison SOFC performance of CaO-SOFC system with conventional SOFC system at varies CO_2 capture efficiency (E_c) and fuel utilization (U_f) (At $T_{ref}=973\text{ K}$, $T_{SOFC}=1073\text{ K}$).



a.)



b.)

Fig. 7.6 Performance improvement of CaO-SOFC system (At $V=0.56$ V, $T_{ref}=973$ K, $T_{SOFC}=1073$ K).

Then economic analysis of the SOFC-CaO systems are compared with those of the conventional SOFC system. Table 7.2 shows the economic analysis of different SOFC-CaO systems at $U_f = 90\%$, operating time = 5 years and the same net electrical power (about 340 kW, $\varepsilon=41.4\%$). It should be noted that the CaO-SOFC systems have to operate at a higher electrical power than that of the conventional SOFC system because additional power is required for operating a compressor. For the lowest compressor power, the amount of CaO in CaO-CO₂ acceptor has to be minimized. Fig. 7.7 shows that minimum of total CaO (F_0+F_R) in the CaO-CO₂ acceptor can be achieved with a proper selection of F_0 . Fig. 7.7.a, Fig. 7.7.b. and Fig. 7.7.c. show the results for the CaO-Before-SOFC, CaO-After-SOFC and CaO-After-Burner, respectively. In Tables 7.2 and 7.3, the minimum F_0+F_R was used to calculate the compressor power and operating cost of CaO. Total added cost was calculated by a summation of cost of SOFC area, cost of compressor and cost of CaO subtracted by cost of the conventional SOFC area. From Table 7.2 and Table 7.3, it was reported that the total amount of CaO in the CaO-Before-SOFC is higher than

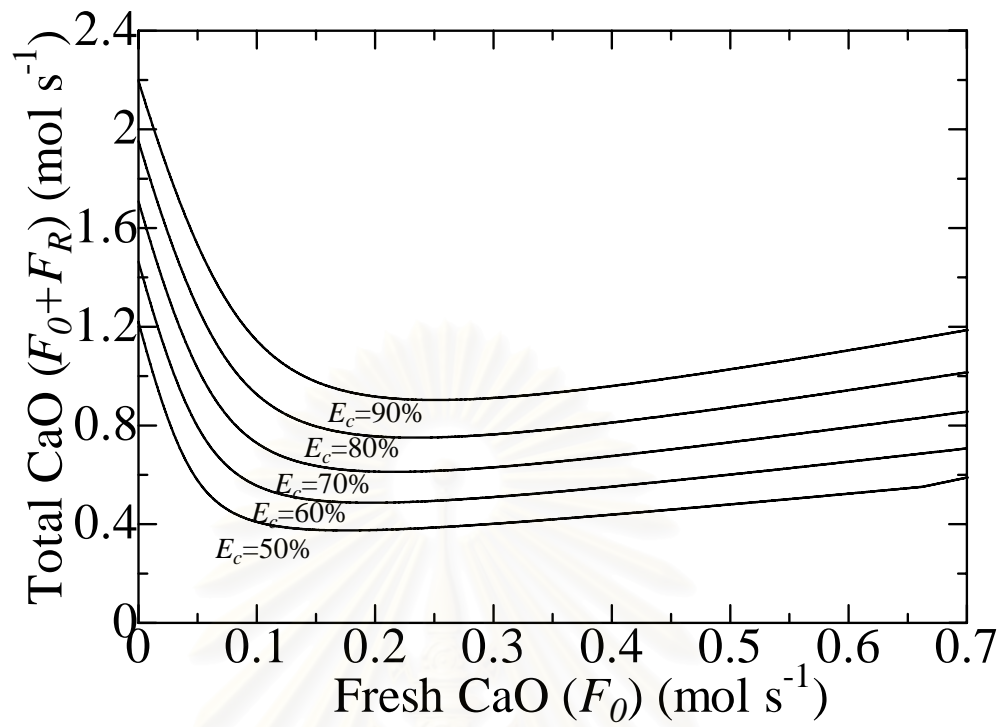
that of the other systems at the same amount of reduced CO₂. This is because amount of CO₂ capture in the CaO-Before-SOFC system is nearly ~100%. CO₂ adsorption almost reaches equilibrium; therefore, much higher amount of CaO is required.

Table 7.2 Economic analysis of CaO-SOFC system and conventional SOFC system ($U_f=80\%$)

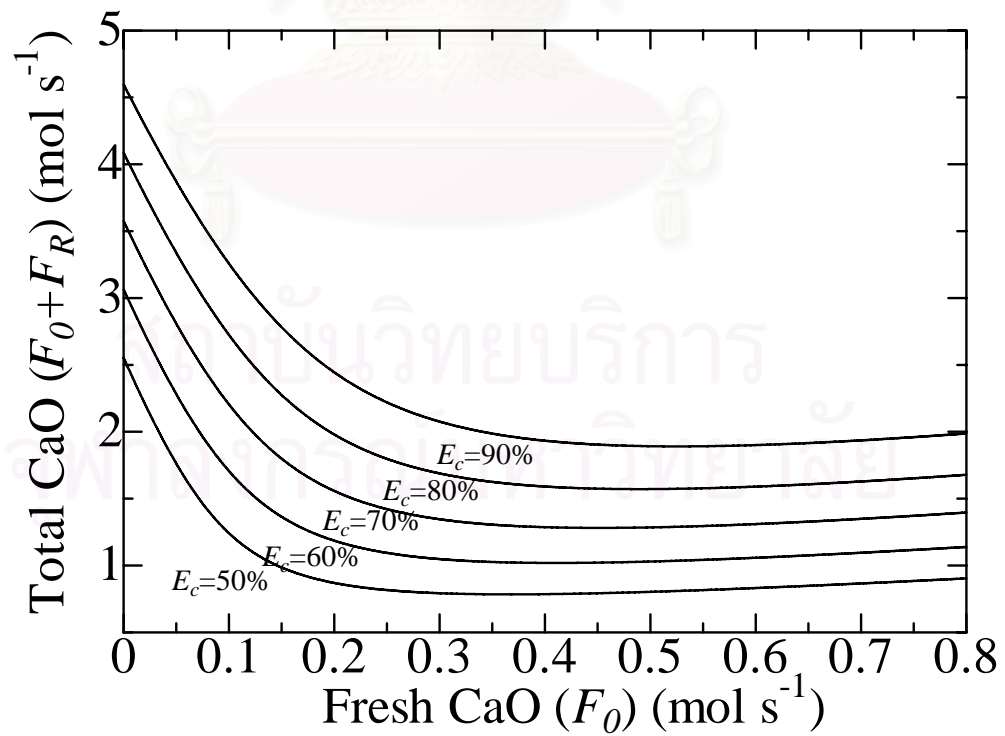
	Conventional	CaO-Before-SOFC	CaO-After-SOFC	CaO-After-Burner
Total net electrical power (kW)	339.64	339.64	339.64	339.64
Electrical power (kW)	339.64	346.78	347.75	376.92
SOFC Area (m ²)	439.96	439.24	471.29	629.04
Compressor power (kW)	-	7.145	8.111	37.283
Compressor cost (\$)	-	6018.955	6585.887	19451.566
Operating voltage (V)	0.55	0.5656	0.5631	0.6428
Cost of SOFC area (\$ (1500 \$ m ⁻²))	659940.43	658860.00	706935.00	943560.00
Reduced CO ₂ (mol s ⁻¹)	-	0.382	0.382	0.382
Added Cost of Area (\$)	-	-1080.43	46994.57	283619.57
F_R of CaO (mol s ⁻¹)	-	0.65269	0.29982	0.28209
F_θ of CaO (mol s ⁻¹)	-	0.25	0.335	0.34
total CaO at start up (mol)	-	0.903	0.635	0.622
Capital cost of CaO (\$)	-	0.0030	0.0021	0.0021
Operation cost of CaO (\$)	-	132639.0	177736.3	180389.04
Total cost add (\$)	-	-1080.4	46994.6	283619.6
Total cost add (\$)	-	131558.6	224730.8	464008.6
CO ₂ reduced (mol)	-	60265296.0	60265296.0	60265296.0
Total cost add/Reduced CO ₂ (\$ mol ⁻¹)	NA	0.002182991	0.003729026	0.007699433

Table 7.3 Economic analysis of CaO-SOFC system and conventional SOFC system
($U_f=90\%$)

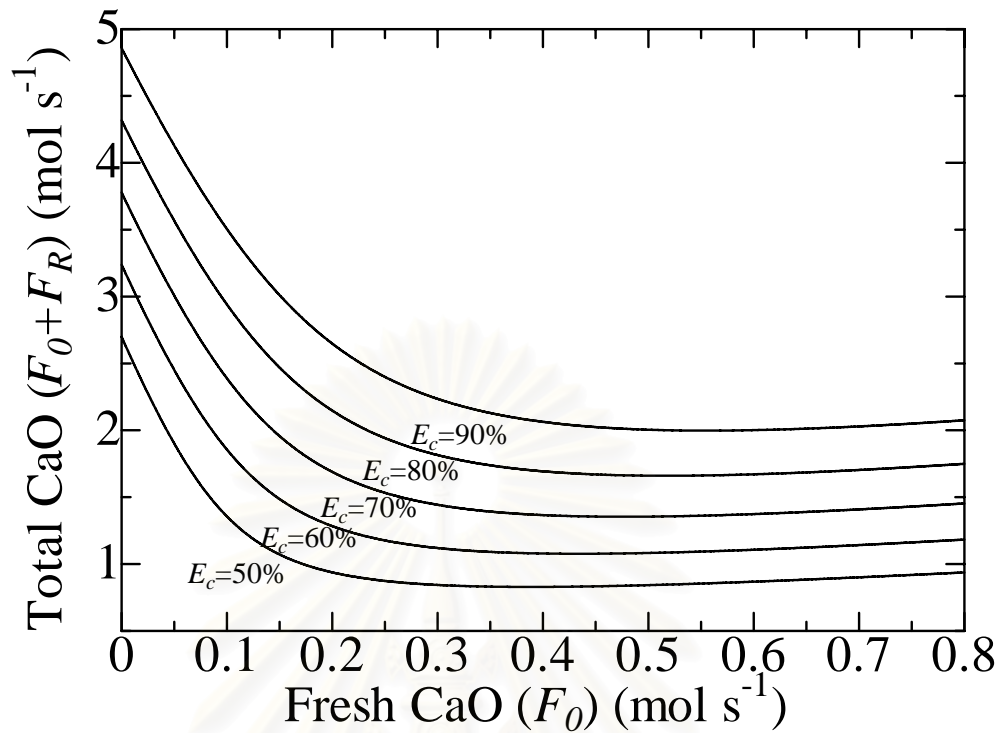
	Conventional	CaO-Before-SOFC	CaO-After-SOFC	CaO-After-Burner
Total net electrical power (kW)	339.64	339.64	339.64	339.64
Electrical power (kW)	339.64	346.78	347.75	376.92
SOFC Area (m ²)	435.399372	428.29	459.9	573.9
Compressor power (kW)	-	7.145	8.111	37.283
Operating voltage (V)	0.4888	0.4991	0.5005	0.5425
Cost of SOFC area (\$) (1500 \$ m ⁻²)	653099.058	642435	689850	860850
Compressor cost (\$)	-	6018.955	6585.887	19451.566
Reduced CO ₂ (mol s ⁻¹)	-	0.382	0.382	0.382
Added Cost of Area (\$)	-	-4645.104	43336.828	227202.508
F_R of CaO (mol/s)	-	0.653	1.365	1.428
F_O of CaO (mol/s)	-	0.250	0.525	0.57
total CaO at start up (mol)	-	0.903	1.890	1.998
Capital cost of CaO (\$)	-	0.0030	0.0064	0.0067
Operation cost of CaO (\$)	-	132639.0	278541.9	302416.9
total cost add (\$)	-	-4645.1	43336.8	227202.5
total cost add (\$)	-	127993.9	321878.7	529619.4
CO ₂ reduced (mol)	-	60265296.0	60265296.0	60265296.0
total cost add / Reduced CO ₂ (\$/mol)	NA	0.002123841	0.00534103	0.008788133



a.)



b.)



c.)

Fig. 7.7 Minimum total CaO (F_0+F_R) a.) CaO-Before-SOFC, b.) CaO-After-SOFC and c.) CaO-After-Burner.

The effects of location of CaO-CO₂ unit and electrical efficiency are shown in Fig. 7.8. Three levels of electrical efficiency (41%, 46% and 53%) are considered. Fig. 7.8.a and Fig. 7.8.b show the required SOFC area (m²) when $U_f = 80\%$ and 90% , respectively. For $U_f = 80\%$, it was found that the SOFC area follows the order: Conventional ~ CaO-Before-SOFC < CaO-After-SOFC < CaO-After-Burner. The higher the electrical efficiency, the higher SOFC area is required. In addition, the SOFC area of CaO-After-Burner enormously increases because the SOFC is operated at a much lower current density. Fig. 7.8.b shows the similar results at a higher fuel utilization (U_f). The required SOFC area is higher at a higher fuel utilization.

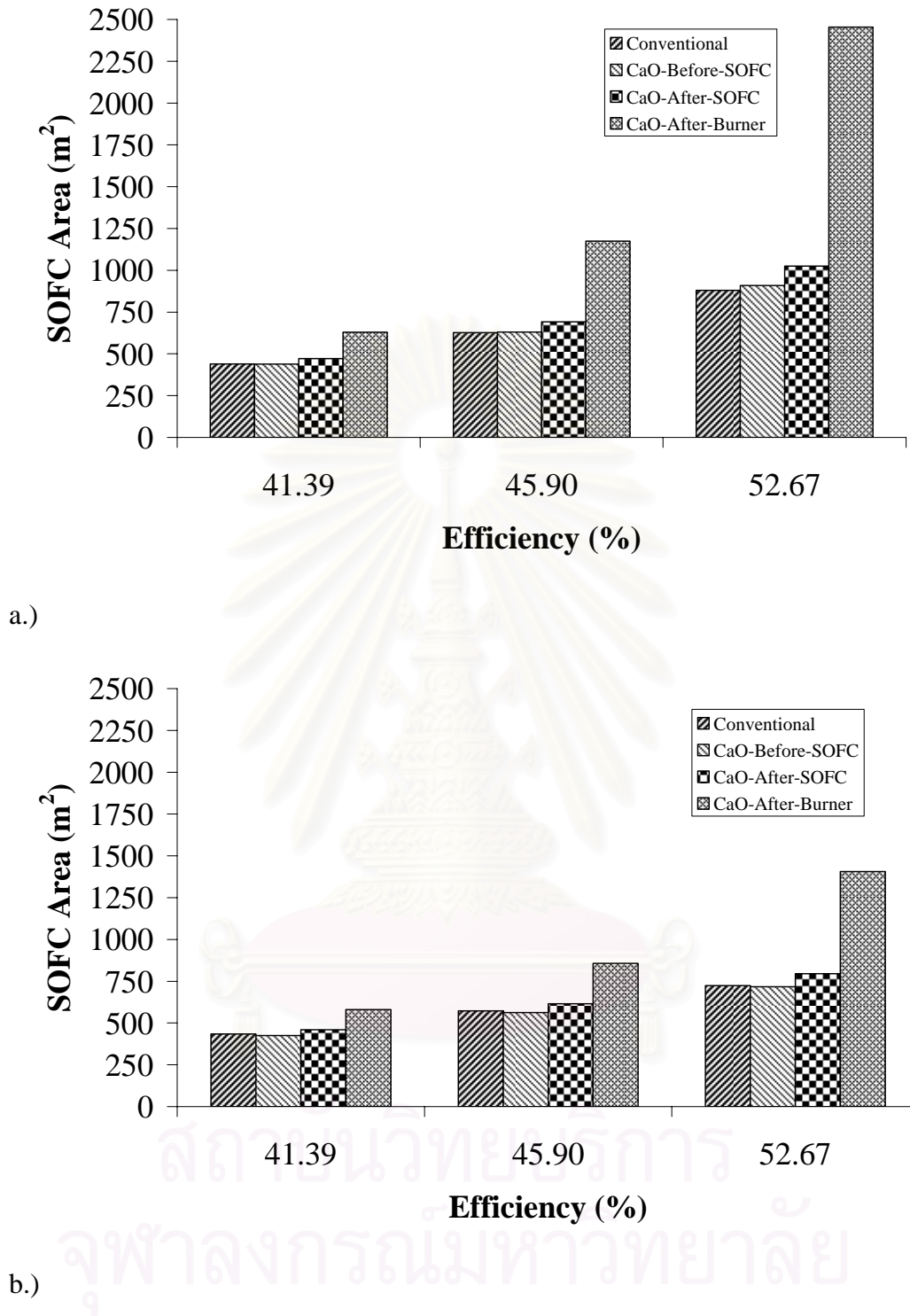


Fig. 7.8 The required SOFC area a). $U_f = 80\%$ and b). $U_f = 90\%$, (At $T_{\text{SOFC}} = 1073 \text{ K}$, $\text{CO}_2 \text{ capture} = 0.424 \text{ mol s}^{-1}$)

The cost of SOFC area can be ordered in the sequence of $\text{CaO-Before-SOFC} < \text{conventional SOFC} < \text{CaO-After-SOFC} < \text{CaO-After-Burner}$. These results show that

the CaO-Before-SOFC can operate at low capital cost of SOFC area. However, CaO-SOFC systems have higher operating cost due to the use of CaO (price of CaO equal 60 \$/ton of CaO). The operating cost of CaO acceptor is in the order: CaO-Before-SOFC < CaO-After-SOFC < CaO-After-Burner for 5 year operating time. Nevertheless, amount of reduced CO₂ depends on types of CaO acceptor and CO₂ capture efficiency. Fig. 7.9 shows that the amount of captured CO₂ follows the sequence: CaO-After-Burner > CaO-After-SOFC > CaO-Before-SOFC.

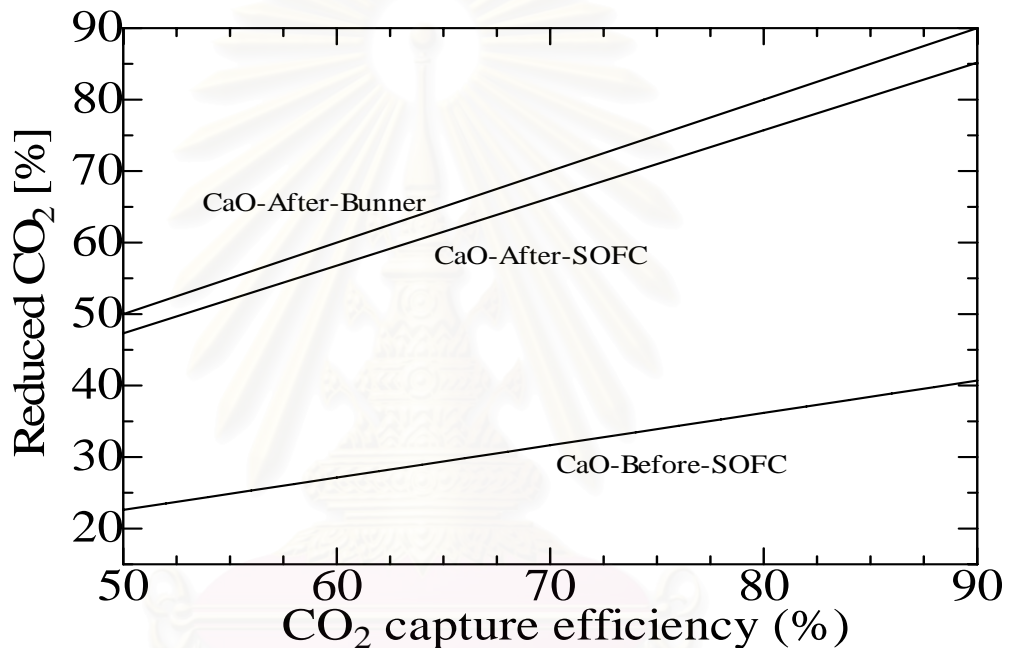


Fig. 7.9 The CO₂ reduction of CaO-SOFC system (CaO-acceptor Before-SOFC, After SOFC and After-burner) from conventional SOFC system (At $T_{ref} = 973$ K, $T_{SOFC} = 1073$ K).

However, it should be noted that the CaO-Before-SOFC system cannot reduce CO₂ more than about 40% as shown in Fig. 7.9. When it is desired to reduce CO₂ more than 40%, only CaO-After-SOFC or CaO-After-Burner are possible. Fig. 7.10 shows economic analysis of the CaO-After-SOFC compared with the CaO-After-Burner at CO₂ capture of 75%. This result shows that the cost of the CaO-After-SOFC is less than that of the CaO-After-Burner. This is due to the much lower partial pressure of CO₂ in the gas stream for the CaO-After-Burner.

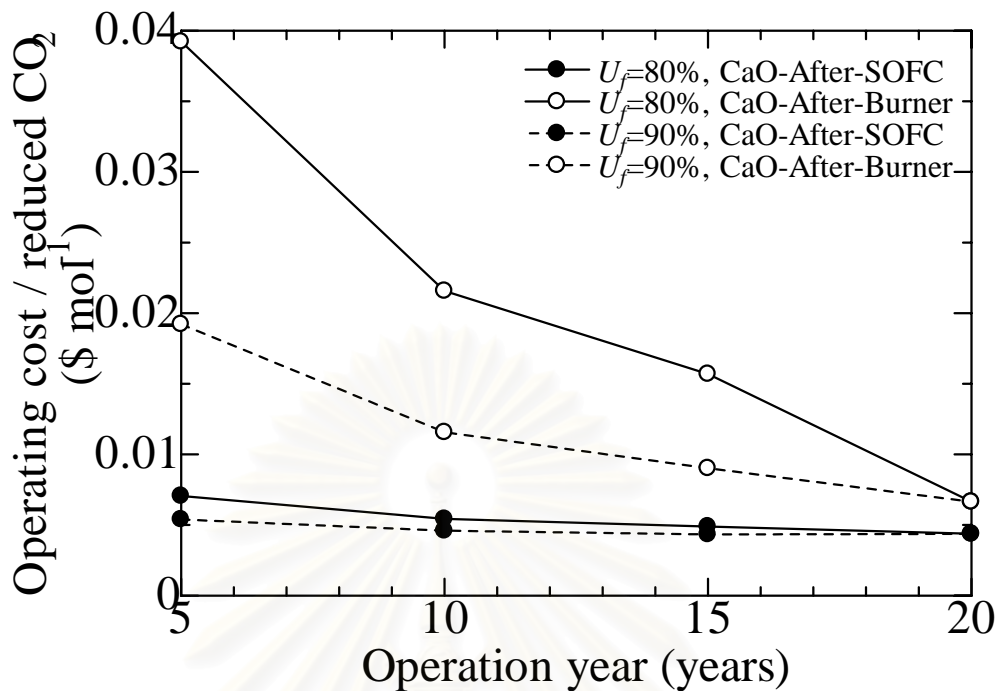


Fig. 7.10 Economic analysis of CaO-After-SOFC and CaO-After-Burner at higher percentage of reduced CO₂ (75%).

Finally, the economical analysis of the use of CO₂ capture unit was considered. It was found that the total added cost/reduced CO₂ (\$·mol⁻¹) follows the order: CaO-After-Burner > CaO-After-SOFC > CaO-Before-SOFC. It was further indicated that the total added cost/reduced CO₂ was reduced by increasing fuel utilization (U_f). Conclusively, the CaO-Before-SOFC shows the potential alternative for reducing CO₂ emitted from SOFC system.

7.2 Conclusion

The SOFC system integrated with a CaO-CO₂ acceptor was investigated in this study. The effect of location of CaO-CO₂ acceptor in the SOFC system (i.e. CaO-Before-SOFC, CaO-After-SOFC and CaO-After-Burner) on reduced CO₂, SOFC performance and economic analysis was considered. It was found that all SOFC-CaO systems can reduce the CO₂ emission; however, only the CaO-Before-SOFC system can improve performance of SOFC. Economic analysis on different CaO-SOFC systems was studied and compared to that of the conventional one. The capital cost of

SOFC area shows that CaO-Before-SOFC < conventional SOFC < CaO-After-SOFC < CaO-After-Burner. Operation cost of CaO was also calculated, the results show conventional SOFC < CaO-Before-SOFC < CaO-After-SOFC < CaO-After-Burner. Unfortunately, percentage of reduced CO₂ higher than ~40% was required, the CaO-After-SOFC is preferable to the CaO-After-Burner due to lower total added cost. The total added cost / reduced CO₂ (\$·mol⁻¹) at reduced CO₂ < 40% are in the sequence of CaO-After-Burner > CaO-After-SOFC > CaO-Before-SOFC.



สถาบันวิทยบริการ
จุฬาลงกรณ์มหาวิทยาลัย

Chapter VIII

CONCLUSION AND RECOMMENDATION FOR FUTURE WORKS

8.1 Conclusion from the study on “Improvement of Solid Oxide Fuel Cell Performance by Using Non-Uniform Potential Operation”

This investigation established that an SOFC-NUP can provide higher power density than a typical SOFC-UP without a reduction of electrical efficiency. The optimum SOFC-NUP was determined by allowing the operating voltage and section split of each section to be appropriately adjusted to achieve the highest power density for each level of electrical efficiency. The maximum power density can be further improved by increasing the number of separated section (n) of the cell; however, it became less pronounced after $n > 3$. Although it is obvious that the non-uniform operation can allow the SOFC to be operated at higher performance, it is still not clear whether the cost reduction by the reduced stack size would be sufficiently attractive compared to the increases of power conditioning cost and complication of the SOFC operation

8.2 Conclusion from the study on “Performance Improvement of Solid Oxide Fuel Cell System Using Palladium Membrane Reactor with Different Operation Modes”

Performance of the SOFC systems fed by methane was analyzed to investigate the potential benefit from replacing the conventional reformer with the palladium membrane reactor. Obviously, the use of the palladium membrane reactor can improve the power density of the SOFC. Three operation modes of membrane reactors; i.e., MR-HPC, MR-V and MR-HPC-V were considered. The economic analysis of the different systems revealed that the total capital cost/net electrical power is dependent on hydrogen recovery, electrical efficiency and operation mode of

the membrane reactor. The use of the palladium membrane reactor becomes attractive over the conventional reformer when the system is operated at high values of electrical efficiency and hydrogen recovery. Finally, it was demonstrated that the MR-HPC-V was the best operation mode for integration with the SOFC system.

8.3 Conclusion from the study on “Solid Oxide Fuel Cell Systems Incorporated with Sequential CaO-CO₂ Capture”

The SOFC system integrated with a CaO-CO₂ acceptor was investigated in this study. The effects of location of CaO-CO₂ acceptor in the SOFC system (i.e. CaO-Before-SOFC, CaO-After-SOFC and CaO-After-Burner) and some operating parameters on the amount of reduced CO₂ and SOFC performance were investigated. It was found that only the CaO-Before-SOFC system can improve performance of SOFC together with the reduction of CO₂ emission. Economic analysis on different CaO-SOFC systems was studied and compared to that of the conventional SOFC. At low level of CO₂ capture (< 40%), the capital cost of SOFC is in the following order: CaO-Before-SOFC < conventional SOFC < CaO-After-SOFC < CaO-After-Burner while the operation cost of CaO-CO₂ acceptor is in the order: conventional SOFC < CaO-Before-SOFC < CaO-After-SOFC < CaO-After-Burner. For higher levels of CO₂ capture, the CaO-After-SOFC is more preferable than the CaO-After-Burner due to lower total added cost. The total added cost/mol of reduced CO₂ (\$.mol⁻¹) at CO₂ capture level < 40% is in the sequence of CaO-Before-SOFC < CaO-After-SOFC < CaO-After-Burner.

8.4 Recommendation for Future Works

- a.) As the results suggest that the performance of solid oxide fuel cell (SOFC) can be improved by employing non-uniform potential operation of SOFC (NUP-SOFC), implementing a membrane reactor to the SOFC system (MR-SOFC) and integrating a CaO-CO₂ acceptor with the SOFC system (CaO-SOFC) (Fig. 8.1). When the SOFC with non-uniform potential operation (NUP-SOFC) is combined with a membrane reactor (MR-SOFC) (Fig. 8.2) or with a CaO-CO₂ acceptor (CaO-SOFC) (Fig.

8.3), the overall performance of the SOFC system should be further improved than its individual operation.

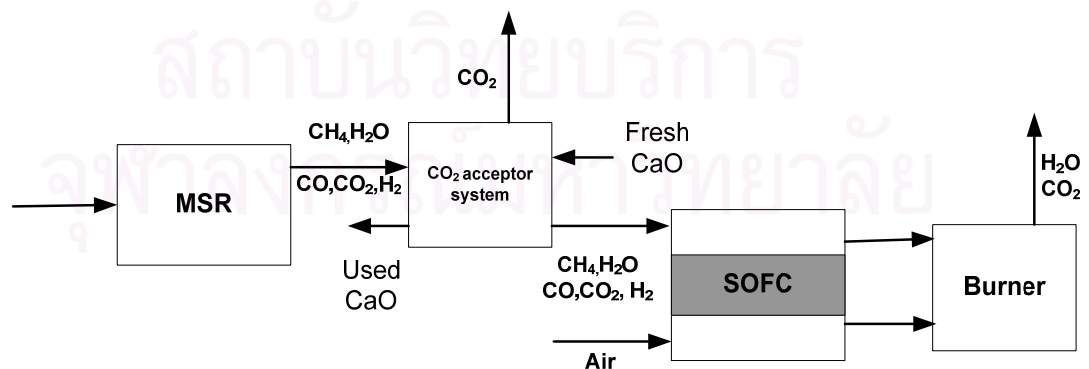
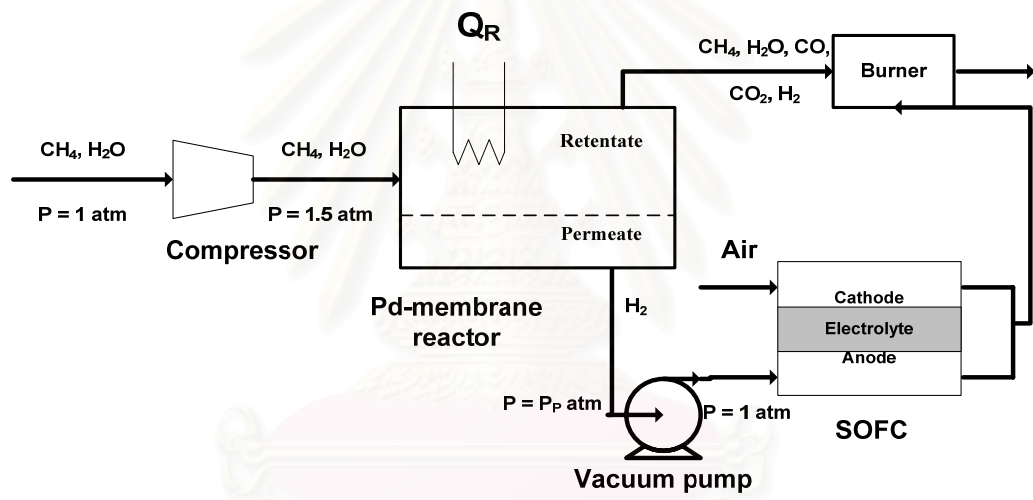
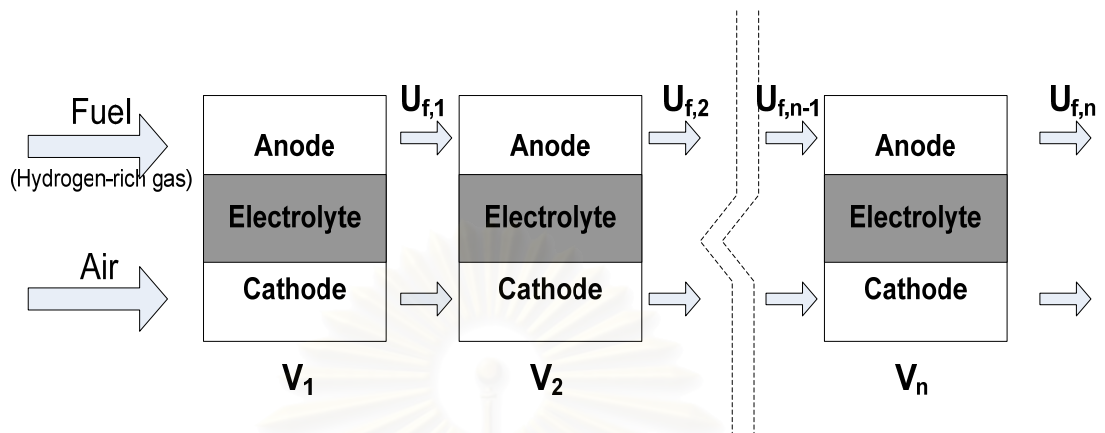


Fig. 8.1 a) non-uniform potential operation of SOFC (NUP-SOFC), b) implementing a membrane reactor to the SOFC system (MR-SOFC) and c) integrating a CaO-CO₂ acceptor with the SOFC system (CaO-SOFC)

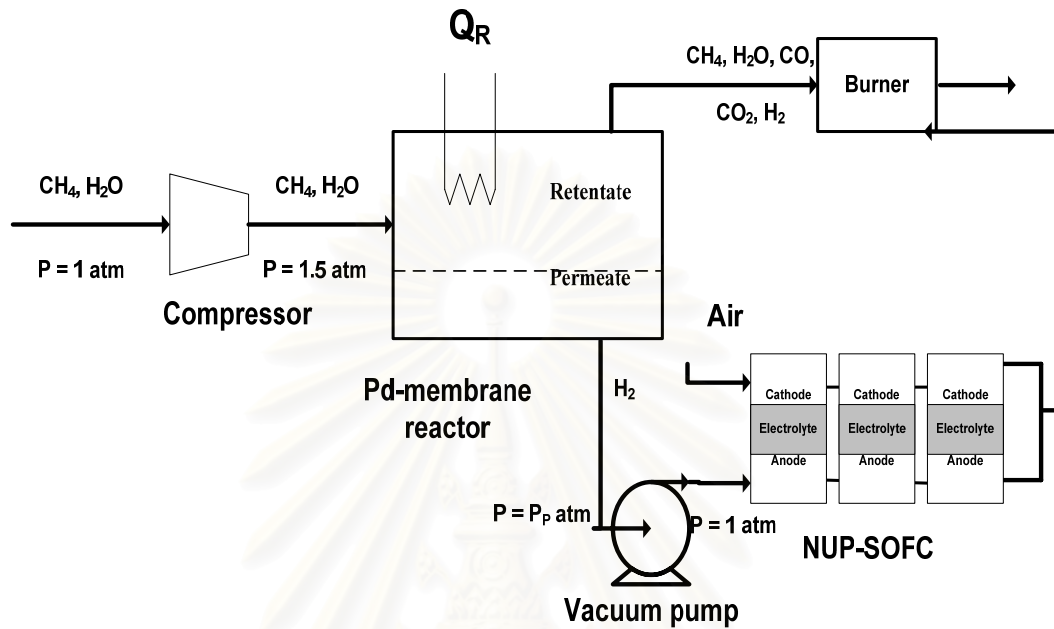


Fig. 8.2 Scheme of the non-uniform potential operation of SOFC (NUP-SOFC) operates with membrane reactor to the SOFC system (MR-SOFC)

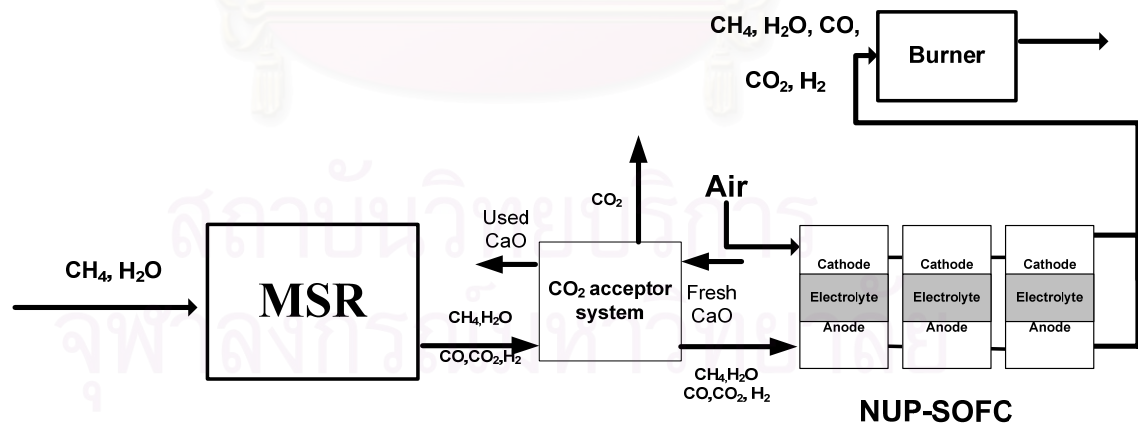
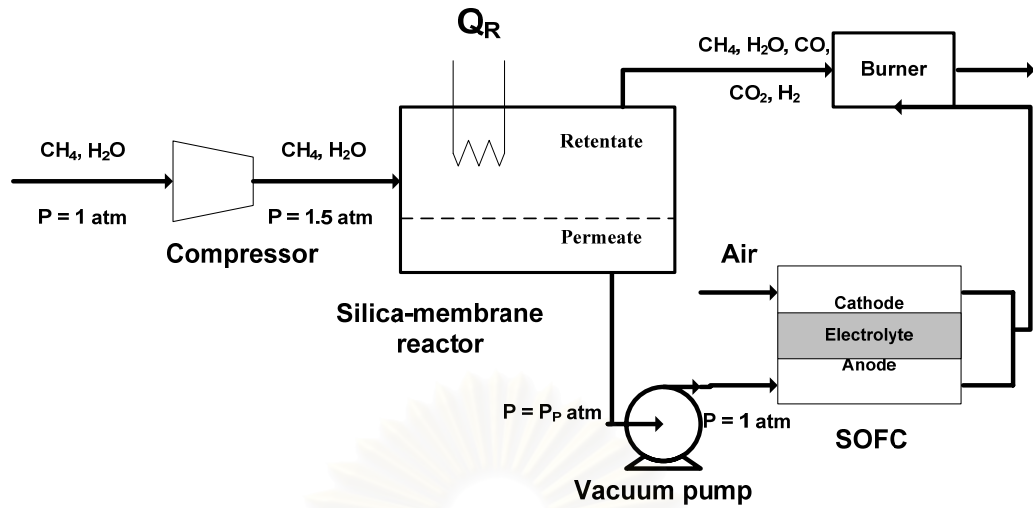


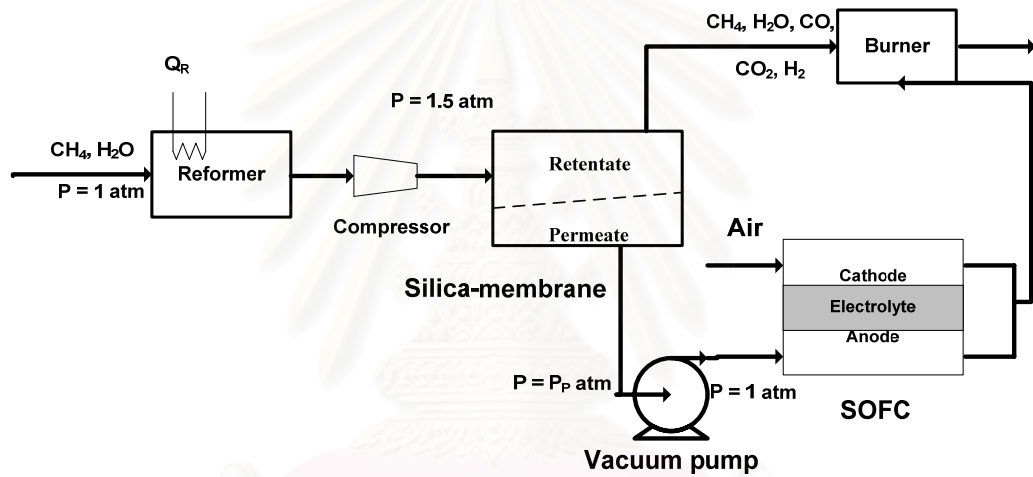
Fig. 8.3 Scheme of the non-uniform potential operation of SOFC (NUP-SOFC) operates with a CaO-CO₂ acceptor with the SOFC system (CaO-SOFC).

From our studies, it was reported that the SOFC-NUP, SOFC-MR and SOFC-CaO could improve maximum performance of the SOFC stack about 10%, 20% and 8%, respectively. Consequently, when the SOFC-NUP is incorporated with SOFC-MR or SOFC-CaO, the performance of the SOFC system should be further improved. However, the economic analysis should be carried out to determine whether the combined operations are really economically attractive compared with the conventional or individual cases.

- b.) From CHAPTER VI, the result shows that the performance of SOFC depends on partial pressure of hydrogen. It was proposed in our study to use a Pd-membrane reactor (Fig. 6.1) to increase the hydrogen partial pressure. However, due to high cost of a palladium membrane, it is interesting to apply other potential membranes with similar characteristics. One of the interesting membranes is porous silica membrane. It is expected that the use of silica membranes exhibit lower module costs, high permeating fluxes, no inhibition effects by chemical species, and high thermal stability, on the contrary to Pd membranes. Its amorphous structures with pores (or spaces) smaller than 1 nm in a wide temperature range below around 1273 K allow the silica membrane to separate hydrogen from the other impurities via molecular sieve mechanism. The study should consider the uses of the silica membrane as a silica membrane reactor (Fig. 8.4a) or as a membrane separation unit (Fig. 8.4b) in the SOFC system.



a.)



b.)

Fig. 8.4 a) SOFC system incorporated with silica membrane reactor, b) SOFC system incorporated with silica membrane.

สถาบันวิทยบริการ
จุฬาลงกรณ์มหาวิทยาลัย

REFERENCES

- Abanades J.C., The maximum capture efficiency of CO₂ using a carbonation/calcination cycle of CaO/CaCO₃. Chem. Eng. J. 90 (2002):303-306.
- Achenbach E. and Riensche E., Methane/steam reforming kinetics for solid oxide fuel cells. J. Power Sources 52 (1994):283-288.
- Achenbach E., Three-dimensional and time-dependent simulation of a planar solid oxide fuel cell stack. J. Power Sources 49 (1994): 333-348.
- Aguiar P., Chadwick D. and Kershenbaun L., Modelling of an Indirect Internal Reforming Solid Oxide Fuel Cell. Chem. Eng. Sci. 57 (2002):1665-1677.
- Aguiar, P., Adjiman C.S., and Brandon N.P., Anode-supported intermediate temperature direct internal reforming solid oxide fuel cell. I: model-based steady -state performance. J. Power Sources 138 (2004):120-136.
- Aguiar, P., Modelling studies of solid oxide fuel cells with internal methane steam reforming. Ph.D. Thesis, University of London, UK, 2002.
- Al-Qahtani H., Effect of ageing on a steam reforming catalyst. Chem. Eng. J. 66 (1997):51-56.
- Amanduson H., Ekedahl L.G. and Dannetun H., Methanol-induced hydrogen permeation through a palladium membrane. Surface Science 442 (1999):199-205.
- Assabumrungrat S., Pavarajarn V., Charojrochkul S. and Laosiripojana N., Thermodynamic analysis for a solid oxide fuel cell with direct internal reforming fueled by ethanol. Chem. Eng. Sci. 59 (2004):6015-6020.
- Au S. F., Woudstra N. and Hemmes K., Study of multistage oxidation by flowsheet calculations on a combined heat and power molten carbonate fuel cell plant. J. Power Sources 122 (2003):28-36.
- Balasubramanian B., Lopez Ortiz A., Kaytakoglu S. and Harrison D.P., Hydrogen from methane in a single-step process. Chem. Eng. Sci. 54 (1999):3543-3552.
- Barelli L., Bidini G., Corradetti A. and Desideri U., Production of hydrogen through the carbonation–calcination reaction applied to CH₄/CO₂ mixtures. Energy 32 (2007):834-843.
- Bedringas K.W., Ertesvag I.S., Byggstotl S. and Magnussen B.F., Exergy analysis of solid oxide fuel cell (SOFC) systems. Energy 22 (1997):403-412.

- Bessette N.F., Wepfer W.J. and Winnick J., A Mathematical Model of a Solid Oxide Fuel Cell. J. Electrochem. Soc. 142 (1995):3792-3800.
- Braun R.J., Klein S.A. and Reindl D.T., Evaluation of system configurations for solid oxide fuel cell-based micro-combined heat and power generators in residential applications. J. Power Sources 158 (2006):1290-1305.
- Brown L.F., A comparative study of fuels for on-board hydrogen production for fuel-cell-powered automobiles. Int. J. Hydrogen Energy 26 (2001):381-397.
- Brunetti A., Caravella A., Barbieri G. and Drioli E., Simulation study of water gas shift reaction in a membrane reactor. J. Membr. Sci. 306 (2007):329-340.
- Buxbaum R.E. and Kinney A.B., Hydrogen transport through tubular membranes of palladium-coated tantalum and niobium. Ind. Eng. Chem. 35 (1996): 530-537.
- Campanari S., Macchi E. and Manzolini G., Innovative membrane reformer for hydrogen production applied to PEM micro-cogeneration: Simulation model and thermodynamic analysis. Int. J. Hydrogen Energy 33 (2008):1361-1373.
- Campanari S., Thermodynamic model and parametric analysis of a tubular SOFC module. J. Power Sources 92 (2001):26-34.
- Chan S.H. and Ding O.L., Simulation of a solid oxide fuel cell power system fed by methane. Int. J. Hydrogen Energy 30 (2005):167-179.
- Chan S.H., Low C.F. and Ding O.L., Energy and exergy analysis of simple solid-oxide fuel-cell power systems. J. Power Source 103 (2002):188-200.
- Chen Z., Po F., Grace J.R., Lim C.J., Elnashaie S., Mahecha-Botero A., Rakib M., Shirasaki Y. and Yasuda I., Sorbent-enhanced/membrane-assisted steam-methane reforming. Chem. Eng. Sci. 63 (2008):170-182.
- Clarke S.H., Dicks A.L., Pointon K., Smith T.A. and Swann A., Catalytic aspects of the steam reforming of hydrocarbons in internal reforming fuel cells. Catal. Today 38 (1997):411-423.
- Comas J., Laborde M. and Amadeo N., Thermodynamic analysis of hydrogen production from ethanol using CaO as a CO₂ sorbent. J. Power Sources 138 (2004):61-67.
- Costamagna P., Selimovic A., Borghi M.D. and Agnew G., Electrochemical model of the integrated planar solid oxide fuel cell (IP-SOFC). Chem. Eng. J. 102 (2004):61-69.
- Criscuoli A., Basile A., Drioli E. and Loiacono O., An economic feasibility study for water gas shift membrane reactor. J. Mem. Sci. 181 (2001): 21-27.

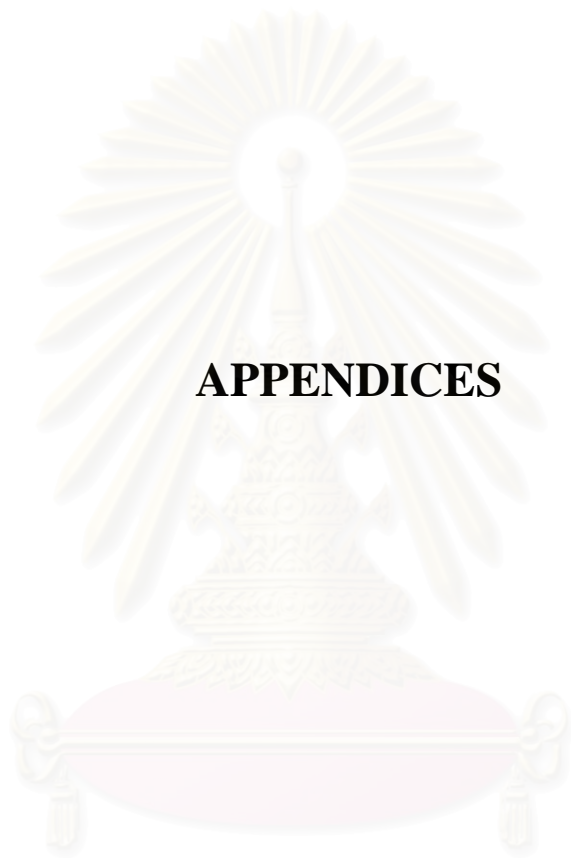
- Demin A.K., and Tsiakaras P., Thermodynamic analysis of a hydrogen fed solid oxide fuel cell based on proton conductor. J. Hydrogen Energy 26 (2001): 1103-1108.
- Demin A.K., Tsiakaras P., Sobyenin V.A. and Hramova S., Thermodynamic analysis of a methane fed SOFC system based on protonic conductor. Solid State Ionics 152 (2002):555-560.
- Demin A. K., Tsiakaras P., Gorbova E. and Hramova S., A SOFC based on a co-ionic electrolyte. J. Power Sources 131 (2004):231-236.
- Dicks A. L., Advances in catalysts for internal reforming in high temperature fuel cells. J. Power Sources 71 (1998):111-122.
- Dicks A. L., Hydrogen generation from natural gas for the fuel cell systems of tomorrow. J. Power Sources 61 (1996):113-124.
- Ding Y. and Alpay E., Adsorption-enhanced steam-methane reforming. Chem. Eng. Sci. 55 (2000):3929–3940.
- Douvartzides S.L., Coutelieris F. and Tsiakaras P., Exergy analysis of a solid oxide fuel cell power plant fed by either ethanol or methane. J. Power Sources 131 (2004):224-230.
- Douvartzides S.L., Coutelieris F. and Tsiakaras P., On the systematic optimization of ethanol fed SOFC-based electricity generating systems in term of energy and exergy. J. Power Sources 114 (2003):203-212.
- Douvartzides S.L., Coutelieris F., Demin A.K. and Tsiakaras P., Fuel options for Solid Oxide Fuel Cells: a thermodynamic Analysis. AIChE J. 49 (2003): 248-257.
- Fredriksson Möller B., Arriagada J., Assadi M. and Potts I., Optimisation of an SOFC/GT system with CO₂-capture. J. Power Sources 131 (2004):320-326.
- Galvita V.V., Belyaev V.D., Frumin A.V., Demin A.K., Tsiakaras P. and Sobyenin V.A., Performance of a SOFC fed by ethanol reforming products. Solid State Ionics 152 (2002):551-554.
- Grasa G.S. and Abanades J.C., Narrow fluidised beds arranged to exchange heat between a combustion chamber and a CO₂ sorbent regenerator. Chem. Eng. Sci. 62 (2007):619-626
- Gupta H. and Fan L.S., Carbonation-calcination cycle using high reactivity calcium oxide for carbon dioxide separation from flue gas. Ind. Eng. Chem. Res. 41 (2002):4035-4042.

- Heinzel A, Roes J. and Brandt H., Increasing the electric efficiency of a fuel cell system by recirculating the anodic offgas. J. Power Sources 145 (2005):312-318.
- Hernandez-Pacheco E., Mann M.D., Hutton P.N., Singh D. and Martin K.E., A cell-level model for a solid oxide fuel cell operated with syngas from a gasification process. Inter. J. Hydrogen Energy 30 (2005):1221-1233.
- Hernandez-Pacheco E., Singh D., Hutton P.N., Patel N. and Mann M.D., A macro-level model for determining the performance characteristics of solid oxide fuel cells. J. Power Sources 138 (2004):174-186.
- Hufton JR., Mayorga S., Sircar S., Sorption-enhanced reaction process for hydrogen production. AIChE. J. 45 (1999):248-256.
- Inui Y., Matsumae T., Koga H. and Nishiura K., High performance SOFC/GT combined power generation system with CO₂ recovery by oxygen combustion method. Energy Conversion and Management 46 (2005):1837-1847.
- Iora P., Aguiar P., Adjiman C.S., and Brandon N.P., Comparison of two IT DIR-SOFC models: Impact of variable thermodynamic, physical, and flow properties. Steady-state and dynamic analysis. Chem. Eng. Sci. 60 (2005):2963-2975.
- Ishihara T., Yamada T., Akbay T. and Takita Y., Partial oxidation of methane over fuel cell type reactor for simultaneous generation of synthesis gas and electric power. Chem. Eng. Sci. 54 (1999):1535-1540.
- Iyer M.V., Gupta H., Sakadjian B.B. and Fan L.S., Multicyclic study on the simultaneous carbonation and sulfation of high-reactivity CaO. Ind. Eng. Chem. Res. 43 (2004):3939-3947.
- Kazim A., Effect of higher operating pressure on the net change in voltage of a proton exchange membrane fuel cell under various operating conditions. J. Power Sources 143 (2005):9-16.
- Khaleel M.A., Lin Z., Singh P., Surdoval W. and Collin D., A finite element analysis modeling tool for solid oxide fuel cell development: coupled electrochemistry, thermal and flow analysis in MARC®. J. Power Sources 130 (2004):136-148.
- Kikuchi E., Membrane reactor application to hydrogen production. Catal. Today 56 (2000):97-101.

- Kim S. D., Hyun S. H., Moon J., Kim J. H., Song R. H., Fabrication and characterization of anode-supported electrolyte thin films for intermediate temperature solid oxide fuel cells. J. Power Sources 139 (2005):67-72.
- Kuchonthara P., Bhattacharya S., Tsutsumi A., Combinations of solid oxide fuel cell and several enhanced gas turbine cycles. J. Power Sources 124 (2003):65-75.
- Lee D.K., An apparent kinetic model for the carbonation of calcium oxide by carbon dioxide. Chem. Eng. J. 100 (2004):71-77.
- Lee D.K., Baek I.H. and Yoon W.L., A simulation study for the hybrid reaction of methane steam reforming and in situ CO₂ removal in a moving bed reactor of a catalyst admixed with a CaO-based CO₂ acceptor for H₂ production. Int. J. of Hydrogen Energy 31 (2006):649-657.
- Lee D.K., Baek I.H. and Yoon W.L., Modeling and simulation for the methane steam reforming enhanced by in situ CO₂ removal utilizing the CaO carbonation for H₂ production. Chem. Eng. Sci. 59 (2004):931-942.
- Levent M., Budak G., Karabulut A., Estimation of concentration and temperature profiles for methane-steam reforming reaction in a porous catalyst. Fuel Proc. Tech. 55 (1998):251-263.
- Li P. W., Chen S.P. and Chyu M.K., Novel gas distributors and optimization for high power density in fuel cells. J. Power Sources 140 (2005):311-318.
- Matelli J.A. and Bazzo E., A methodology for thermodynamic simulation of high temperature, internal reforming fuel cell systems. J. Power Sources 142 (2005):160-168.
- Nagata S., Momma A., Kato T. and Kasuga Y., Numerical analysis of output characteristics of tubular SOFC with internal reformer. J. Power Sources 101 (2001):60-71.
- Palsson J., Selimovic A. and Sjunnesson L., Combined solid oxide fuel cell and gas turbine systems for efficient power and heat generation. J. Power Sources 86 (2000):442-448.
- Patel K.S. and Sunol A.K., Modeling and simulation of methane steam reforming in a thermally coupled membrane reactor. Int. J. Hydrogen Energy 32 (2007):2344-2358.
- Pedernera M.N., Piña J. and Borio D.O., Kinetic evaluation of carbon formation in a membrane reactor for methane reforming. Chem. Eng. J. 134 (2007):138-144.

- Pfafferodt M., Heidebrecht P., Stelter M. and Sundmacher K., Model-based prediction of suitable operating range of a SOFC for an Auxiliary Power Unit. J. Power Sources 149 (2005):53-62.
- Renner H.J. and Marschner R., Catalytic reforming of natural gas and other hydrocarbon, Ullmann's Encyclopedia of Industrial Chemistry fifth edition, VCH Verlagsgesellschaft, Weinheim, Germany. A2 (1985):186-204.
- Riensch E., Stimming U., Unverzagt G., Optimization of a 200 kW SOFC cogeneration power plant: Part I: Variation of process parameter. J. Power Sources 73 (1998):251-256.
- Rostrup-Nielsen J. R., Conversion of hydrocarbons and alcohols for fuel cells. Phys. Chem. Chem. Phys. 3 (2001):283-288.
- Sangtongkitcharoen W., Assabumrungrat S., Pavarajarn V., Laosiripojana N. and Praserttham P., Comparison of carbon formation boundary in different modes of solid oxide fuel cells fueled by methane. J. Power Source 142 (2005):75-80.
- Sangtongkitcharoen W., Vivanpatarakij S., Laosiripojana N., Arpornwichanop A. and Assabumrungrat S., Performance analysis of methanol-fueled solid oxide fuel cell system incorporated with palladium membrane reactor. Chem. Eng. J. 138 (2008):436-441.
- Selimovic A., Palsson J. Networked solid oxide fuel cell stacks combined with gas turbine cycle, J. Power Sources 106 (2002):76-82.
- Senn S.M. and Poulidakos D., Multistage polymer electrolyte fuel cell based on nonuniform cell potential distribution functions. Electrochemistry Communications 7 (2005):773-780.
- Shu J., Grandjean B.P.A. and Kaliaguine S., Methane steam reforming in asymmetric Pd- and Pd-Ag/porous SS membrane reactors. Appl. Catal. A 119 (1994):305-325.
- Simner S.P., Bonnett J.F., Canfield N.L., Meinhardt K.D., Shelton J.P., Sprenkle V.L. and Stevenson J.W., Development of lanthanum ferrite SOFC cathodes, J. Power Sources 113 (2003):1-10.
- Simpson A.P. and Lutz A.E., Exergy analysis of hydrogen production via steam methane reforming. Int. J. Hydrogen Energy 32 (2007):4811-4820.
- Standaert F., Analytical Fuel Cell Modelling and Exergy Analysis of Fuel Cells, Ph.D. Thesis, Delft University of Technology, 1998.

- Tagawa T., Moe K.K., Ito M. and Goto S., Fuel cell type reactor for Chemicals-energy co-generation. Chem. Eng. Sci. 54 (1999):1553-1557.
- Tosti S., Basile A., Borgognoni F., Capaldo V., Cordiner S., Di Cave S., Gallucci F., Rizzello C., Santucci A. and Traversa E., Low temperature ethanol steam reforming in a Pd-Ag membrane reactor Part 1: Ru-based catalyst. J. Membr. Sci. 308 (2008):250-257.
- Tosti S., Basile A., Borgognoni F., Capaldo V., Cordiner S., Di Cave S., Gallucci F., Rizzello C., Santucci A. and Traversa E., Low-temperature ethanol steam reforming in a Pd-Ag membrane reactor Part 2: Pt-based and Ni-based catalysts and general comparison. J. Membr. Sci. 308 (2008): 258–263.
- Vivanpatarakij S., Assabumrungrat S. and Laosiripojana N., Improvement of solid oxide fuel cell performance by using non-uniform potential operation. J. Power Sources 167 (2007):139-144.
- Walas S.M., Chemical Process Equipment Selection and Design, Butterworth, Inc. (1988):665-668.
- Wang Z., Zhou J., Wang Q., Fan J. and Cen K., Thermodynamic equilibrium analysis of hydrogen production by coal based on Coal/CaO/H₂O gasification system. Int. J. Hydrogen Energy 31 (2006):945-952.
- Xiua G.H., Lia P. and Rodrigues A.E., Sorption-enhanced reaction process with reactive regeneration. Chem. Eng. Sci. 57 (2002):3893-3908.
- Xu J. and Froment G.F., Methane steam reforming, methanation and water. gas shift: I. Intrinsic kinetics. AIChE J. 35 (1989):88-96.
- Yoon S. P., Han J., Nam S. W., Lim T.H. and Hong S. A., Improvement of anode performance by surface modification for solid oxide fuel cell running on hydrocarbon fuel. J. Power Sources 136 (2004):30-36.
- Yoon Y.G., Lee W.Y., Park G.G., Yang T.H. and Kim C.S., Effects of channel configurations of flow field plates on the performance of a PEMFC. Electrochimica Acta. 50 (2004):709-712.



APPENDICES

สถาบันวิทยบริการ
จุฬาลงกรณ์มหาวิทยาลัย

APPENDIX A

THERMODYNAMIC DATA OF SELECTED COMPONENTS

Table A.1 Heat capacities of selected components (C_p)

Components	$C_p = a + bT + cT^2 + dT^3 + eT^4$ [J/mol]				
	a	$b \times 10^3$	$c \times 10^5$	$d \times 10^8$	$e \times 10^{13}$
Methane	34.942	-39.957	19.184	35.103	393.21
Carbon monoxide	29.556	-6.5807	2.0130	-1.2227	22.617
Carbon dioxide	27.437	42.315	-1.9555	0.3997	-2.9872
Water	33.933	-8.4186	2.9906	-1.7825	36.934
Hydrogen	25.399	20.178	-3.8549	3.1880	-87.585

Table A.2 Heat of formation (H_f), and entropy (S^0) of selected components

Components	$H_f = a + bT + cT^2$ [kJ/mol]			S^0 [J/mol.K]
	a	$b \times 10^3$	$c \times 10^5$	
Methane	-63.425	-43.355	1.7220	186.27
Carbon monoxide	-112.19	8.1182	-8.0425	197.54
Carbon dioxide	-393.42	0.1591	-0.1395	213.69
Water	-241.80	0	0	188.72
Hydrogen	0	0	0	130.57

APPENDIX B

CALCULATIONS OF GIBBS ENERGY AND EQUILIBRIUM CONSTANT

B.1. Determining Gibbs energy (G) at any temperatures by equations below:

$$G = H - TS \quad (\text{B1})$$

$$dG = dH - d(TS) \quad (\text{B2})$$

Take integration to the equation above:

$$\int dG = \int dH - \int d(TS) \quad (\text{B3})$$

$$G_T - G_{STD} = \int_{298}^T dH - \int_{298}^T d(TS) \quad (\text{B4})$$

where: $H = H(T) = a + bT + cT^2$ (B5)

$$S = S(T) = S^0 + \int_{298}^T C_p dT \quad (\text{B6})$$

where: T = the temperature range of 500 - 1,500 K

S^0 = the entropy at standard state (298 K, 1 atm)

B.2. Determining the equilibrium constant (K)

$$G_T = -RT \ln K \quad (\text{B7})$$

Rearrange the above equation;

$$K = \exp\left(-\frac{G_T}{RT}\right) \quad (\text{B8})$$

And from thermodynamic concept

$$K = \prod a_i^{v_i} \quad (\text{B9})$$

When gas phase is considered, we can substitute activity with partial pressure term.

$$K = \prod \left(\Phi_i y_i \frac{P}{P^o} \right)^{v_i} \quad (\text{B10})$$

Since it was studied at the pressure of 1 atm, the equation (B10) became the following equation:

$$K = \prod (y_i)^{v_i} \quad (\text{B11})$$

From equation (B11), the converted moles associated to the reactions involved in the production of hydrogen from steam reforming (x_1, x_2, x_3) can be calculated.

สถาบันวิทยบริการ
จุฬาลงกรณ์มหาวิทยาลัย

APPENDIX C

NEWTON'S METHOD

Newton's method is used to solve several unknown answers from equations. This method was applied from Taylor's series expansion to estimate the answers of non-linear equations. The first-order differentiated equations are considered. Then the equations can be applied as follow:

$$f(x+\Delta x) = f(x) + J(x) \Delta x \quad (C1)$$

When $J(x)$ = Jacobian matrix

$$J(x) = \begin{bmatrix} \frac{\partial f_1(x)}{\partial x_1} & \dots & \frac{\partial f_1(x)}{\partial x_n} \\ \vdots & \ddots & \vdots \\ \frac{\partial f_n(x)}{\partial x_1} & \dots & \frac{\partial f_n(x)}{\partial x_n} \end{bmatrix} \quad (C2)$$

To solve the answers is to find Δx which provides:

$$0 = f(x) + J(x) \Delta x \quad (C3)$$

Δx is calculated by the linear equation below:

$$J(x) \Delta x = -f(x) \quad (C4)$$

The procedure of the calculation:

1. Set the value of $k = 1$
2. If $k \leq N$ (The largest amount of loops in the operation)

- 2.1 Find $f(x)$ and $J(x)$
 - 2.2 Solve the equation: $J(x) \Delta x = -f(x)$ to get Δx
 - 2.3 Set $x = x + \Delta x$
 - 2.4 $|f(\Delta x)| < TOLX$ or $|f(x)| < TOLF$, end the calculation
 - 2.5 Set $k = k+1$ and repeat item 2.1
3. If $i > N$, and the answer hasn't been solved, it would be presumed that the amount of N is too small or the starting value is not appropriate.



สถาบันวิทยบริการ
จุฬาลงกรณ์มหาวิทยาลัย

APPENDIX D

CALCULATION OF POWER CONSUMPTION OF COMPRESSOR BY USING *Aspen Plus*TM SIMULATOR

In Chapter 6 and Chapter 7, the compressor is considered in the SOFC system. The power consumption for operating the compressor can be determined using *Aspen Plus*TM. Fig. D1 shows the schematic diagram of a compressor.

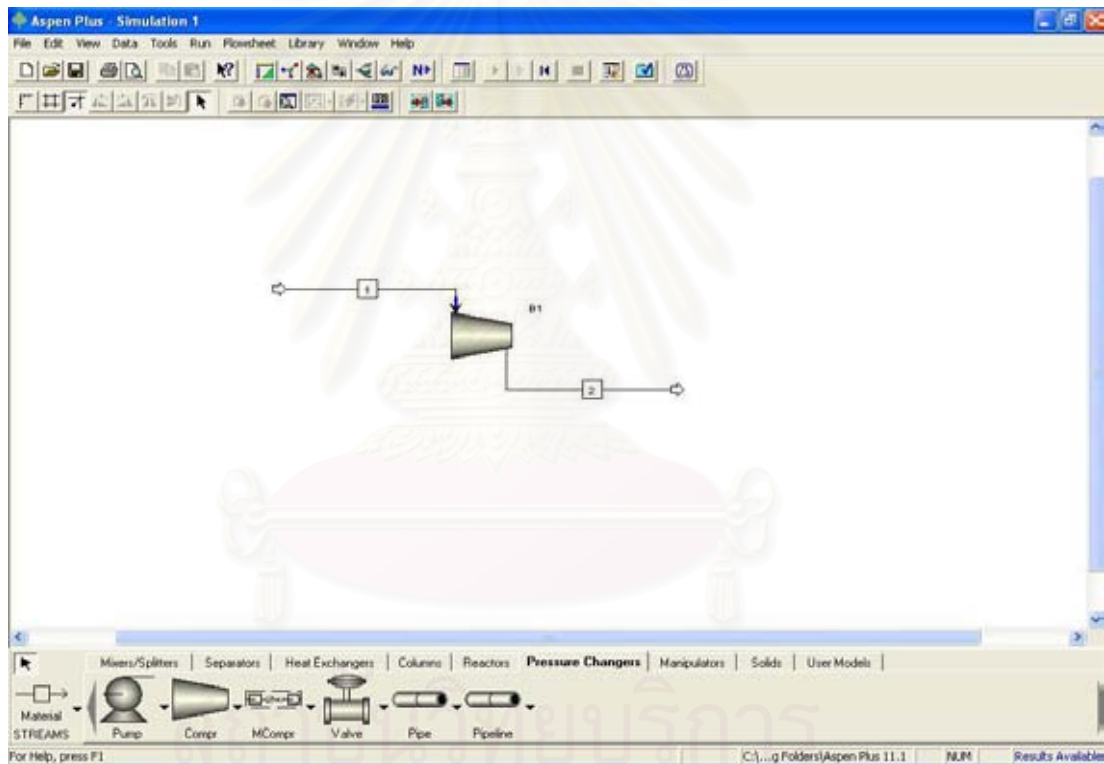


Fig. D1 Schematic diagram of compressor

First, Input parameters, temperature, pressure and mole flow rate, at *Stream 1* (Fig. D2)

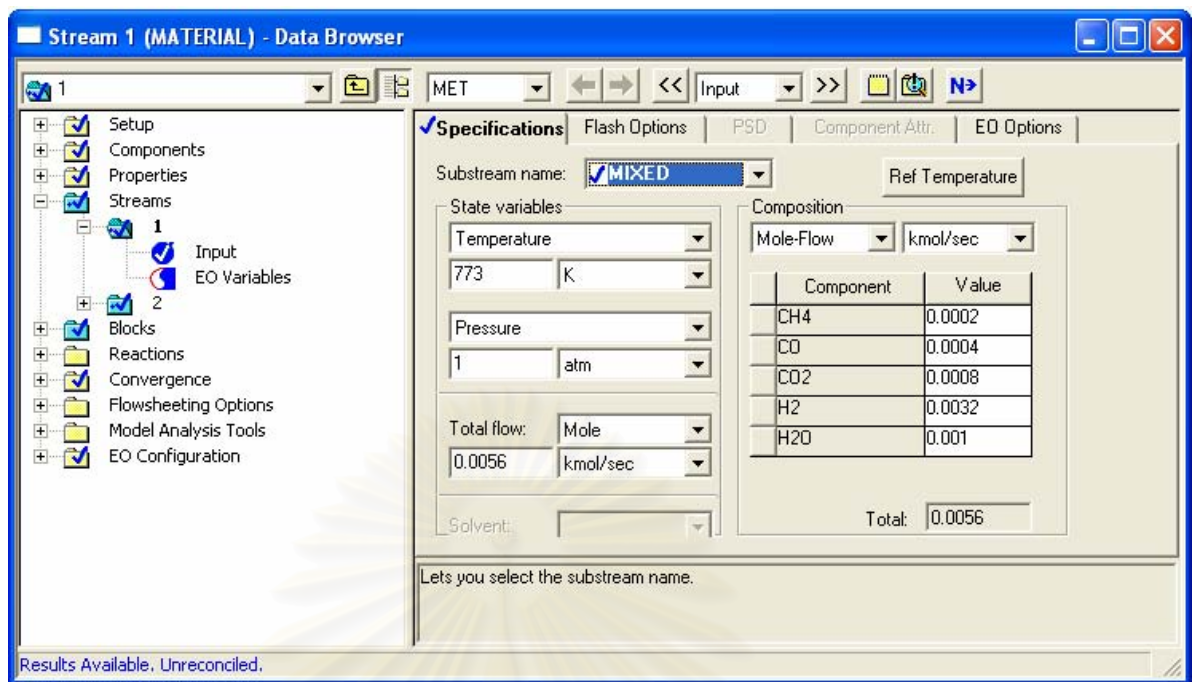


Fig. D.2 Inputting parameter at *Stream 1 (Material)*.

Then, Set Compressor model and Outlet specification (Fig. D3)

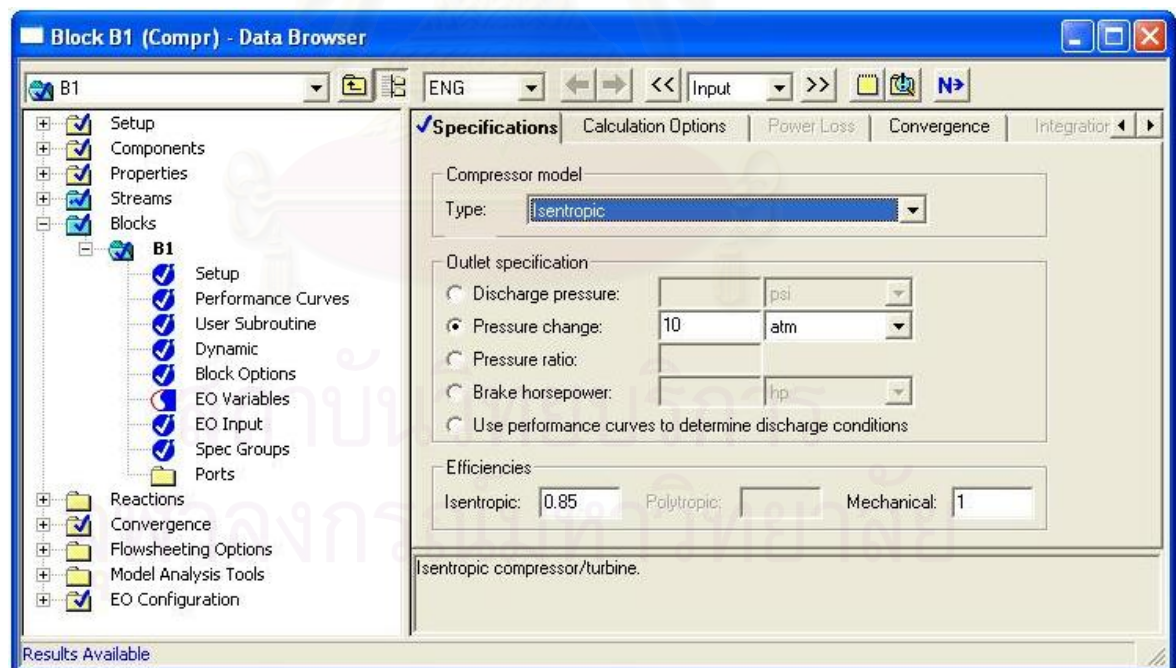


Fig. D.3 Setting compressor parameter at Block B1 (Compr).

After that, start for calculation. Results of the calculation will be obtained as illustrated in Fig. D4.

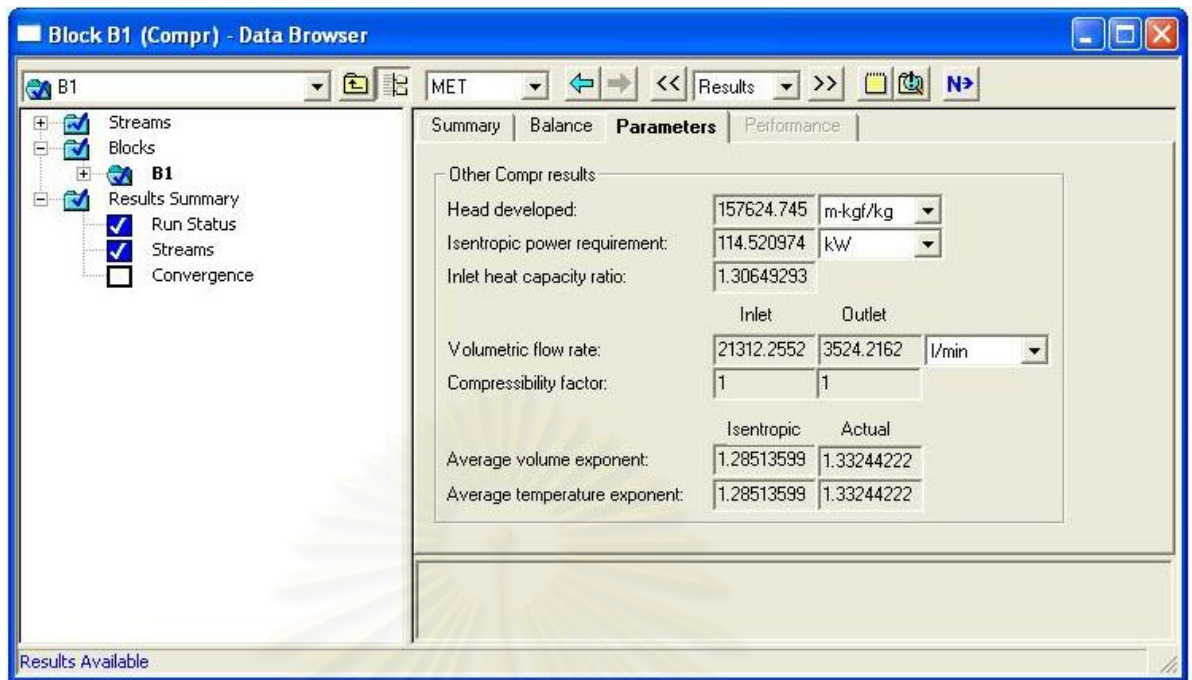


Fig. D4 Calculation results.

สถาบันวิทยบริการ
จุฬาลงกรณ์มหาวิทยาลัย

APPENDIX E

LIST OF PUBLICATIONS

International Publications

- 1) **Vivanpatarakij S.**, Assabumrungrat S. and Laosiripojana N., Improvement of solid oxide fuel cell performance by using non-uniform potential operation. J. Power Source 167 (2007):11-18.
- 2) Sangtongkitcharoen W., **Vivanpatarakij S.**, Laosiripojana N., Arpornwichanop A. and Assabumrungrat S., Performance analysis of methanol-fueled solid oxide fuel cell system incorporated with palladium membrane reactor. Chem. Eng. J. 138 (2008):436-441.

International Conferences

- 1) **Vivanpatarakij S.**, Assabumrungrat S., Laosiripojana N. and Praserthdam P., Improvement of Solid Oxide Fuel Cell Performance by Using Non-uniform Potential Operation. CAMURE-6 and ISMR-5 by National Chemical Laboratory, Pune, India, January 14-17, 2007 (Poster presentation).
- 2) Sangtongkitcharoen W., **Vivanpatarakij S.**, Assabumrungrat S., Laosiripojana N., Arpornwichanop A. and Praserthdam P., Performance Analysis of Methanol-Fuel Solid Oxide Fuel Cell System Incorporated with Palladium Membrane Reactor. CAMURE-6 and ISMR-5 by National Chemical Laboratory, Pune, India, January 14-17, 2007 (Oral presentation).

National Conferences

- 1) **S. Vivanpatarakij**, S. Assabumrungrat and N. Laosiripojana “Improvement of solid oxide fuel cell performance by using non-uniform potential operation” The 56th RGJ Seminar Series: Chemical Engineering Science and Technology supported by Thailand Research Fund (TRF), Chulalongkorn University, Thailand, September 28, 2007 (Oral presentation).



สถาบันวิทยบริการ
จุฬาลงกรณ์มหาวิทยาลัย

VITAE

Mister Supawat Vivanpatarakij was born in March 5, 1982 in Bangkok, Thailand. He finished high school from Wat Rajabopit School, Bangkok in 2000. He received his Bachelor's Degree in Chemical Engineering (2nd Honor), from the Department of Chemical Engineering, Thammasat University in 2004. Afterward, He continued studying Doctoral degree of Chemical Engineering, Chulalongkorn University since June 2004.



สถาบันวิทยบริการ
จุฬาลงกรณ์มหาวิทยาลัย